Studies on Peripherally Functionalized 2,7-Diazapyrenes

周辺修飾された 2,7-ジアザピレンに関する研究

NAKAZATO Takumi

仲里　巧

Department of Molecular and Macromolecular Chemistry, Graduate School of Engineering

Nagoya University

2020

Table of Contents

List of Abbreviations

Å	ångström unit
Ac	acetyl
ACID	anisotropy of the induced current density
aq	aqueous solution
Ar	aryl
B3	Becke's three-parameter hybrid exchange functional
BCOD	bicyclo[2,2,2]octadiene
BLA	bond length alternation
BS	symmetry-broken
Bu	*n*-butyl
calcd	calculated
cod	1,5-cyclooctadiene
CT	charge transfer
δ	chemical shift
DFT	density functional theory
DMF	*N*,*N*-dimethylformamide
ε	absorption coefficient
ESI-MS	electrospray ionization mass spectrometry
ESR	electron spin resonance
Eq.	equation
equiv	equivalent(s)
Et	ethyl
f	oscillator strength
Fc	ferrocene
FI-TRMC	flash-induced time-resolved microwave conductivity
h	hour(s)
HOMA	harmonic oscillator model of aromaticity
HOMO	highest occupied molecular orbital
HR-MS	high resolution mass spectrometry infrared
J	coupling constant (NMR)
λ	wavelength
LUMO	lowest occupied molecular orbital
LYP	Lee–Yang–Parr correlation functional
M	metal or molar
Me	methyl
Mes	mesityl

List of Abbreviations

min	minute(s)
MO	molecular orbital
MV	methyl viologen
NICS	nucleus-independent chemical shift
NIR	near infrared
NMR	nuclear magnetic resonance
Ph	phenyl
OEFT	organic field-effect transistor
PAH	polycyclic aromatic hydrocarbon
OPiv	pivaloxy
ppm	parts per million
R	an organic group or restricted
RT	room temperature
$TBAPF_6$	tetrabutylammonium hexafluorophosphate
TD	time-dependent
TEA	triethylamine
TFA	trifluoro aceticacid
THF	tetrahydrofuran
TMS	tetramethylsilane
Tol	tolyl
UV	ultraviolet
vis	visible
VT	variable temperature

Chapter 1.

General Introduction

Contents

1-1. Polycyclic aromatic hydrocarbons (PAHs)

Benzene is the most important and fundamental motif in the chemistry since its discovery in 1825. Its derivatives are widely used in pharmaceuticals and organic materials.[1,2] Polycyclic aromatic hydrocarbons (PAHs) which are consisted with annulated several benzene rings are key materials in the field of organic-, physical-, environmental-, and biochemistry for more than 100 years.[3] Since Clar and Scholl reported their pioneering works for the synthesis and characterization of PAHs, various PAHs have been developed. Photophysical and electrochemical properties of PAHs depend on the number and arrangement of fused rings (Figure 1-1).[4,5] In the last 20th century, the discovery of electrical conductivity in organic materials[6] fascinated organic and physical chemists to elucidate the synthesis and properties of PAHs as promising candidates for organic materials such as organic light emitting diodes (OLED),[7] organic field effect transistors (OFET),[8] organic photovoltaic cells (OPVs),[9] and organic solid lasers (OSLs).[10]

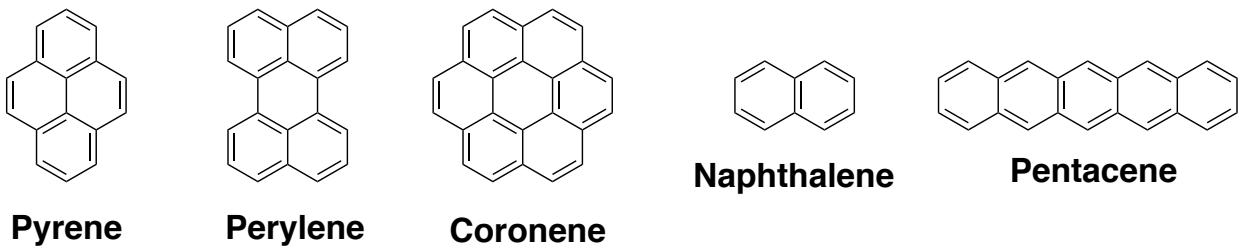

Figure 1-1. Polycyclic aromatic hydrocarbons.

Peripheral substituents of PAHs play an important role to tune their optical and electrochemical properties. For example, the parent pyrene shows weak fluorescence ($\Phi = 0.29$) in THF because the $S_1 \rightarrow S_0$ transition is symmetry forbidden. On the other hand the introduction the *tert*-butylphenyl groups into 1,3,6 and 8 positions of the pyrene core dramatically increase their fluorescence quantum yield ($\Phi = 0.90$) because the symmetry is broken by introduction of peripheral substituents and $S_1 \rightarrow S_0$ transition becomes symmetry allowed (Figure 1-2-a).[11] Perylene is a widely investigated PAH. Generally, perylene is electron donating molecule as represented by the perylene-bromine complex.[6a] On the other hand, perylene diimides (PDIs) exhibit the high electron deficient nature. Therefore, PDI derivatives have been studied as candidates for the n-type semiconductor or the electron-accepting unit for supramolecular structures (Figure 1-2-b).[12]

Peripheral substituents can also increase the solubility and chemical stability of compounds and modify the aggregation behavior of PAHs in solution and solid state. Pentacene is one of the representative PAHs which exhibits high charge transporting ability.[13] Parent pentacene is insoluble in typical organic solvents and easily oxidized in ambient atmosphere. On the other hand, the introduction of triisopropylsilylethynyl (TIPS-ethynyl) groups to 6 and 13 positions of pentacene increase the solubility due to the bulky silyl groups and improve the oxidative stability by stabilizing the HOMO level with ethynyl groups. Furthermore, the installation of substituents also changes the packing structure from herringbone to 2D brickwork ar-

rangement (Figure 1-3).[14] Consequently, the developments of efficient substituent introduction methods are important topics in organic chemistry.

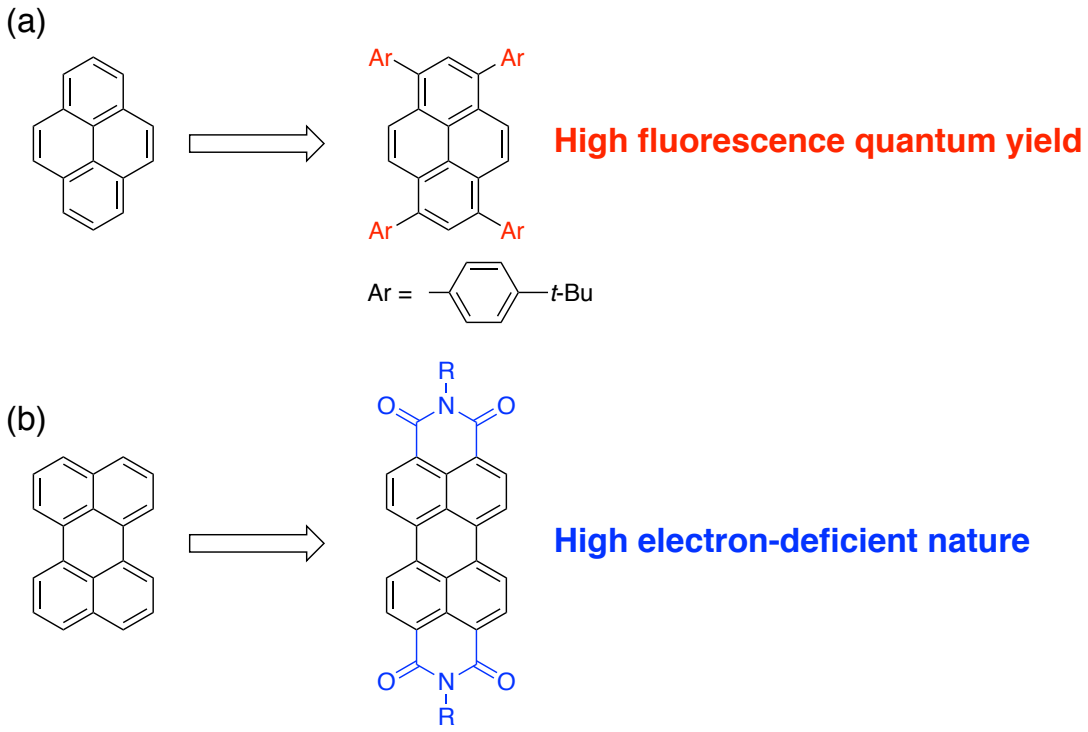

Figure 1-2. Peripheral functionalization of PAHs.

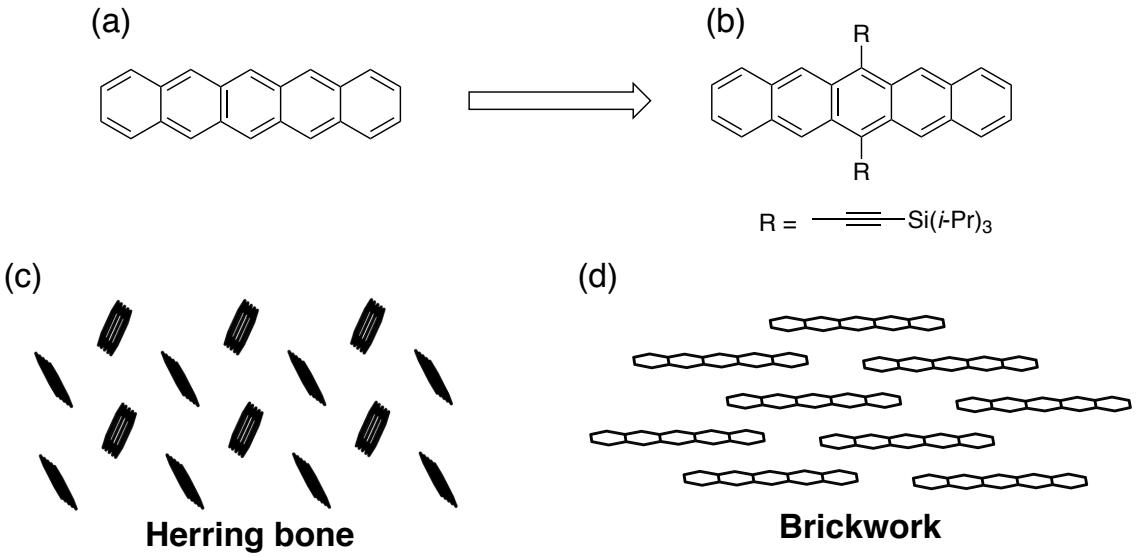

Figure 1-3. (a) The chemical structure of pentacene. (b) The chemical structure of pentacene with TIPS groups. (c) Packing structure of parent pentacene. (d) Packing structure of pentacene with TIPS groups. Hydrogen atoms and TIPS groups are omitted for clarity.

Transition metal-catalyzed cross-coupling reactions are useful methods for the introduction the peripheral substituents to PAHs. The use of the cross-coupling reactions enables the diversity-oriented synthesis of PAHs. In other words, one synthetic intermediate is transformed to a variety of peripherally functionalized PAHs. Aryl halides are commonly employed as the synthetic intermediate, where halogen atoms work as leaving groups. Recently, phenol derivatives are also applicable for the electrophilic coupling partners by using nickel catalysts. In 1979, Wenkert reported the pioneering work of the cross-coupling reaction of anisole derivatives with aryl Grignard reagents using $NiCl_2(PPh_3)_2$ catalyst (Scheme 1-1a). In 2008, Garg *et al.* demonstrated the cross-coupling reactions of naphthalene derivatives with pivaloxy groups in the presence of $NiCl_2(PCy_3)_2$ (Scheme 1-1b). Tobisu, Chatani, and co-workers developed the cross-coupling reaction for the alkylation of anisole derivatives (Scheme 1-1c). Consequently, PAHs with ether or ester groups on their peripheral area can be useful intermediates to synthesize various derivatives of them.

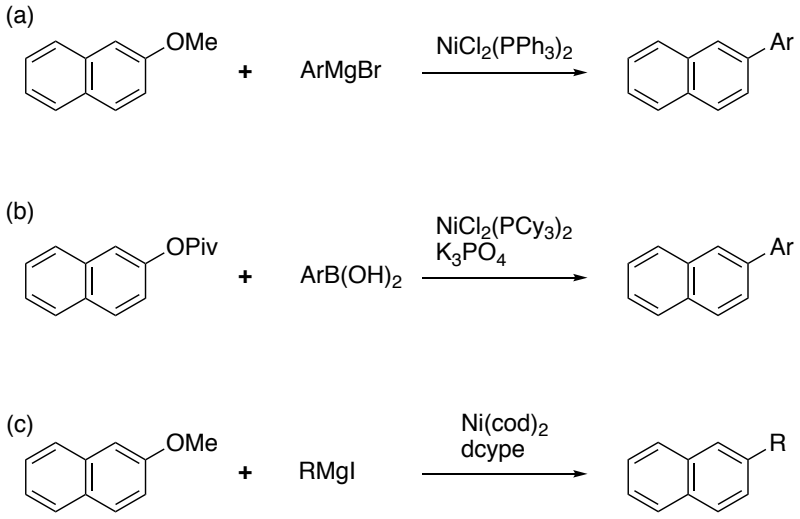

Scheme 1-1. Cross-coupling reactions of phenol derivatives.

1-2. Nitrogen containing PAHs (aza-PAHs)

Introduction of heteroatoms into PAHs backbones substantially alters their electronic nature and imparts novel functions derived from introduced heteroatoms.[15] Nitrogen is an attractive element to introduce to π-conjugated systems because of (1) the larger electron negativity than carbon, (2) the existence of a lone pair, and (3) the similar van der Waals radius to that of carbon. Consequently, incorporation of nitrogen atoms into PAHs renders the electron-deficient nature, coordination ability, and nucleophilicity without significant change of the structure of the parent PAHs.

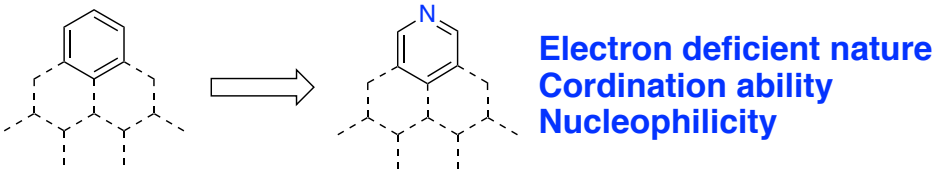

Figure 1-4. Nitrogen containing PAHs.

Scheme 1-2 shows examples of the synthetic method for aza-PAHs. Intramolecular Vilismeier reaction of biaryl compounds with amide moiety is one of the basic method to provide quinoline-annulated PAHs (Scheme 1-2a).[16] The condensation of *o*-quinone derivatives with aromatic diamines effectively affords the corresponding pyrazine-annulated acenes (Scheme 1-2b).[17] The reductive aromatization reaction of imide compounds is known as one of the synthetic method for pyridine with acetyl groups.[18] In this reaction, acetyl groups can be introduced by the reaction with acetic anhydride after constructing the pyridine skeleton (Scheme 1-2c).[18]

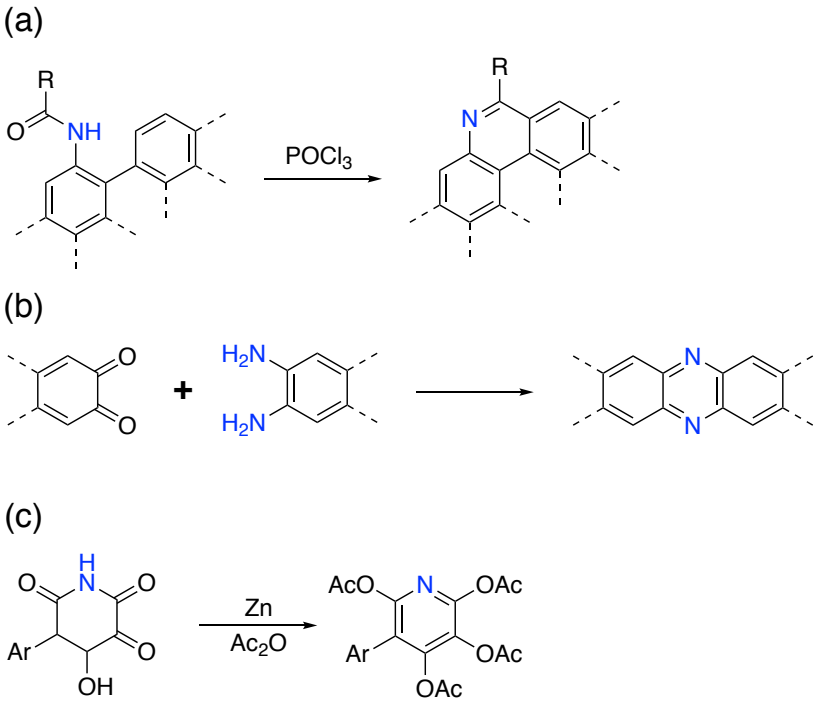

Scheme 1-2. (a) A synthetic method for quinoline annulated PAHs. (b) A synthetic method for pyradine annulated acene compounds. (c) A synthetic method for peripherally functionalized pyridine.

Peripheral modification is also a useful method for tuning the electronic nature of aza-PAHs. On the other hand, the modifications on nitrogen atoms such as the coordination to the metal or quaternarization using the lone pair of nitrogen atoms in aza-PAHs are efficient methods to modify the photophysical and electronic properties of π-conjugated systems. Coordination of Lewis basic nitrogen atoms of *N*-PAH with Lewis acidic boron center is effective method for reducing the LUMO level of the coordinated *N*-PAH. Consequently, B–N units are often employed in the molecular design toward organic n-type semiconductor. Dou, Dong, and Liu *et al*. reported the synthesis of dibenzooctaacene containing four B–N units via one pot multifold boron complexation on the dibenzotetraazaoctacene with four amino groups (Scheme 1-3). This boron complex exhibits low LUMO level as low as –4.58 eV which facilitates the efficient electron injection. Furthermore, the boron complex shows high electron mobility up to 1.60 $cm^2\ V^{-1}\ s^{-1}$.[19]

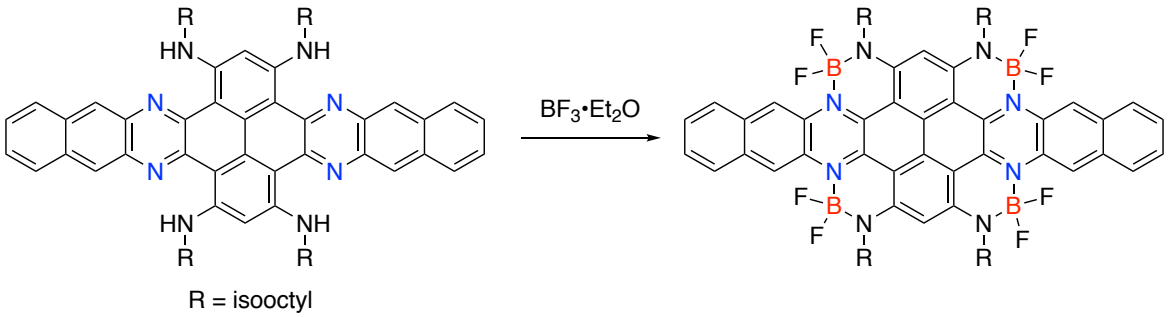

Scheme 1-3. Boron complexation of the azaacene compound.

Intramolecular B–N bond formation is also used to lock the two aromatic rings configurationally. Wakamiya and Yamaguchi *et al*. synthesized the boron complex of thienyl thiazole (scheme 1-4). The intramolecular B–N bond formation constrained the thiophene and thiazole moieties in s-*cis* conformation. In addition, the coordination bond locked the π-conjugated skeleton in planar with dihedral angle of 7.4°.[20]

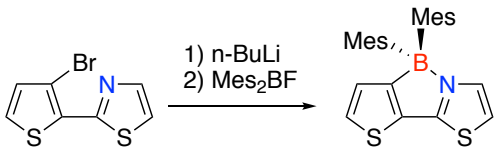

Scheme 1-4. Boron complexation of thienyl thiazole.

Quaternarization of imine-type nitrogen atoms is an efficient method to lower the LUMO level of the aza-PAHs reflecting their cationic nature. Consequently, PAHs with cationic nitrogen are often used as electron receptor and components of charge-transfer complexes. The simple synthetic method to create cationic nitrogen is the alkylation of peripheral imine-type nitrogen atoms of PAHs. For instance, Fukuzumi and Lemmetyinen *et al*. reported that 9-mesityl-10-methylacridinium ion which has an electron-donating mesityl group and an electron-accepting methylacridinium unit afforded the electron-transfer state with long lifetime upon photoirradiation (Scheme 1-5).[21]

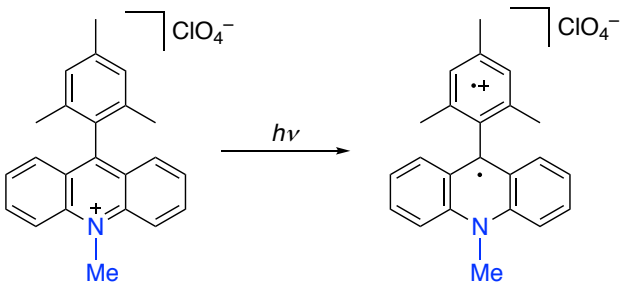

Scheme 1-5. Irradiation of 9-mesityl-10-methylacridinium salt.

N,N'-Dialkylated 4,4'-bipyridyls have been employed as components of supramolecular structures such as catenanes or rotaxanes using donor acceptor interaction. In 1989, Stoddart *et al*. reported the synthesis of

[2]catenane using donor–acceptor interaction between *N,N′*-dialkylated 4,4'-bipyridyls and 1,4-dialkoxybenzene as a template.[22] The structure was clearly determined by X-ray analysis (Figure 1-5). Each 4,4'-bipyridyl and 1,4-dialkoxybenzene unit exists at the center of each ring with the distance between the π-planes of *ca*. 3.5 Å.

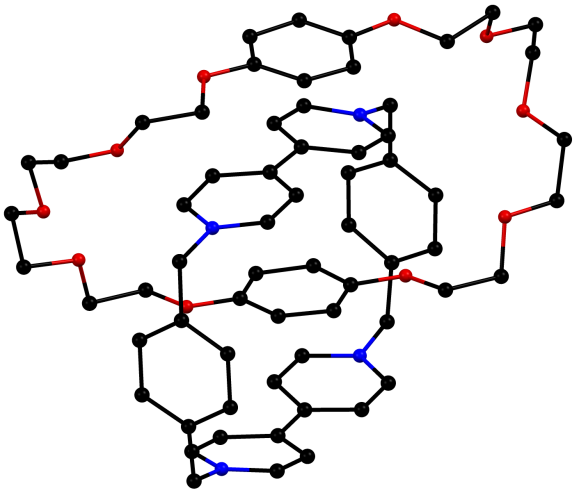

Figure 1-5. Crystal structure of the [2]catenane. Hydrogen atoms and counterions are omitted for clarity.

1-3. Pyrenes

Pyrene is a well-studied PAH. Pyrene has excellent optical properties such as high fluorescence efficiency and efficient excimer emission. Pyrene derivatives are promising candidates for organic materials. For instance, as described in the earlier part of this chapter, pyrene derivatives with four aryl groups on 1,3,6, and 8-positions were developed as the emitter for OLEDs.[11] Receptor-introduced pyrene can be used as a chemical sensor using excimer emission caused by the association with guest molecules such as heavy metals.[23] Recently, pyrenes have also been developed as organic semiconductors. The thiophene derivative of pyrene exhibits decent hole mobility of 2.1 cm^{-2} V^{-1} S^{-1}.[24]

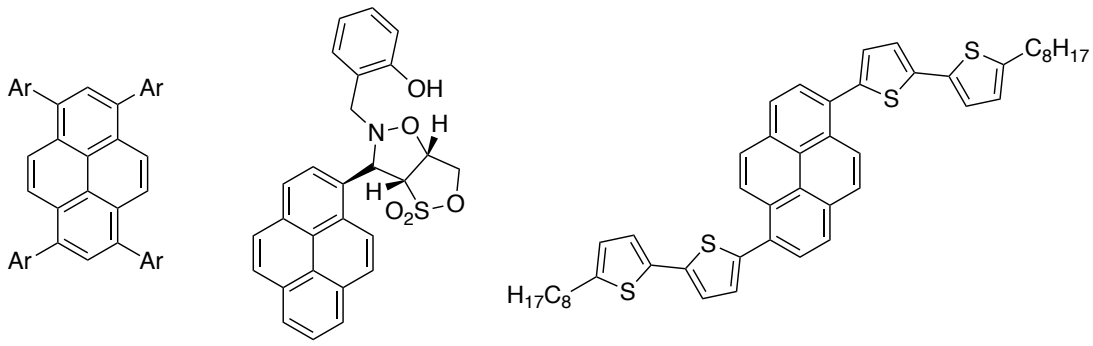

Emitter **Chemical sensor** **Organic semiconductor**

Figure 1-6. Applications of pyrene derivatives.

These successful studies on pyrene are due to not only excellent optical properties of pyrene and its derivatives but also the established peripheral modification methods for pyrene. In particular, 1,3,6,8-positions are functionalized via various cross-coupling reactions followed by the regioselective bromination reaction.[25] Accordingly, pyrene derivatives with various substituents on 1,3,6,8-positions have been synthesized and investigated.

1-4. Back ground of 2,7-diazapyrenes

As the author mentioned in previous section, pyrene has excellent optical properties. The incorporation of nitrogen atoms to pyrene skeleton is expected to impart the electron deficient nature, coordination ability, and nucleophilicity. Consequently, various types of nitrogen containing pyrenes have been synthesized and characterized. 2,7-Diazapyrene is regarded as not only nitrogen analogous to pyrene but also π-extended 4,4'-bipyridine. Thus 2,7-diazapyrene and its derivatives are expected to exhibit optical properties derived from pyrene skeleton and electron deficient nature, coordination ability and reactivity derived from 4,4'-bipyridine skeleton.

The first synthesis of a parent 2,7-diazapyrene was achieved in 1968 via dehydrogenation of [2.2]-(3,5)-pyridinophane (Scheme 1-6a).[26] In 2000, Sotiriou-Leventis *et al*. developed the efficient synthetic method for the parent 2,7-diazapyrene via oxidative aromatization followed by reduction of carbonyl groups of naphthalene diimide (Scheme 1-6b).[27] Peripheral functionalization of 2,7-diazapyrene with siloxy groups was achieved by Sachidev (Scheme 1-6c).[28]

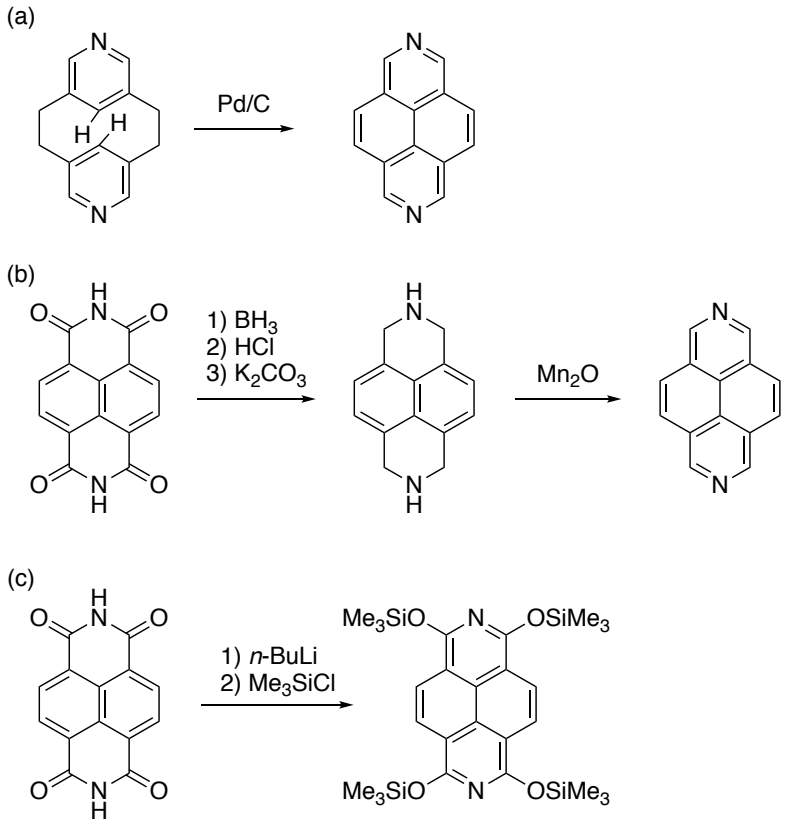

Scheme 1-6. Synthetic methods for 2,7-diazapyrenes.

Similar to pyrene, modification of the peripheral area should be important for exploring functions of 2,7-diazapyrenes. However, unfortunately, peripheral functionalization of the parent 2,7-diazapyrene has not been achieved. This is because the poor solubility of the parent 2,7-diazapyrene hinder the introduction of substituents into the peripheral area of the diazapyrene skeleton. Although the diazapyrene with siloxy groups has been synthesized, the siloxy groups cannot be used as a leaving group for cross-coupling reactions because they are easily hydrolyzed.

1-5. Overview of this thesis

Reductive aromatization shown in Scheme 1-2c is an effective method to synthesize peripherally substituted pyridines. The author envisaged that application of the reductive aromatization to naphthalene diimide should provide 2,7-diazapyrene with leaving groups on 1,3,6 and 8-positions which are used as synthetic intermediates capable of synthesizing various derivatives. This thesis describes the novel synthetic methods for peripherally functionalized 2,7-diazapyrenes and the investigation of 2,7-diazapyrene derivative. In chapter 2 and chapter 3, the author attempted to establish efficient synthetic methods for aryl- and alkyl-introduced 2,7-diazapyrenes at the peripheral positions, respectively. In chapter 2, the synthesis of tetraaryl-2,7-diazapyrenes is discussed. Reductive aromatization of naphthalene diimide with pivalic anhydride as an electrophile afforded 2,7-diazapyrene with pivaloxy groups. Introduced pivaloxy groups were available for transformation to other aryl groups via cross-coupling reactions with arylboronic acids. In

chapter 3, the author discloses the synthesis of tetraalkyl-2,7-diazapyrenes. 2,7-Diazapyrene having methoxy groups was synthesized by reductive aromatization as the synthetic intermediate of tetraalkyl-2,7-diazapyrenes. Subsequent cross-coupling reactions with alkyl Grignard reagents afforded tetraalkyl-2,7-diazapyrenes. In chapter 4 and chapter 5, the functionalization on nitrogen atoms of 2,7-diazapyrenes was explored. In chapter 4, synthesis of 2,7-diazapyrene boron complex are discussed. Boron complexation of 2,7-diazapyrene with *o*-hydroxyphenyl groups afforded corresponding boron-diazapyrene complex of syn-form and anti-form respectively. The author disclosed that anti-form quantitatively isomerizes to the syn-form under heating conditions, and that the syn-form forms a dimer in solution and solid. In chapter 5, synthesis of *N*,*N*′-dimethyl-2,7-diazapyrenium dications with peripheral aryl groups and two-electron reduction of them are discussed. Dimethyldiazapyrenes exhibited significantly low-lying LUMO level reflecting their dicationic nature. Furthermore, two-electron reduced *N*,*N*′-dimethyl-2,7-diazapyrenium dications showed antiaromatic character derived from peripheral 16π electron conjugation.

1-6. References

1. Faraday, M. On new compounds of carbon and hydrogen, and on certain other products obtained during the decomposition of oil by heat. *Phil. Trans. R. Soc. Lond.* 1825, **115**, 440–466.

2. Taylor, R. D.; MacCoss, M.; MacCoss, Lawson, A. D. G.; *J. Med. Chem.* **2014**, *57*, 5845–5859.

3. (a) Harvey, R. G. Polycyclic Aromatic Hydrocarbons, Wiley-VCH, Weinheim, 1997; (b) Müllen, K.; Wegner, G. Electronic Materials: The Oligomer Approach, Wiley-VCH, Weinheim, 1998; (c) Carbon-Rich Compounds, ed. Haley, M. M.; Tykwinski, R. R. Wiley-VCH, Weinheim, 2006; (d) Functional Organic Materials, ed. Muller, T. J. J.; Bunz, U. H. F. Wiley-VCH, Weinheim, 2007.

4. (a) Scholl, R.: Seer, C.: Weitzenböck, R.: *Chem. Ber.* **1910**, *43*, 2202-2209. (b) Scholl, R.; Seer, C. *Leibigs. Ann. Chem.* **1912**, *394*, 111-123. (c) Clar, E.; D. Stewart, G. *J. Am. Chem. Soc.* **1953**, *75*, 2667-2672. (d) Clar, E.; Schmidt, W. *Tetrahedron* **1979**, *35*, 2673-2680.

5. (a) Herwig, P.; Kayser, C. W.; Müllen, K.; Spiess, H. W. *Adv. Mater*. **1996**, *8*, 510-513. (b) Ito, H.; Ozaki, K. Itami, K. *Angew. Chem. Int. Ed*. **2017**, *56*, 11144-11164.

6. (a) Akamatsu, H.; Inokuchi, H.; Matsunaga, Y. *Nature* **1954**, *173*, 168-169. (b) Sano, M.; Akamatu, H. *Bull. Chem. Soc. Jpn.* **1961**, *39*, 1569-1571.

7. (a) Jarikov, V. V. *J. Appl. Phys*. **2006**, *100*, 014901. (b) Anthony, J. E. *Chem. Rev*. **2006**, *106*, 5028-5048. (c) Mi, B. X.; Gao, Z. Q.; Lee, C. S.; Lee, S. T.; Kwong, H. L.; Wong, N. B. *Appl. Phys. Lett*. **1999**, *75*, 4055-4057; (d) Jiang, X. Y.; Zhang, Z. L.; Zheng, X. Y.; Wu, Y. Z.; Xu, S. H. *Thin Solid Films* **2001**, *401*, 251-254.

8. (a) Klauk, H.; Halik, M.; Zschieschang, U.; Eder, F.; Schmid, G.; Dehm, C.; *App. Phys. Lett*. **2003**, *82*, 4175-4177. (b) Zhang, L.; Fonari, A.; Liu, Y.; Hoyt, A.-L. M.; Lee, H.; Granger, D.; Parkin, S.; Russell, T. P.; Anthony, J. E.; Brédas, J. -L.; Coropceanu, V.; Briseno, A. L.; *J. Am. Chem. Soc.* **2014**, *136*, 9248-9251.

9. (a) Yo, S.; Domercq, B.; Kippelen, B. *Appl. Phys. Lett*. **2004**, *85*, 5427-5429. (b) Sakai, J.; Taima, T.; Yamanari, T.; Yoshida, Y.; Fujii, A.; Ozaki, M.; *Jpn. J. Appl. Phys*. **2010**, *49*, 032301-1.

10. (a) Aimono, T.; Kawamura, Y.; Goushi, K.; Yamamoto, H.; Sasabe, H.; Adachi, C. *Appl. Phys. Lett.* **2005**, *86*, 071110. (b) Sandanayaka, A. S. D.; Matsushima, T.; Bencheikh, F.; Yoshida, K.; Inoue, M.; Fujihara, T.; Goushi, K.; Ribierre, J. -C.; Adachi C. *Sci. Adv.* **2017**, *3*, e1602570. (c) Sandanayaka, A. S. D.; Matsushima, T.; Bencheikh,F.; Terakawa, S.; Potscavage, W. J.; Qin, C.; Fujihara, T.; Goushi, K.; Ribierre, J. -C.; Adachi, C.; *Appl. Phys. Express* **2019**, *12*, 1-6. (d) Jiang, Y.; Liu, Y.-Y.; Liu, X.; Lin, H.; Gao, K.; Lai, W. -Y. *Chem. Soc. Rev.* **2020**, *49*, 5885-5944.

11. Assaad, T. H. E.; Auer, M.; Castaneda, R.; Hallal, K. M.; Jradi, F. M.; Mosca, L.; Khnayzer, R. S.; Patra, D.; Timofeeva, T. V.; Bredas, J. L.; Kratochvil, E. J. W. L.; Wex, B.; Kaafarani, B. R.; *J. Mater. Chem., C* **2016**, *4*, 3041-3058.

12. (a) Struijk, C. W.; Sieval, A. B.; Dakhorst, J. E. J.; van Dijk, M.; Kimkes, P.; Koehorst, R. B. M.; Donker, H.; Schaafsma, T. J.; Picken, S. J.; van de Craats, A. M.; Warman, J. M.; Zuilhof, H.; Sudhölter, E. J.; *J. Am. Chem. Soc*. **2000**, *122*, 11057-11066. (b) Gregg, B. A.; Cormier, R. A.; *J. Am. Chem. Soc*. **2001**, *123*, 7959-7960. (c) Wang, C.; Dong, H.; Hu, W.; Liu, Y.; Zhu, D.; *Chem. Rev.* **2012**, *112*, 2208-2267. (d) Würthner, F.; Saha-Möller, C. R.; Fimmel, B.; Ogi, S.; Leowanawat, P.; Schmidt, D. *Chem. Rev*. **2016**, *116*, 962-1052.

13. (a) Lin, Y. Y.; Gundlach, D. J.; Nelson, S.; Jackson, T. N.; *IEEE Trans. Electron Devices* **1997**, 44, 1325-1331. (b) Kelley, T. W.; Muyres, D. V.; Baude, P. F.; Smith, T. P.; Jones, T. D. *Mater. Res. Soc. Symp. Proc*. **2003**, *771*, L6.5.1.

14. Anthony, J. E.; Brooks, J. S.; Eaton, D. L.; Parkin, S. R. *J. Am. Chem. Soc*. **2001**, *123*, 9482-9483.

15. Stępień, M.; Gońka, E.; Żyła, M.; Sprutta, N. *Chem. Rev*. **2017**, *117*, 3479-3716.

16. Bischler, A.; Napieralski, B. *Ber. Dtsch. Chem. Ges*. **1893**, *26*, 1903-1908.

17. Miao, S.; S. Brombosz, M.; Schleyer, P. V. R.; Wu, J. I.; Barlow, S.; Marder, S. R.; Hardcastle, K. I.; Bunz, U. H. F.; *J. Am. Chem. Soc*. **2008**, *130*, 7339-7344.

18. Poschenrieder, H.; Stachel, H. -D.; Wiesend, B.; Polborn, K. J. *Heterocyclic Chem.* **2003**, *40*, 61-69.

19. Min, Y.; Dou, C.; Liu, D.; Dong, H.; Liu, J. *J. Am. Chem. Soc*. **2019**, *141*, 17015-17021.

20. Wakamiya, A.; Taniguchi, T.; Yamaguchi, S.; *Angew. Chem. Int. Ed*. **2006**, *45*, 3170-3173.

21. Fukuzumi, S.; Kotani, H.; Ohkubo, K.; Ogo, S.; Tkachenko, N. V.; Lemmetyinen, H.; *J. Am. Chem. Soc*. **2004**, *126*, 1600-1601.

22. Ashton, R.; Goodnow, T. T.; Kaijer, A. E.; Reddington, M. I.; Slawin, A. M. Z.; Spencer, N.; Stoddart, J. F.; Vicent, C.; Williams, D. J.; *Angew. Chem. Int. Ed. Engl*. **1989**, *28*, 1396-1399.

23. (a) B.; Bodenant, F.; Fages, M. H.; Delville, *J. Am. Chem. Soc*. **1998**, *120*, 7511-7519. (b) B.; Valeur, I.; Leray, *Coord. Chem. Rev*. **2000**, *205*, 3-40. (b) Yang, R. H.; Chan, W. H.; Lee, A. W. M.; Xia, P. E.; Zhang, H. K.; Li, K. A. *J. Am. Chem. Soc.* **2003**, *125*, 2884-2885. (c) Strauss, J.; Daub, J. *Org. Lett*. **2002**, *4*, 683-686.

24. Cho, H.; Lee, S.; N. Cho, S.; Jabbour, G. E.; Kwak, J.; Hwang, D. -H.; Lee, C. *ACS Appl. Mater. Interfaces* **2013**, *5***,** 3855-3860.

25. Kathayat, R. S.; Finney, N. S.; *J. Am. Chem. Soc*. **2013**, *135*, 12612-12614. (b) Heng, W. Hu, Y.; J.; Yip, J. H. K. *Organometallics* **2007**, *26*, 6760-6768. (c) K.; Thakur, D.; Wang, S.; Mirzaei, R.; Rathore *Chem.- Eur. J*. **2020**, *26*, 14085-14089.

26. Jenny, W.; Holtzrichter, H. *Chimia* **1968**, *22*, 247.

27. Sotiriou-Leventis, C.; Mao, Z. J. *Heterocyclic Chem*. **2000**, *37*, 1665-1667.

28. Sachdev, H. Patent: EP2 390 253 A1, November 30, 2011.

Chapter 2.

Synthesis of tetraaryl-2,7-diazapyrenes via reductive aromatization of naphthalene diimide

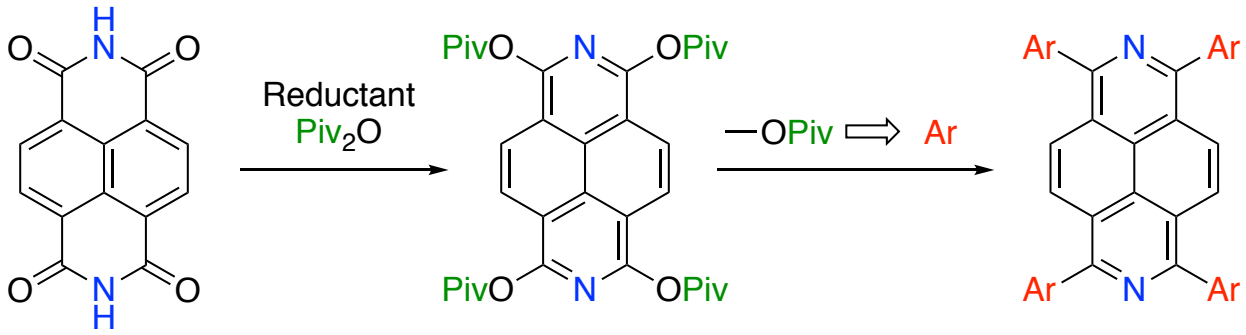

Contents

2-1. Introduction

Nitrogen-doped PAHs are promising candidates for organic materials such as n-type semiconductors due to their electron-deficient nature and stimuli responsive materials derived from the reactivity of nitrogen atoms.[1-5] 2,7-Diazapyrenes are attractive molecules because they should show electron affinity and Brønsted basicity due to nitrogen atoms with excellent optical properties of pyrene. However peripheral functionalization has not been achieved because of the lack of efficient synthetic methods of 2,7-diazapyrenes. In this chapter, the author discloses the reductive aromatization of naphthalene diimide. The reductive aromatization of naphthalene diimide provides a 2,7-diazapyrene with leaving groups on 1,3,6, and 8 positions, which serves as a synthetic intermediate for the synthesis of a versatile 2,7-diazapyrenes.

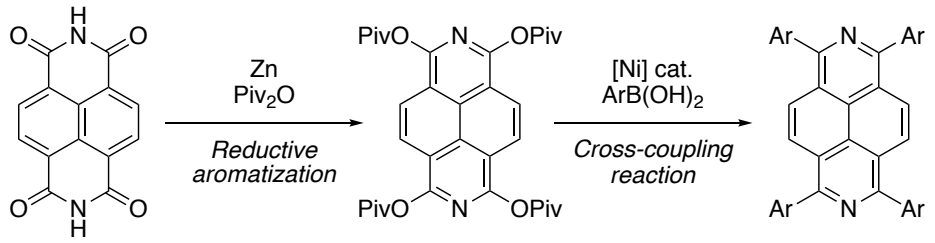

Scheme 2-1. Synthetic strategy for peripherally functionalized 2,7-diazapyrenes via reductive aromatization of naphthalene diimide.

2-2. Synthesis of peripherally functionalized 2,7-diazapyrenes

Scheme 2-2 shows the synthesis of 2,7-diazapyrene with pivaloxy groups. Treatment of naphthalene diimide with 16 equiv of zinc powder and 16 equiv of pivalic anhydride (Piv_2O) provided pivaloxydiazapyrene (**2-1**) in 85% yield. Ni-catalyzed cross-coupling reactions successfully transformed the introduced pivaloxy groups into various aryl groups.[7]

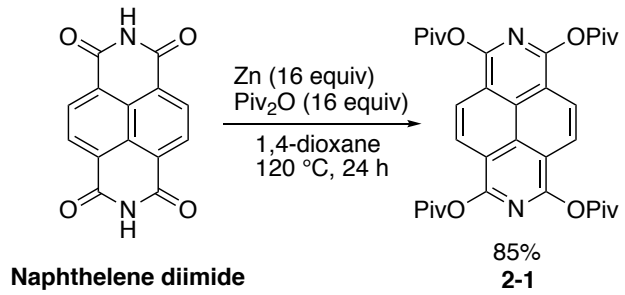

Scheme 2-2. Reductive aromatization of naphthalene diimide.

The synthetic route to diazapyrenes **2-2a-f** is shown in Scheme 2-3. The reaction of **2-1** with 4-*tert*-butylphenylboronic acid in the presence of $Ni(cod)_2$ (cod: 1,5-cyclooctadiene), tricyclohexylphosphine (PCy_3), and K_3PO_4 in toluene at 60 °C for 18 h afforded the corresponding diazapyrene (**2-2a**) in 59% yield. A variety of arylboronic acids were applicable to this reaction system, and **2-2b-f** were obtained in moderate yields.

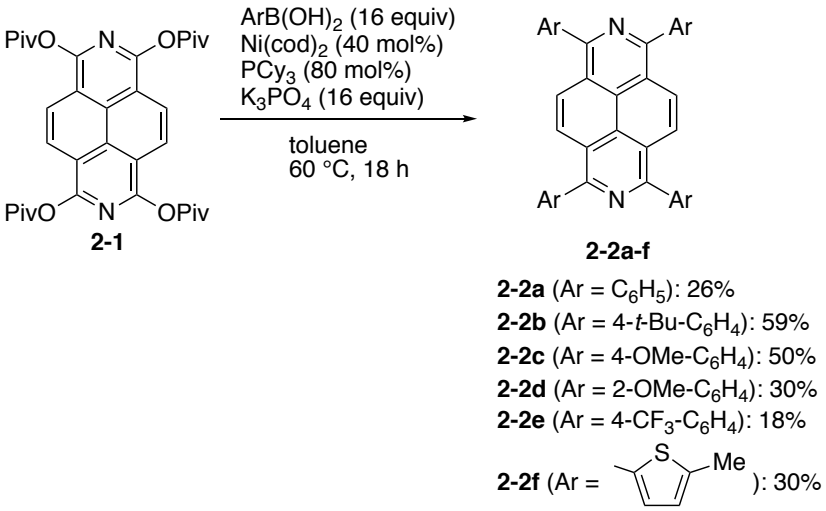

Scheme 2-3. Cross-coupling reactions of **2-1**.

Unfortunately, attempts to use alkylboronic acids for the introduction of alkyl groups were not successful. However, **2-3** was prepared in 77% yield from the desulfurization of the thiophene rings of **2-2f** with Raney nickel (Scheme 2-4).

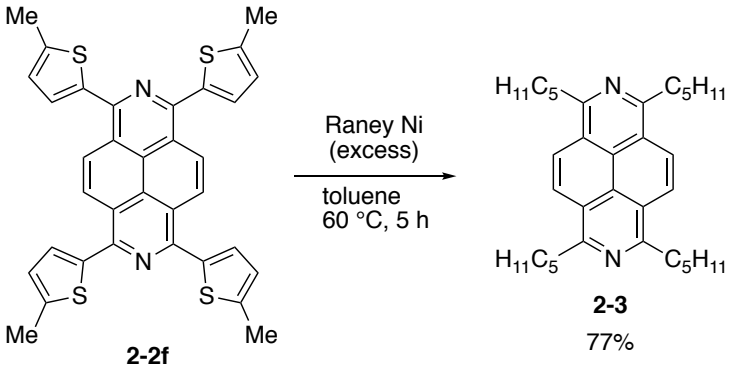

Scheme 2-4. Desulfurization of **2-2f** into **2-3**.

2-3. Structural analyses

X-ray diffraction analyses clearly revealed the molecular structures of **2-2a**, **2-2f**, and **2-3**. The MPD value of the diazapyrene core in **2-2a** is 0.079 Å, which indicates that diazapyrene core adopts the highly planar conformation of the diazapyrene core (Figure 2-1a). The dihedral angles (~32–33°) between the pyri-

dine rings and peripheral 4-*tert*-butylphenyl groups of **2-2a** are smaller than those corresponding pyrene (51–55°). This result clearly shows that the replacement of the C–H moieties at the 2 and 7 positions in pyrene with nitrogen atoms reduces the steric repulsion between the central core and the peripheral aryl groups. Diazapyrene **2-2f** (mean plane deviation: 0.056 Å) also has a planar core and the dihedral angles (~15-18°) between the pyridine moiety and thiophene rings in **2-2f** are smaller than those of **2-2a** (Figure 2-1a and d). These dihedral angles in **2-2a** and **2-2f** clearly show the presence of π-conjugation through the tetraaryl diazapyrenes. The packing structure of **2-3** is different from those of **2-2a** and **2-2f** (Figure 2-1h and i). While π-stacking between the diazapyrene cores was not observed for molecules of **2-2a** and **2-2f**, those of **2-3** are stacked in a face-to-face manner with an interplanar distance of 3.406 Å.

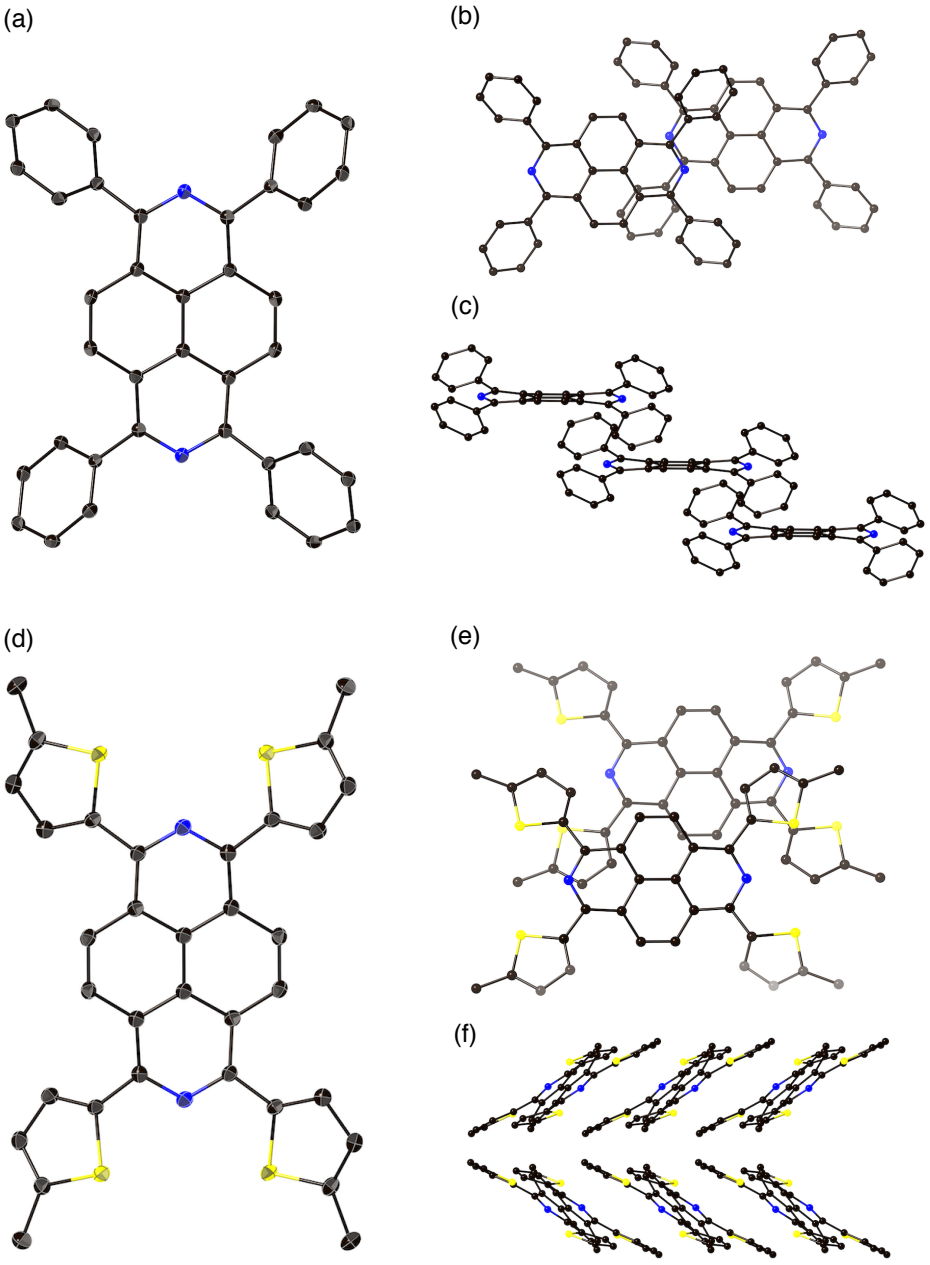

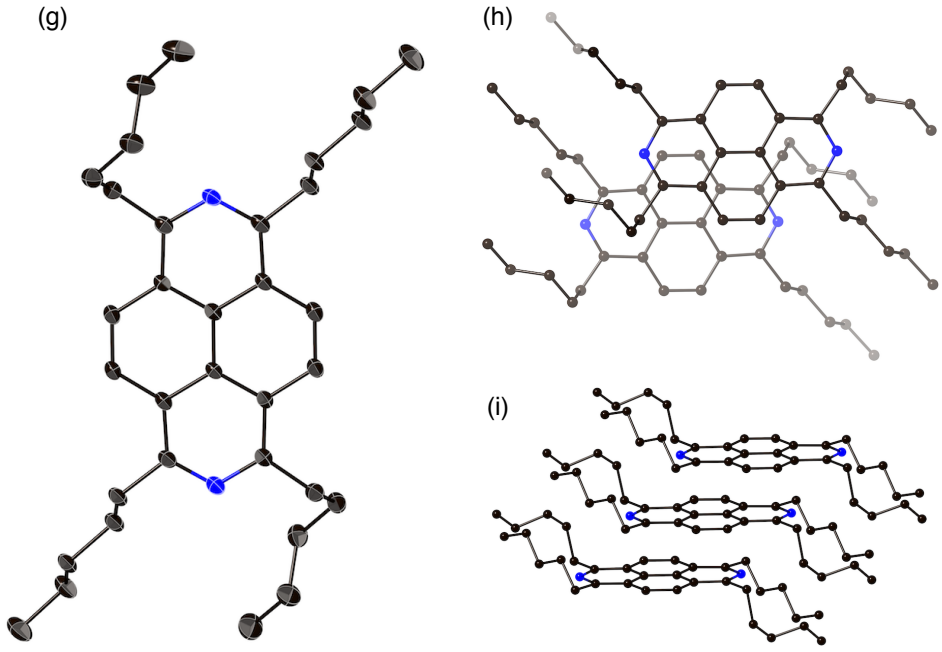

Figure 2-1. Molecular structures of **2-2a**, **2-2f**, and **2-3**. (a) Top view, (b) top view of the packing, and (c) side view of the packing of **2-2a**. (d) Top view, (e) top view of the packing, and (f) side view of the packing of **2-2f**. (g) Top view, (h) top view of the packing, and (i) side view of the packing of **2-3**. Hydrogen atoms are omitted for clarity. Thermal ellipsoids are set to 50% probability.

2-4. Optical properties

Figure 2-2a exhibits the UV-vis absorption spectra of **2-2a-f** and **2-3** in CH_2Cl_2. The longest-wavelength absorption bands of aryl groups introduced 2,7-diazapyrenes exhibit a bathochromic shift compared to that of **2-3**, suggesting an efficient π-conjugation between aryl groups on the peripheral area and the diazapyrene skeleton. In CH_2Cl_2, diazapyrenes **2-2a-f** and **2-3** exhibit fluorescence (Φ = 0.13~0.47) spectra (Figure 2-2b).

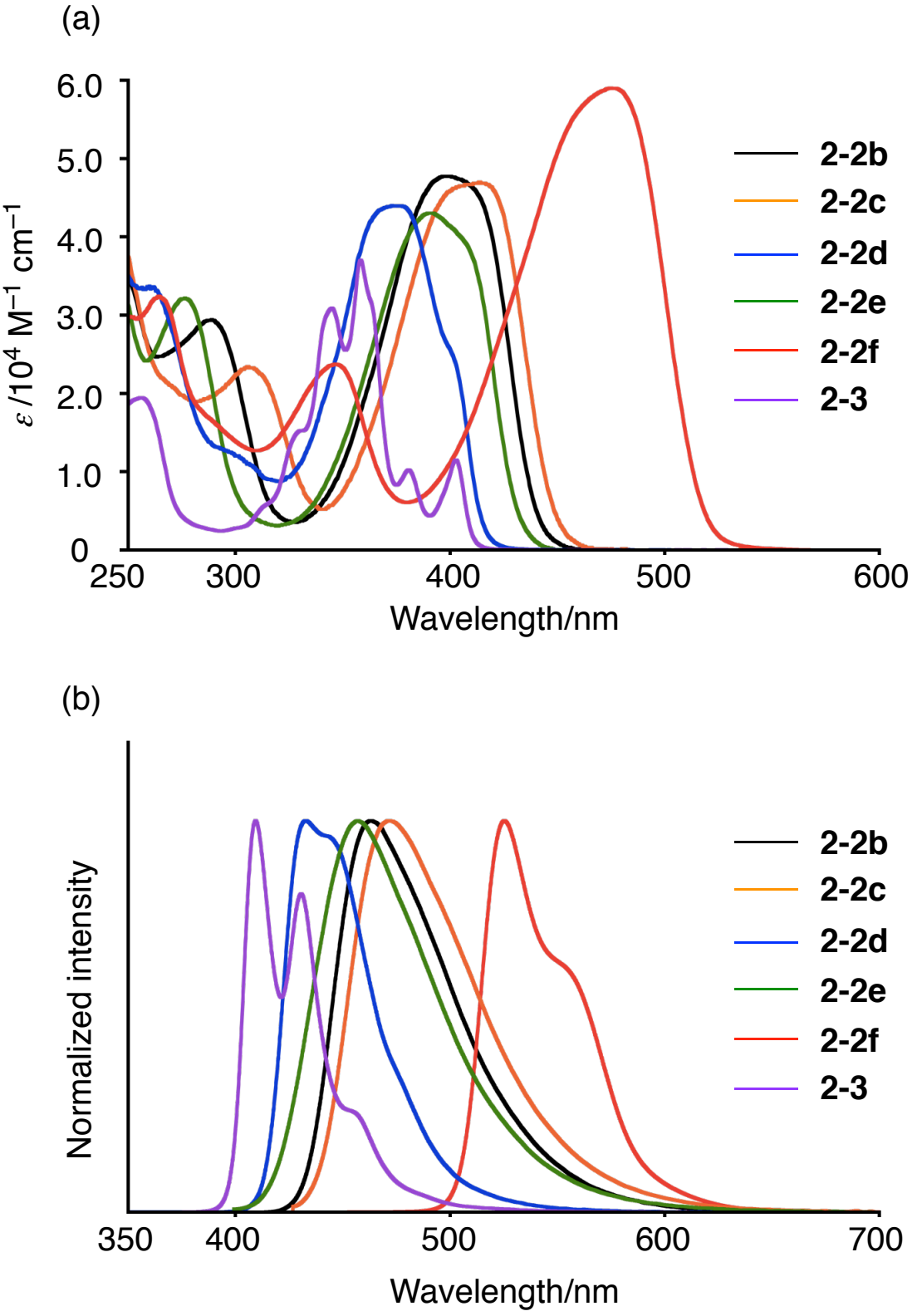

Figure 2-2. (a) UV-vis absorption spectra of **2-2b-f** and **2-3** in CH_2Cl_2. (b) Emission spectra of **2-2b-f** and **2-3** in CH_2Cl_2.

Table 2-1. Excited wavelengths and absolute fluorescence quantum yields of **2-2b**-**f** and **2-3** in CH_2Cl_2.

Compound	λ_{ex} (nm)	Φ (in CH_2Cl_2)
2-2b	380	0.38
2-2c	380	0.36
2-2d	380	0.46
2-2e	380	0.32
2-2f	400	0.13
2-3	340	0.47

2-5. Protonation behavior

To investigate the potential of **2-3** to serve as an acid-responsive material, protonation experiments of **2-3** in CH_2Cl_2 were performed (Figure 2-3). The addition of trifluoroacetic acid (TFA) to a CH_2Cl_2 solution of **2-3** resulted to appear a new absorption band at 427 nm (Figure 2-3a). The observation of isosbestic points supports the direct transformation of **2-3** into the monoprotonated species **A** (Figure 2-3e). After 2.5 equiv of TFA had been added, the absorption band bathochromically shifted to 444 nm as shown in Figure 2-3b. For the sake of comparison, the author prepared the diprotonated compound **2-4** (OTs = *p*-toluenesulfonate), which exhibited a similar absorption band at 441 nm (Figure 2-4); this result confirms that the absorption band at 444 nm in Figure 2-3b originates from the diprotonated species B. Similar changes were also observed in the fluorescence spectra of 1g upon protonation (Figure 2-3c and d). On the basis of these titration experiments, the equilibrium constant of the first step was estimated to be 270000, and the second step was estimated to be 1200 from the absorption spectrum.

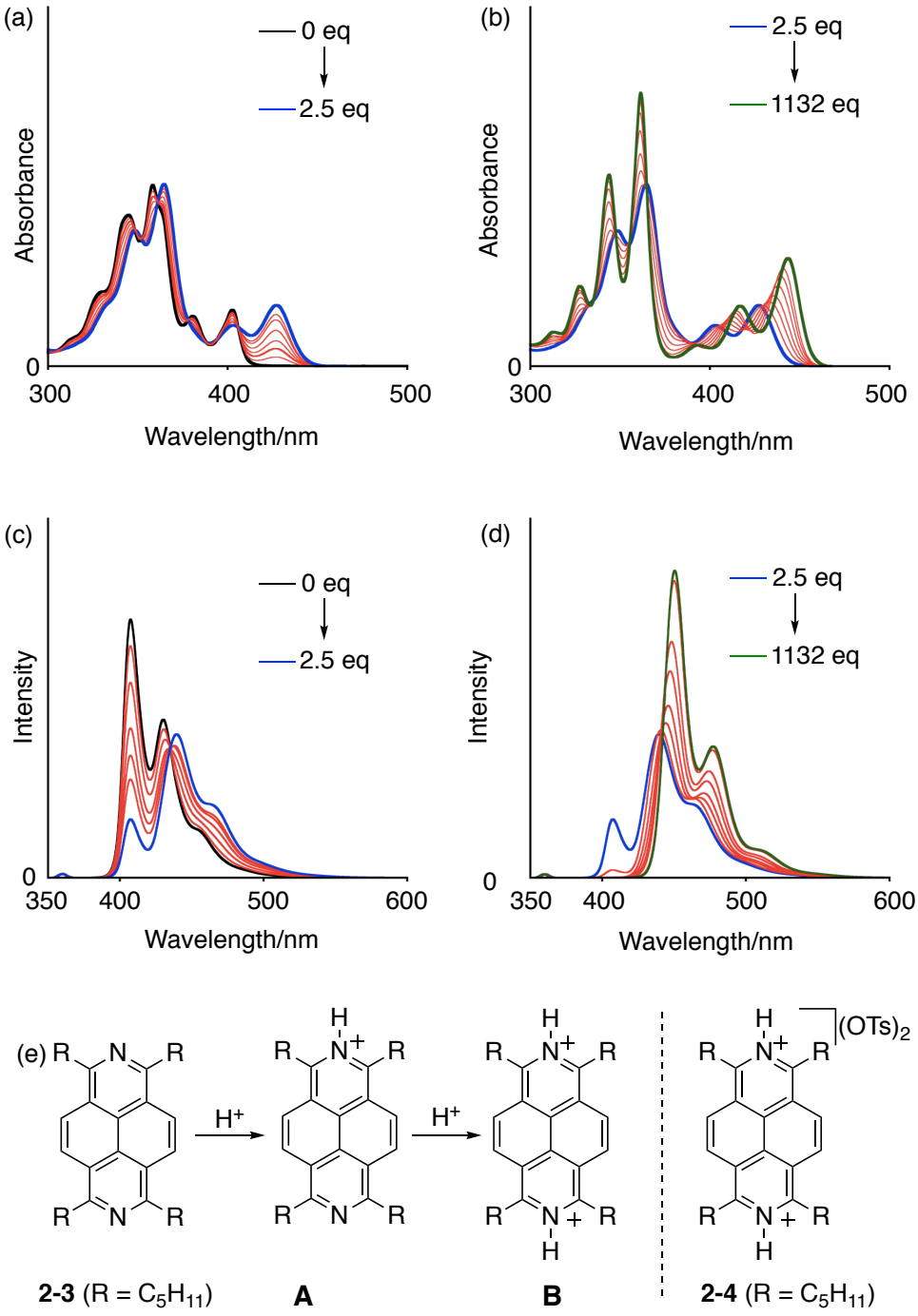

Figure 2-3. Spectral changes in the absorption spectra of **2-3** in CH_2Cl_2 (2.7×10^{-5} M) upon addition of TFA (a) (0–2.5 equiv) and (b) (2.5–1132 equiv). Spectral changes in the fluorescence spectra of **2-3** in CH_2Cl_2 (2.7×10^{-6} M) upon addition of TFA (c) (0–2.5 equiv) and (d) (2.5–1132 equiv). (e) Stepwise protonation of **2-3**.

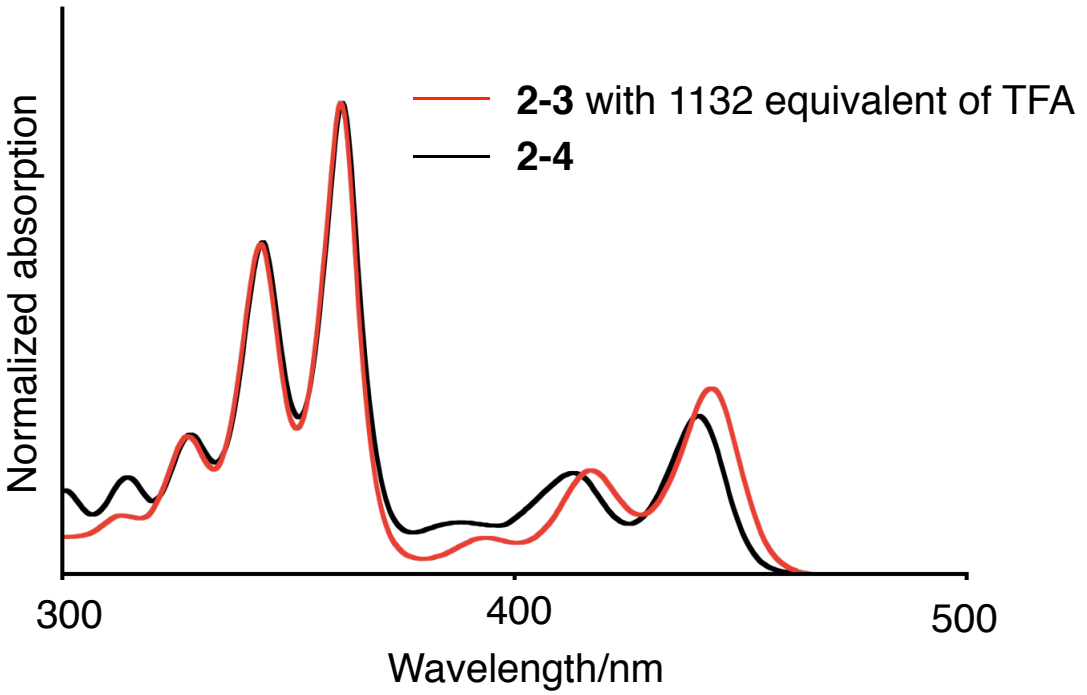

Figure 2-4. Absorption spectra of **2-4** and **2-3** with 1132 equivalent of TFA.

2-6. Cyclic voltammetry

Figure 2-5 shows results of cyclic voltammetry measurement in **2-3** and **2-5**. Diazapyrene **2-3** exhibits one reversible reduction potential (2.56 V; vs. Fc/Fc^{+}), while a reduction peak was not observed for pyrene **2-5** up to 3.0 V, supporting the notion that the LUMO level of **2-3** is lower than that in **2-5**.

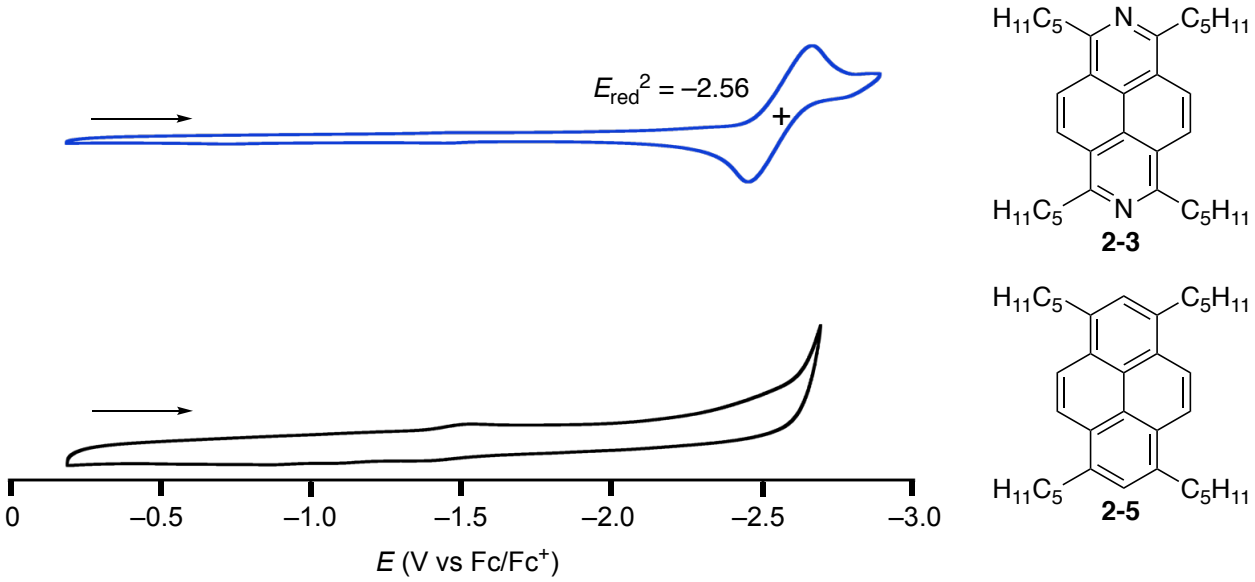

Figure 2-5. Cyclic voltammogram of **2-3** and **2-5** in THF.

2-7. Electron mobility

The electron mobility of **2-3** was measured using FI-TRMC measurements.[8] Using FI-TRMC, the intrinsic carrier mobility at semiconductor-insulator interfaces was evaluated by monitoring microwaves reflected by a simple metal-insulator-semiconductor (MIS) device that contains the target semiconductor materials. Here, a hexane solution of **2-3** was spin-coated onto poly(methyl methacrylate)/SiO_2 layers to form a thin film, and gold electrodes were deposited to inject charge carriers. A powder X-ray diffraction analysis revealed that **2-3** exhibits a lamellar periodicity of 14.4 Å (Figure 2-6), suggesting that the 2,7-diazapyrene cores form 2D π-electron layers parallel to the substrate. Upon applying a gate bias to the MIS devices, current flows were observed (Figure 2-7), indicating that the injection of electrons into the **2-3** layer and the reflected microwave power changed simultaneously (Figure 2-8). The number of charge carriers (N_e) was calculated from the integration of the flow current, while the pseudoconductivity ($N_e\mu_e$) was estimated from the reflected microwave power.[8a] The N_e and $N_e\mu_e$ values were plotted as a function of the gate bias, and the slope of the resulting plots describes the electron mobility (Figure 2-9a). For **2-3**, a value of μ_e = 0.6 cm^2 V^{-1} s^{-1} (electron mobility) was estimated. In sharp contrast, pyrene **2-5** showed little microwave response for both holes and electrons, i.e., the mobilities were below the instrument detection limit (< 0.1 cm^2 V^{-1} s^{-1}) (Figure 2-9b and 2-10). This is due to the 2D alignment of 2,7-diazapyrene cores in parallel with the semiconductor-insulator interfaces which is advantageous to suppress thermal breakdown of in-plane electron conductive pathways. This clear contrast suggests that nitrogen-doping PAHs dramatically alters their electronic properties, inducing e.g. electron mobility in the solid state. It should be noted that the devices were prepared by spin-coating from a non-halogenated solvent, the use of which has not been demonstrated for common n-type materials such as arylene diimides.

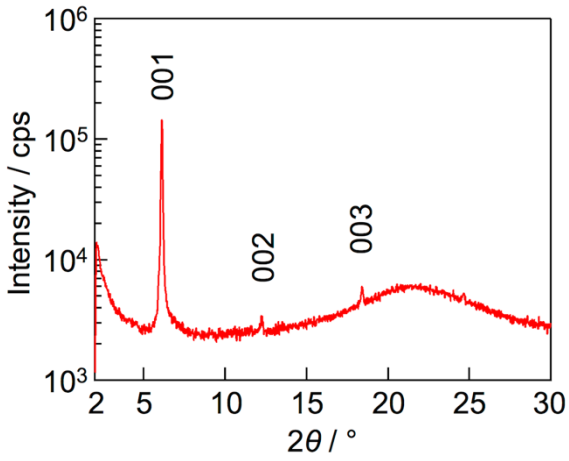

Figure 2-6. X-ray diffraction patterns of **2-3**-based MIS device used in FI-TRMC measurements. The estimated d values from the three peaks were d001 = 14.4 Å, d_{002} = 7.2 Å, and d_{003} = 4.8 Å.

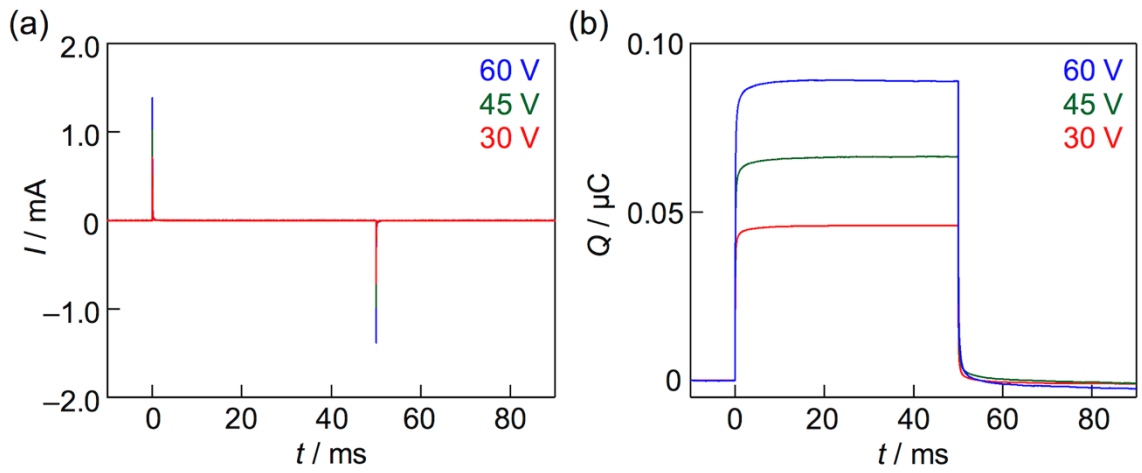

Figure 2-7. (a) Flowed electric current plot against the time in **2-3**-based MIS device by injecting electrons. (b) An number of accumulated charges plotted against the time by electron injection to the time in **2-3**-based device. The charge amount was calculated from integration of the value of flowed current.

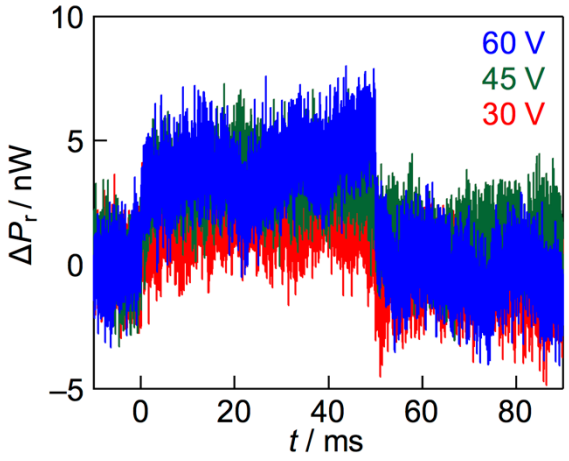

Figure 2-8. The change in reflected microwave power by electron injection plotted against the time in **2-3**-based MIS device.

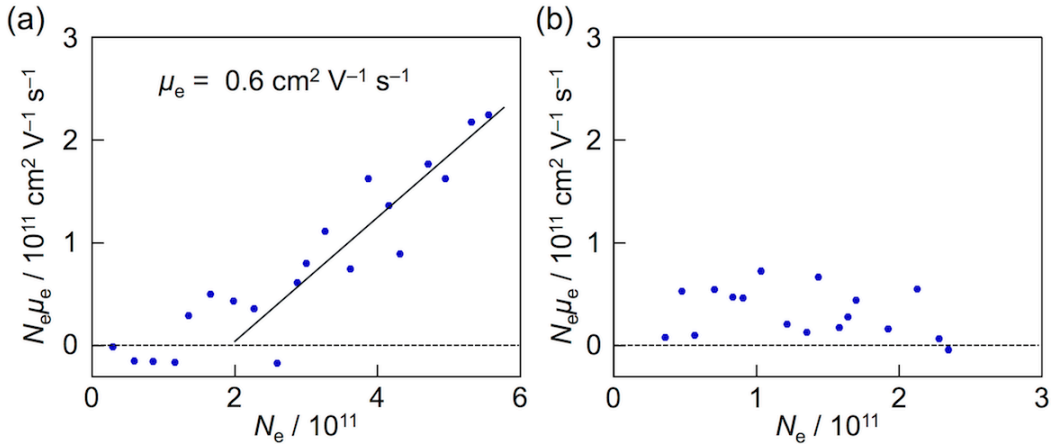

Figure 2-9. Tthe pseudo-electrical conductivity ($N\mu$) plotted against the amount of injected electrons (N) in MIS devices using (a) **2-3** and (b) **2-5**.

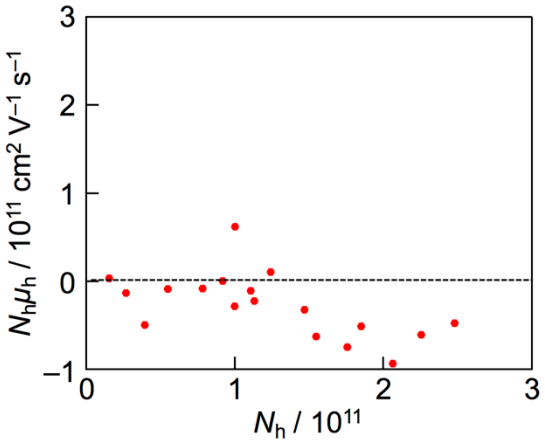

Figure 2-10. The pseudo-electrical conductivity ($N_h\mu_h$) plotted against the amount (N_h) of injected holes in **2-5**-based MIS device.

2-8. Summary of Chapter 2

In summary, a novel protocol for the synthesis of various 2,7-diazapyrenes was accomplished on the basis of a combination of a reductive aromatization of naphthalene diimide and Ni-catalyzed cross-coupling reactions. 2,7-Diazapyrene with pentyl groups **2-3** exhibited acid-responsive changes in the absorption and fluorescence spectra. The electrochemical studies of **2-3** confirmed that the electronegativity of the nitrogen atoms lowers the LUMO level. Furthermore, FI-TRMC measurements clearly demonstrated a higher electron mobility for **2-3** compared to pyrene, suggesting that diazapyrenes **2** should be promising n-type organic semiconductors.

2-9. Refenences

1. (a) Tonzola, C. J.; Alam, M. M.; Kaminsky, W.; Jenekhe, S. A. *J. Am. Chem. Soc.* **2003**, *125*, 13548-13558. (b) Winkler, M.; Houk, N. K.; *J. Am. Chem. Soc.* **2007**, *129*, 1805-1815. (c) Lakshminarayana, A. N.; Ong, A.; Chi, C.; *J. Mater. Chem. C* **2018**, *6*, 3551-3563.

2. (a) Lemaur, V.; da Silva Filho, D. A.; Coropceanu, V.; Lehmann, M.; Geerts, Y.; Piris, J.; Debije, M. G.; van de Craats, A. M.; Senthilkumar, K.; Siebbeles, L. D. A.; Warman, J. M.; Brédas, J.-L.; Cornil, J. *J. Am. Chem. Soc.* **2004**, *126*, 3271-3279. (b) Kaafarani, B. R.; Kondo, T.; Yu, J.; Zhang, Q.; Dattilo, D.; Risko, C.; Jones, S. C.; Barlow, S.; Domercq, B.; Amy, F.; Kahn, A.; Brédas, J.-L.; Kippelen, B.; Marder, S. R. *J. Am. Chem. Soc.* **2005**, *127*, 16358-16359.

3. Martens, S. C.; Zschieschang, U.; Wadepohl, H.; Klauk, H.; Gade, L. H. *Chem. Eur. J.* **2012**, *18*, 3498-3509.

4. a) Li, Y.; Li, Y.; Li, J.; Li, C.; Liu, X.; Yuan, M.; Liu, H.; Wang, S. *Chem. Eur. J.* **2006**, *12*, 8378-8385. (b) He, B.; Dai, J.; Zherebetskyy, D.; Chen, T. L.; Zhang, B. A.; Teat, S. J.; Zhang, Q.; Wang, L.; Liu, Y. A. *Chem. Sci.* **2015**, *6*, 3180-3186. (c) Hattori, Y.; Kimura, S.; Kusamoto, T.; Maeda, H.; Nishihara, H. *Chem.Commun.* **2018**, *54*, 615-618. (d) Hisaki, I.; Suzuki, Y.; Gomez, E.; Ji, Q.; Tohnai, N.; Nakamura, T.; Douhal, A. *J. Am. Chem. Soc*. **2019**, *141*, 2111−2121.

5. (a) Würthner, F.; Sautter, A.; Thalacker, C. *Angew. Chem., Int. Ed.* **2000**, *39*, 1243-1245. (b) Sautter, A.; Thalacker, C.; Würthner, F. *Angew. Chem., Int. Ed.* **2001**, *40*, 4425-4428. (c) Sautter, A.; Schmid, D. G.; Jung, G.; Würthner, F. *J. Am. Chem. Soc.* **2001**, *123*, 5424-5430. (d) Würthner, F.; Sautter, A.; Schilling, J. *J. Org. Chem.* **2002**, *67*, 3037-3044.

6. Poschenrieder, H.; Stachel, H. -D.; Wiesend, B.; Polborn, K. J. *Heterocyclic Chem.* **2003**, *40*, 61-69.

7. Quasdorf, K. W.; Tian, X.; Garg, N. K. *J. Am. Chem. Soc.* **2008**, *130*, 14422-14423.

8. (a) Honsho, Y.; Miyakai, T.; Sakurai, T.; Saeki, A.; Seki, S. *Sci. Rep.* **2013**, *3*, 3182. (b) Tsutsui, Y.; Schweicher, G.; Chattopadhyay, B.; Sakurai, T.; Arlin, J.-B.; Ruzié, C.; Aliev, A.; Ciesielski, A.; Colella, S.; Kennedy, A. R.; Lemaur, V.; Olivier, Y.; Hadji, R.; Sanguinet, L.; Castet, F.; Osella, S.; Dudenko, D.; Beljonne, D.; Cornil, J.; Samorì, P.; Seki, S.; Geerts, Y. H.; *Adv. Mater*. **2016**, *28*, 7106-7114. (c) Inoue, J.; Tsutsui, Y.; Choi, W.; Kubota, K.; Sakurai, T.; Seki, S.; *ACS Omega* **2017**, *2*, 164-170.

9.

Chapter 3.

Synthesis and crystal packing structures of tetraalkyl-2,7-diazapyrenes

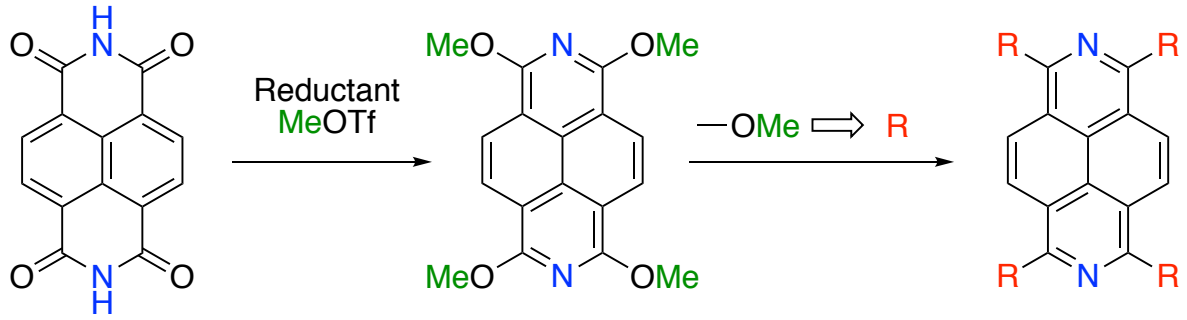

Contents

3-1. Introduction

In Chapter 2, it was described that 2,7-diazapyrene with pentyl groups exhibits the moderate the electron mobility. This result suggests tetraalkyl-2,7-diazapyrenes are promising candidates for n-type semiconductor. To investigate the potential of 2,7-diazapyrenes for electron transporting materials, their arrangement in the solid state should be engineered by the proper peripheral alkyl groups.[1] However, the desulfurization strategy is not straightforward route for the synthesis of 2,7-diazapyrenes with various alkyl groups. Furthermore, this method only provides 2,7-diazapyrenes with alkyl groups longer than a butyl group (Scheme 2-4).

To overcome the shortcomings, a more efficient method for the introduction of various alkyl groups at the peripheral position of 2,7-diazapyrenes is desirable. This Chapter discloses the reductive aromatization of naphthalene diimide into 1,3,6,8-tetramethoxy-2,7-diazapyrene **3-1** (Scheme 3-1). Furthermore, the transformation of the methoxy groups to alkyl groups via cross-coupling reaction with alkyl Grignard reagents is described.[2-4]

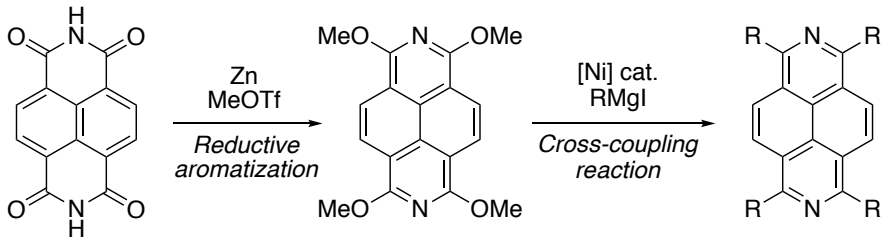

Scheme 3-1. Synthetic strategy for tetraalkyl-2,7-diazapyrenes via reductive aromatization of naphthalene diimide and cross-coupling reaction.

3-2. Synthesis of tetraalkyl-2,7-diazapyrenes

Scheme 3-2 shows the synthetic procedure of 2,7-diazadiazapyrene with methoxy groups **3-1**. The reaction of naphthalene diimide with 6 equiv of methyl triflate (MeOTf) in the presence of 16 equiv of zinc powder provided tetramethoxy-2,7-diazapyrene (**3-1**) in 41% yield.

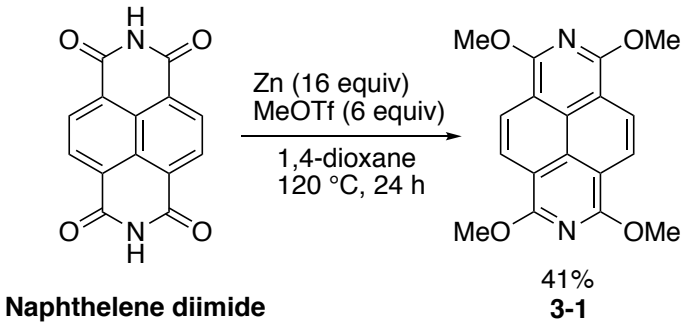

Scheme 3-2. Reductive aromatization of naphthalene diimide with methyl triflate.

The methoxy groups in **3-1** were readily converted to various alkyl groups through the cross-coupling reaction with alkyl Grignard reagents to provide tetraalkyl-2,7-diazapyrenes **3-2a-c**.[3e] Treatment of **3-1** with methylmagnesium iodide, catalytic amounts of $Ni(cod)_2$ (cod: 1,5-cyclooctadiene) and bis(dicyclohexylphosphino)ethane (dcype) afforded tetramethyldiazapyrene (**3-2a**) in 37% yield. The use of ethyl and propyl Grignard reagents furnished tetraethyldiazapyrene (**3-2b**) and tetrapropyldiazapyrene (**3-2c**) in 16% and 12% yields, respectively.

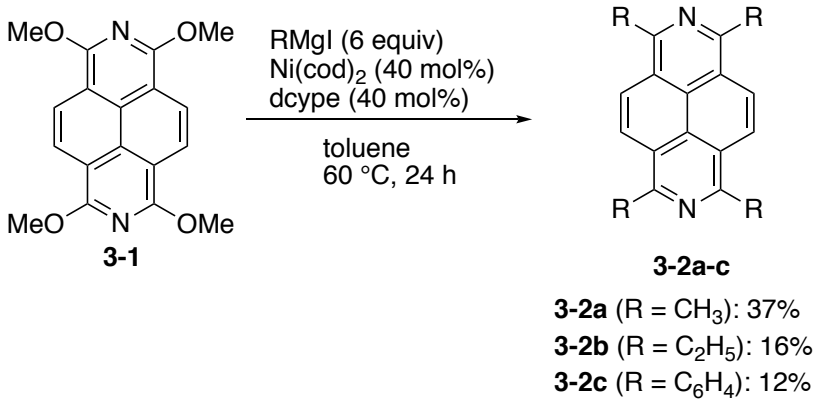

Scheme 3-3. Cross-coupling reaction of **3-1**.

3-3. Structural analyses

X-ray analysis successfully revealed structures of **3-1**, **3-2a**, and **3-2b** (Figure 3-1). The diazapyrene core in **3-1**, **3-2a**, and **3-2b** adopts highly planar conformation. Each molecule of **3-2b** adopts the slipped stacking formation in packing structure. The distance between π-planes is 3.364 Å (Figure 3-1h, i). This packing structure is similar to that of **2-3**. In sharp contrast, **3-2a** forms face-to-face stacking in the crystal with an interplanar distance of 3.385 Å (Figure 3-1e, f). A brickwork packing structure was observed in **3-1** (Figure 3-1b, c). The distance between π-planes in **3-1** (3.448 Å) is longer than those of **3-2a** and **3-2b** having alkyl groups. It is noteworthy that such small differences in peripheral substituents dramatically changed the morphology of the solid state.

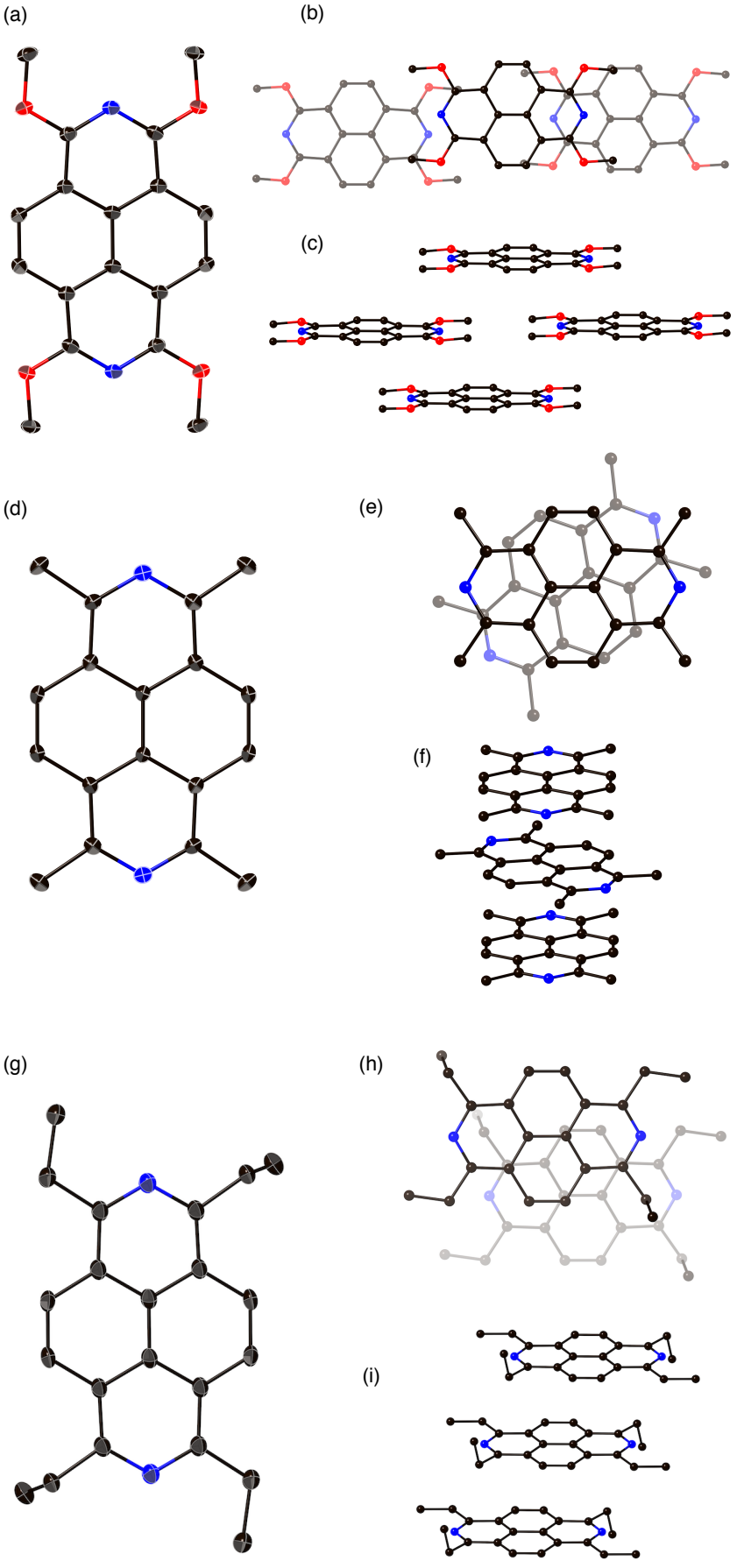
(a)
(b)
(c)
(d)
(e)
(f)
(g)
(h)
(i)

Figure 3-1. Molecular structures of **3-1**, **3-2a**, and **3-2b**. (a) Top view, (b) top view of the packing, and (c) side view of the packing of **3-1**. (d) Top view, (e) top view of the packing, and (f) side view of the packing of **3-2a**. (g) Top view, (h) top view of the packing, and (i) side view of the packing of **3-2b**.

3-4. Optical properties

Figure 3-2a shows electronic absorption spectra of **3-1** and **3-2a-c** in CH_2Cl_2. While the change of the alkyl groups did not alter the absorption spectra of tetraalkyldiazapyrene **3-2a-c**, bathochromic shift was observed in tetramethoxydiazapyrene **3-1**. Diazapyrenes **3-1** and **3-2a-c** show fluorescence (Φ = 0.28–0.49) in CH_2Cl_2. In accordance with the absorption spectra, the emission band of **3-1** also bathochromically shifted compared to **3-2a-c** (Figure 3-2b).

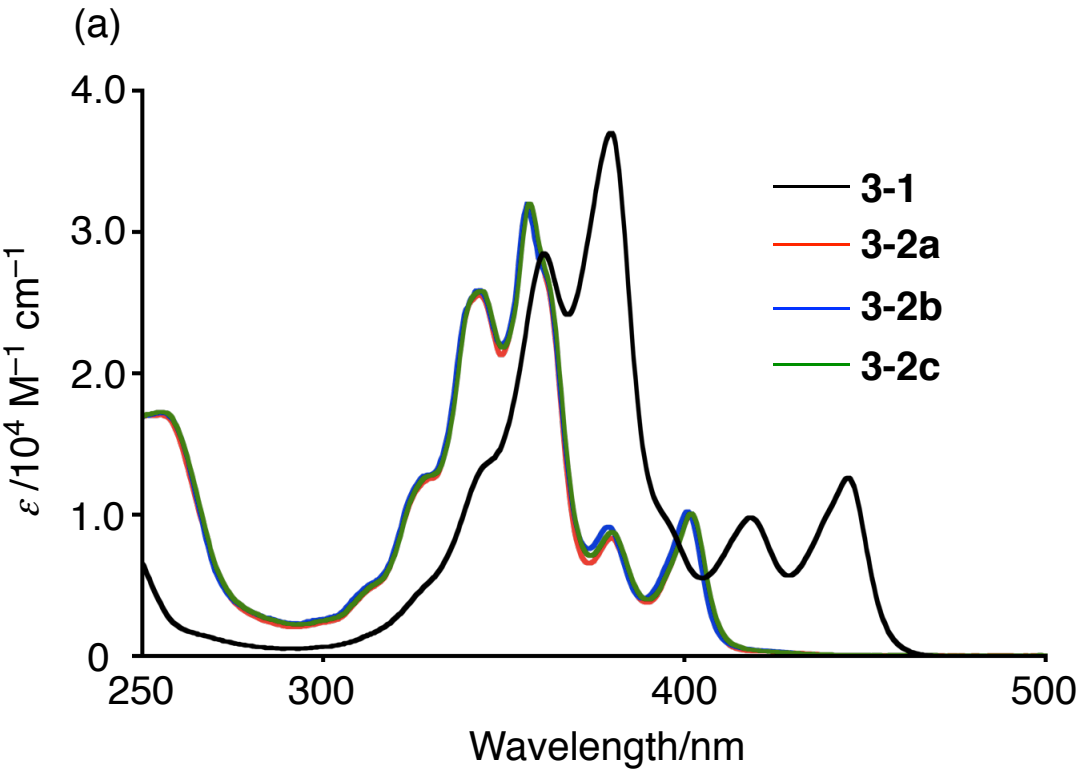

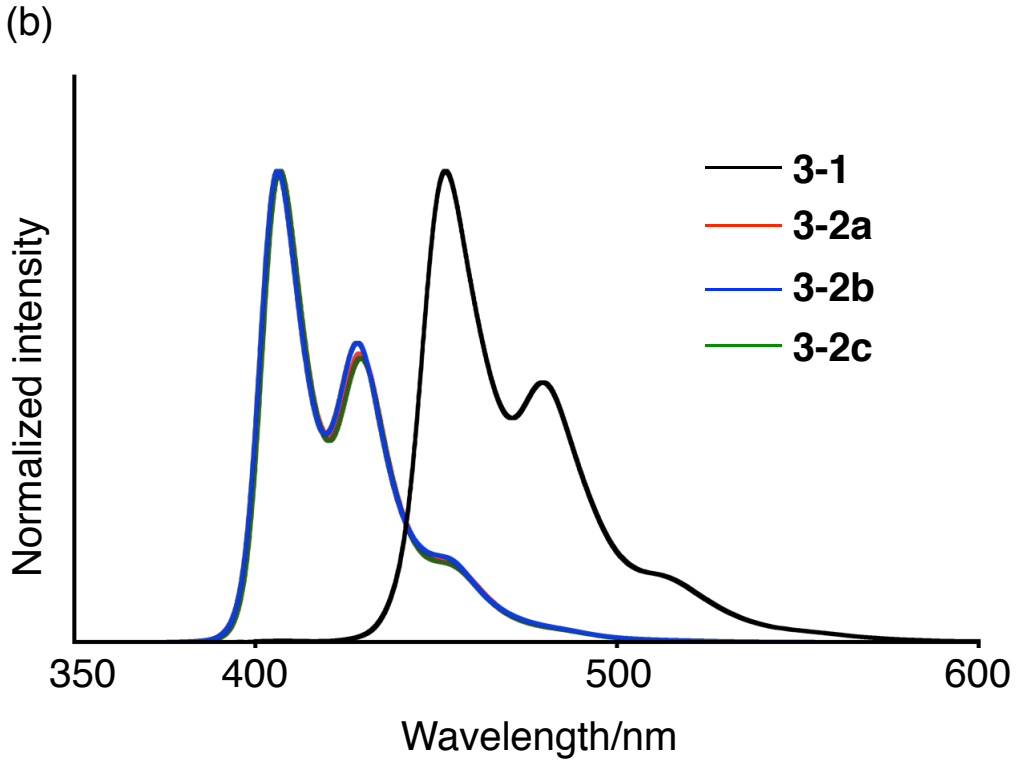

Figure 3-2. (a) Electronic absorption spectra of **3-1** and **3-2a-c** in CH_2Cl_2. (b) Emission spectra of **3-1** and **3-2a-c** in CH_2Cl_2.

Table 2-1. Excited wavelengths and absolute fluorescence quantum yields of **3-1** and **3-2a-c** in CH_2Cl_2.

Compound	λ_{ex} (nm)	Φ (in CH_2Cl_2)
3-1	400	0.28
3-2a	380	0.48
3-2b	380	0.41
3-2c	380	0.49

As the concentration increased, a new emission band was observed around 500 nm in **3-2a** (Figure 3-3a).[5] The emission lifetime measured at 425 nm in a dilute solution was 6.5 ns, while the lifetime measured at 500 nm in a concentrated solution was 26 ns. These results clearly suggest that the newly observed emission was the excimer emission. Interestingly, the stronger excimer emission of **3-2a** was observed than that of **2-3** which has longer alkyl groups (Figure 3-3d). This result clearly indicates that peripheral substituents affect the ease of the formation of excimer.[5]

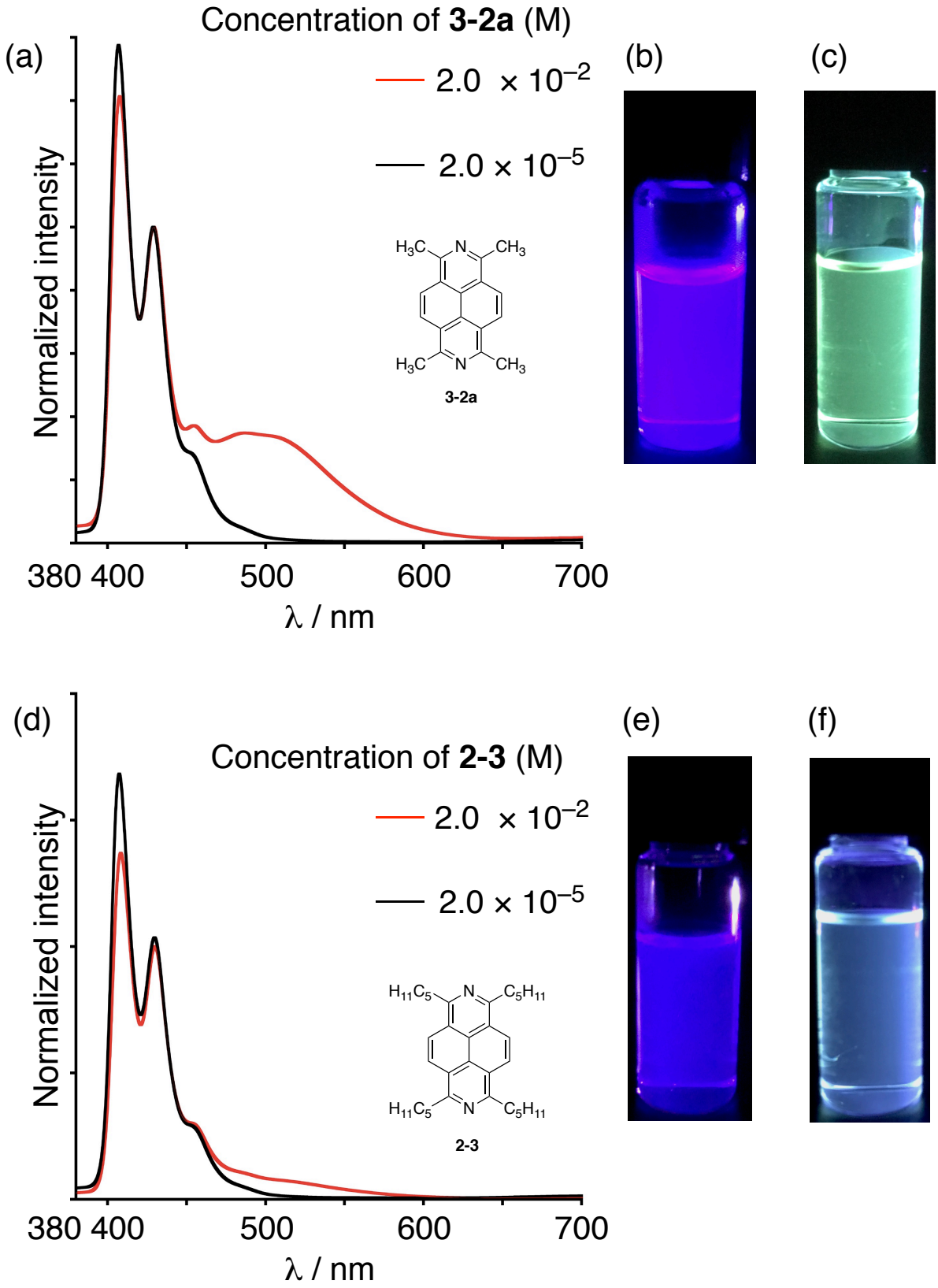

Figure 3-3. (a) Emission spectra of **3-2a** in CH_2Cl_2. Photo images of **3-2a** in CH_2Cl_2 (2.0×10^{-5} M) under excitation (λ_{ex} = 360 nm) at (b) 2.0×10^{-5} M and (c) 2.0×10^{-2} M. (d) Emission spectra of **2-3** in CH_2Cl_2. Photo images of **2-3** in CH_2Cl_2 under excitation (λ_{ex} = 360 nm) at (e) 2.0×10^{-5} M and (f) 2.0×10^{-2}

M. Triangular fluorescence cell (T-81 TOSOH QUARTS) was used for the measurement of the excimer emission.

Figure 3-4.

3-5. Electrochemical properties

The reduction potentials of **3-1** and **3-2a-c** were evaluated with cyclic voltammetry and differential-pulse voltammetry (Figure. 3-4). Diazapyrene **3-2a** exhibits one reversible reduction potential (–2.58 V; vs $[Fc]/[Fc]^+$), which is similar to those of **3-2b** and **3-2c**. While no reduction wave was observed in **3-1** up to –3.0 V. These results suggest that the introduction of methoxy groups to the diazapyrene core raises the LUMO level.

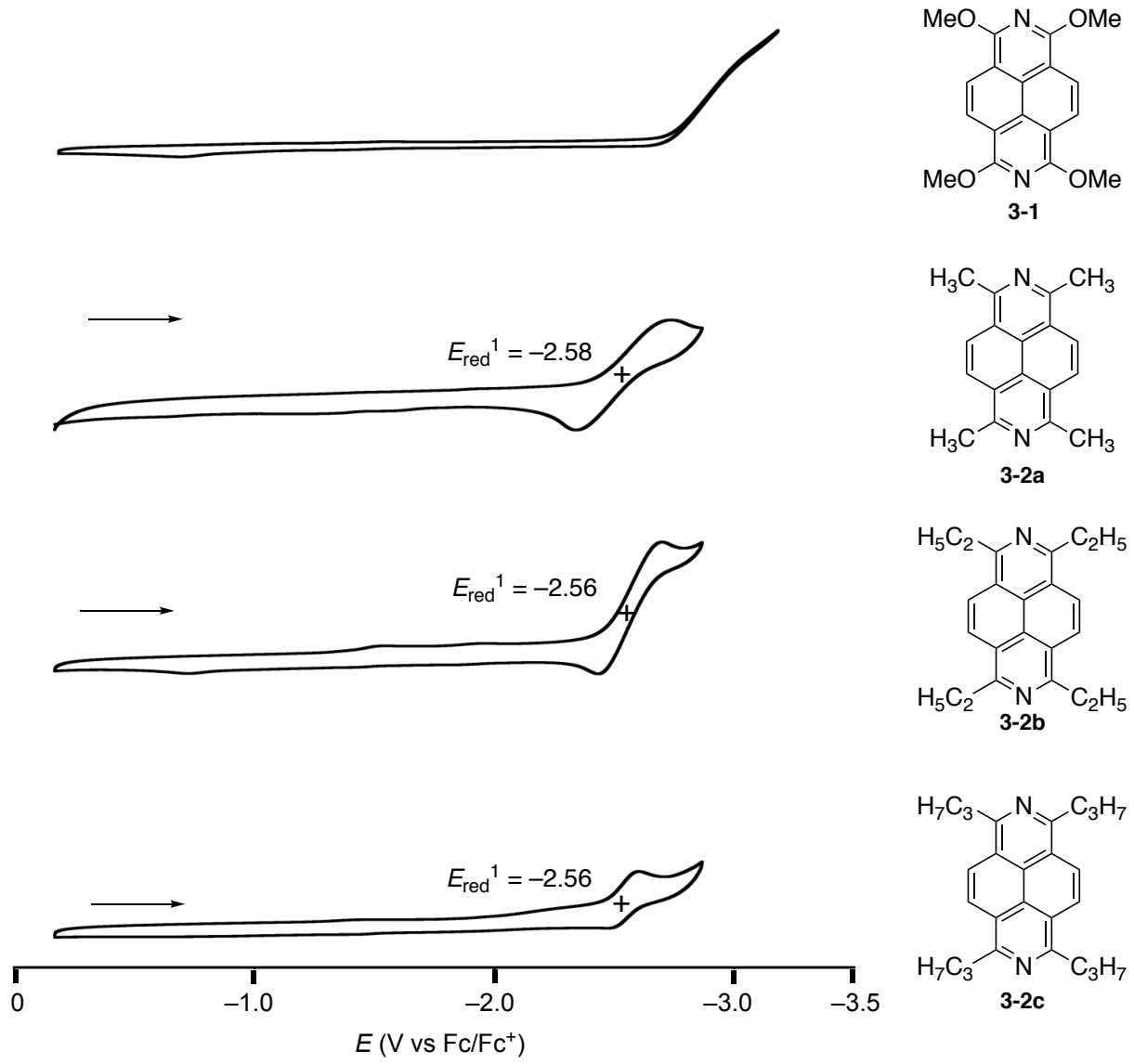

Figure 3-5. Cyclic voltammogram of **3-1** and **3-2a-c** in THF.

3-6. Electron mobility

The unique face-to-face packing structure of **3-2a** in its single crystal stimulated the author to investigate its conductivity. The FI-TRMC technique was employed to investigate the local-scale charge transport properties for both positive (hole) and negative (electron) carriers.[6] A $CHCl_3$ solution of **3-2a** was spincoated to form a thin film on polyimide-coated SiO_2 insulating layers on gold electrode-patterned quartz substrate. A top gold electrode was deposited on the **3-2a** layer to fabricate the metal–insulator–semiconductor (MIS) device. The metal–insulator–semiconductor device, placed on the resonant cavity, was monitored by microwave spectroscopy. With a square wave gate bias applied to the MIS devices, current flows were appeared (Figure 3-5a), indicating the injection of electrons to the **3-2a** layer. By integrating the flow current, the profiles of the number of accumulated charges were obtained (Figure 3-5b). The amount of injected charge carriers (N_{inj}) was calculated from the saturated values in each bias voltage. Accordingly, the reflected microwave power changed in response to the accumulated charges (Figure 3-5c). The pseudoconductivity ($\Delta N\mu_e$) was estimated based on the saturated reflected microwave power.[18a] As the N_{inj} and $\Delta N\mu_e$ values were plotted at each gate bias, the slope of the resulting plots represents electron mobility (Figure 3-5d), yielding $\mu_e = 0.07$ cm^2 V^{-1} s^{-1} for films in **3-2a**. Similarly, the charge carrier mobility of a spincoated film of **3-2b** was evaluated by the FI-TRMC method, recording $\mu_e = 0.06$ cm^2 V^{-1} s^{-1} (Figure 3-6). These values are almost same as the electron mobility of **2-3** measured under the similar conditions ($\mu_e = 0.09$ cm^2 V^{-1} s^{-1}) (Figure. 3-7). Powder X-ray diffraction (PXRD) measurements of the spincoated film of **3-2a** revealed that the packing structure in the film was close to that of the single crystal (Figure. S11a). On the other hand, the patterns obtained from the spincoated film and simulation from the single crystal data were different for **3-2b** (Figure. 3-8). Control of the packing structures and the degree of crystallinity in the film state are worthy of further investigation. Nevertheless, the comparable electron mobility values evaluated for **3-2a** and **3-2b** suggests that the overlaps of low LUMOs of the 2,7-diazapyrene derivatives contribute to the observed good electron mobility for **3-2a** and **3-2c**.

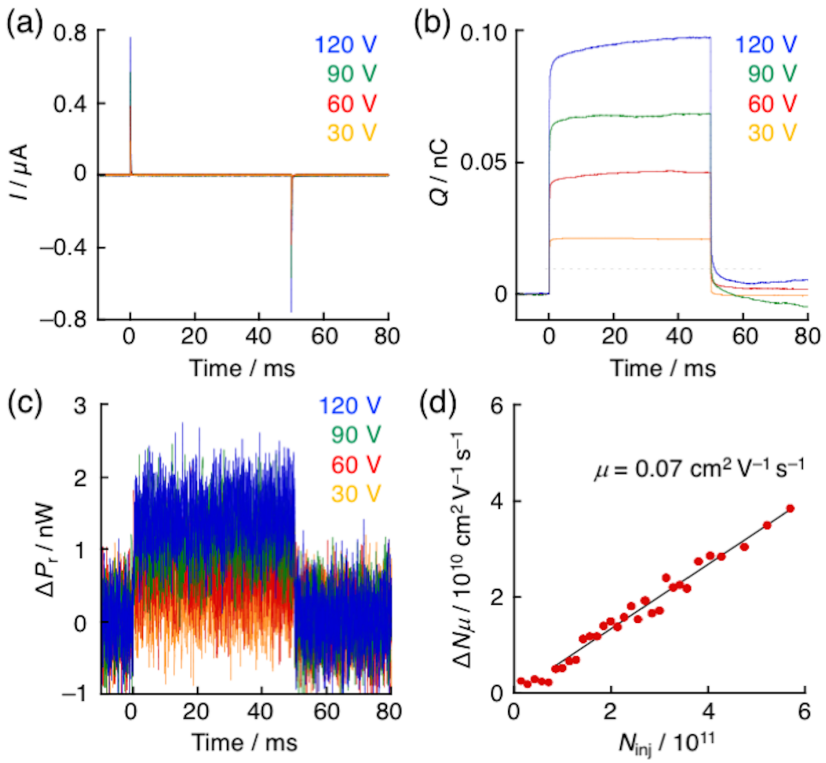

Figure 3-6. (a) Time profiles of the flowed electric current in **3-2a**-based MIS device by injecting electrons. (b) Time profiles of accumulated charge amounts by electron injection in **3-2a**-based device. The charge amount was calculated from integration of the value of flowed current. (c) The change in reflected microwave power by electron injection plotted against the time in **3-2a**-based MIS device. (d) Pseudo-electrical conductivity ($\Delta N\mu$) plotted against the amount of injected electrons (N_{inj}).

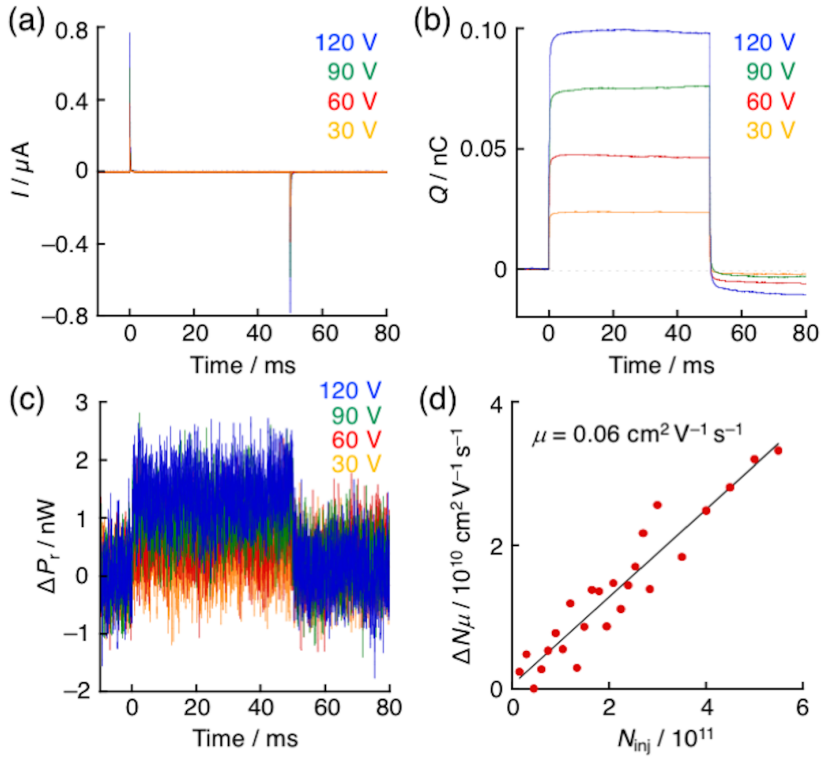

Figure 3-1. (a) Time profiles of the flowed electric current in **3-2b**-based MIS device by injecting electrons. (b) Time profiles of accumulated charge amounts by electron injection in **3-2b** -based device. The charge amount was calculated from integration of the value of flowed current. (c) The change in reflected microwave power by electron injection plotted against the time in **3-2b**-based MIS device. (d) Pseudo-electrical conductivity ($\Delta N\mu$) plotted against the amount of injected electrons (N_{inj}).

Figure 3-2.

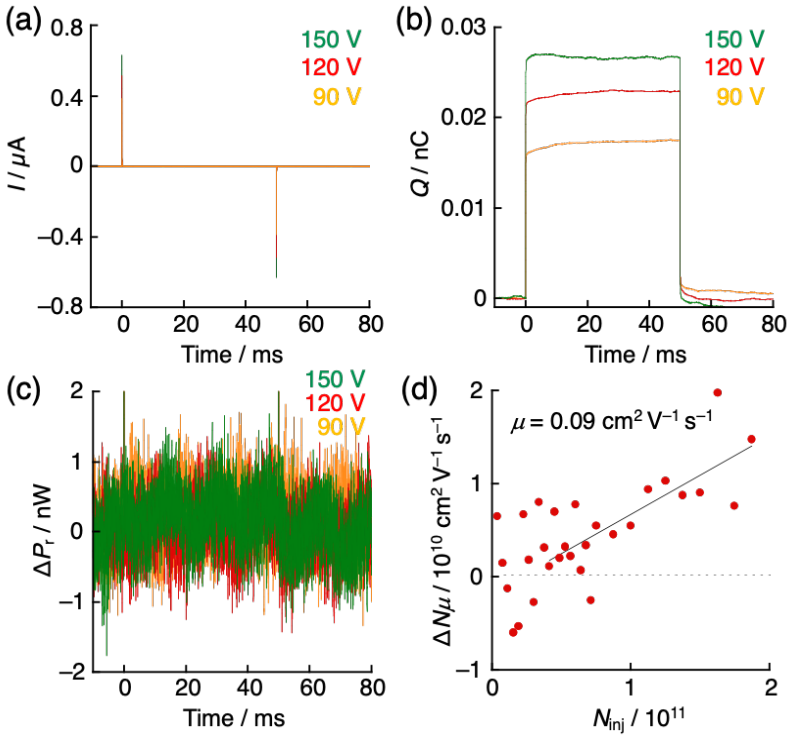

Figure 3-3. (a) Time profiles of the flowed electric current in **2-3**-based MIS device by injecting electrons. (b) Time profiles of accumulated charge amounts by electron injection in **2-3**-based device. The charge amount was calculated from integration of the value of flowed current. (c) Time profiles of change in reflected microwave power by electron injection in **2-3**-based MIS device. (d) Correlation between the pseudo-electrical conductivity ($\Delta N\mu$), and the number of injected electrons (N_{inj}).

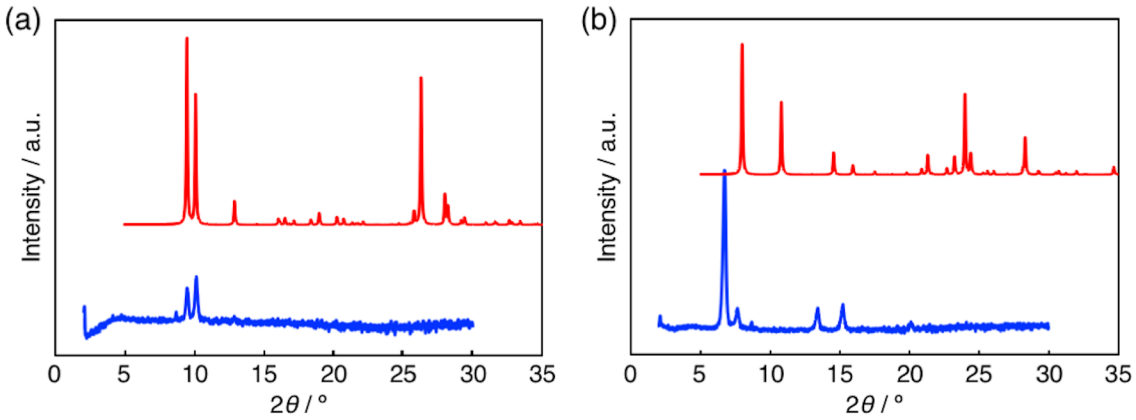

Figure 3-4. Experimental (blue) and simulated (red) XRD patterns of (a) **3-2a** and (b) **3-2b**. The experimental patterns were obtained from spincoated films, while simulated patterns were calculated from the single crystal structural analysis.

3-7. Summary of Chapter 3

In summary, this chapter developed the synthesis of 1,3,6,8-tetramethoxy-2,7-diazapyrene **3-1** through reductive aromatization of naphthalene diimide. The methoxy groups were converted to a variety of alkyl units via Kumada-Tamao cross-coupling reaction with alkyl Grignard reagents. The X-ray crystallographic analysis of **3-2** elucidated that the length of the alkyl groups dramatically affected the packing structure in the solid state. Tetramethyl-2,7-diazapyrene **3-2a** exhibited more distinct excimer emission as compared to tetrapentyl-2,7-diazapyrene **2-3**, indicating that the length of the alkyl groups modulates the intermolecular interactions in solution. Furthermore, FI-TRMC measurements clearly revealed the intrinsic high electron mobility of **3-2a** and **3-2b**.

3-8. References

1. (a) Lei, T.; Wang, J.-Y.; Pei, J. *Chem. Mater.* **2013**, *26*, 594-603. (b) Kang, I.; Yun, H.-J.; Chung, D. S.; Kwon, S.-K.; Kim, Y.-H. *J. Am. Chem. Soc.* **2013**, *135*, 14896-14899. (c) Pei, J.; Wang, X.-Y.; Zhuang, F.-D.; Zhou, X.; Yang, D.-C.; Wang, J.-Y. *J. Mater. Chem. C* **2014**, *2*, 8152-8161. (d) Labban, E. A.; Warnan, J.; Cabanetos, C.; Ratel, O.; Tassone, C.; Toney, F. M.; Beaujuge, M. P. *ACS Appl Mater Interfaces* **2014**, *6*, 19477-19481. (e) Back, J. Y.; An, T. K.; Cheon, Y. R. Cha, H.; Jang, J.; Kim, Y.; Beak, Y.; Chung D. S.; Kwon, S.-K.; Park, C. E.; Kim, Y.-H. *ACS Appl. Mater. Interfaces* **2015**, *7*, 351-358.

2. (a) Dankwardt, J. W. *Angew. Chem., Int. Ed.* **2004**, *43*, 2428-2432. (b) Tobisu, M.; Shimasaki, T.; Chatani, N. *Angew. Chem., Int. Ed.* **2008**, *47*, 4866-4869. (c) Wang, C.; Ozaki, T.; Takita, R.; Uchiyama, M. *Chem. - Eur. J.* **2012**, *18*, 3482-3485.

3. (a) Guan, B.-T.; Xiang, S.-K.; Wu, T.; Sun, Z.-P.; Wang, Z. B.-Q.; Zhaob, K.-Q;. Shi, Z.-J.; *Chem. Commun.* **2008**, *12*, 1437-1439. (b) Yang, Z.-K.; Wang, D.-Y.; Minami, H.; Ogawa, H.; Ozaki, T. Saito, T. Minamoto, K.; Wang, C.; Uchiyama, M. *Chem. - Eur. J.* **2016**, *22*, 15693-15699. (c) Morioka, T.; Nishizawa, A.; Nakamura, K.; Tobisu, M.; Chatani, N. *Chem. Lett.* **2015**, *44*, 1729-1731. (d) Tobisu, M.; Takahira, T.; Chatani, N. *Org. Lett.* **2015**, *17*, 4352-4355. (e) Tobisu, M.; Takahira, T.; Morioka, T. Chatani, N. *J. Am. Chem. Soc.* **2016**, *138*, 6711-6714.

4. (a) Tobisu, M.; Shimasaki, T.; Chatani, N.; *Chem. Lett.* **2009**, *38*, 710-711. (b) Tobisu, M.; Yasutome, A.; Yamakawa, K.; Shimasaki, T.; Chatani, N. *Tetrahedron* **2012**, *68*, 5157-5161. (c) Zarate, C.; Manzano, R.; Martin, R. *J. Am. Chem. Soc.* **2015**, *137*, 6754-6757. (d) Tobisu, M.; Takahira, T.; Ohtsuki, A.; Chatani, N. *Org. Lett.* **2015**, *17*, 680-683. (e) Zarate, C.; Nakajima, M.; Martin, R. *J. Am. Chem. Soc.* **2017**, *139*, 1191-1197.

5. Cho, Y.-J.; Kim, S.-Y.; Son, H.-J.; Cho, D. W.; Kang, S. O. *Phys. Chem. Chem. Phys*. **2017**, *19*, 5486-5494 (b) Lee, J.; Kim, B.; Kwon, J. E.; Kim, J.; Yokoyama, D.; Suzuki, K.; Nishimura, H.; Wakamiya, A.; Park, S. Y.; Park, J. *Chem. Commun.* **2014**, *50*, 14145-14148. (c) Sherwood, G. A.; Cheng, R.; Chacon-Madrid, K.; Smith, T. M. Smith.; Peteanu, L. A. *J. Phys. Chem. C* **2010**, *114*, 12078–12089.

Chapter 3

6. (a) Honsho, Y.; Miyakai, T.; Sakurai, T.; Saeki, A.; Seki, S. *Sci. Rep.* **2013**, *3,* 3182. (b) Choi, W.; Tsutsui, Y.; Sakurai, T.; Seki, S. *Appl. Phys. Lett.* **2017**, *110*, 153303. (c) Choi, W.; Nishiyama, H.; Ogawa, Y.; Ueno, Y.; Furukawa K.; Takeuchi, T.; Tsutsui, Y.; Sakurai, T.; Seki, S. *Adv. Opt. Mater.* **2018**, *306*, 1701402.

Chapter 4.

Complexation of 2,7-diazapyrene with boron for structural and electronic tuning

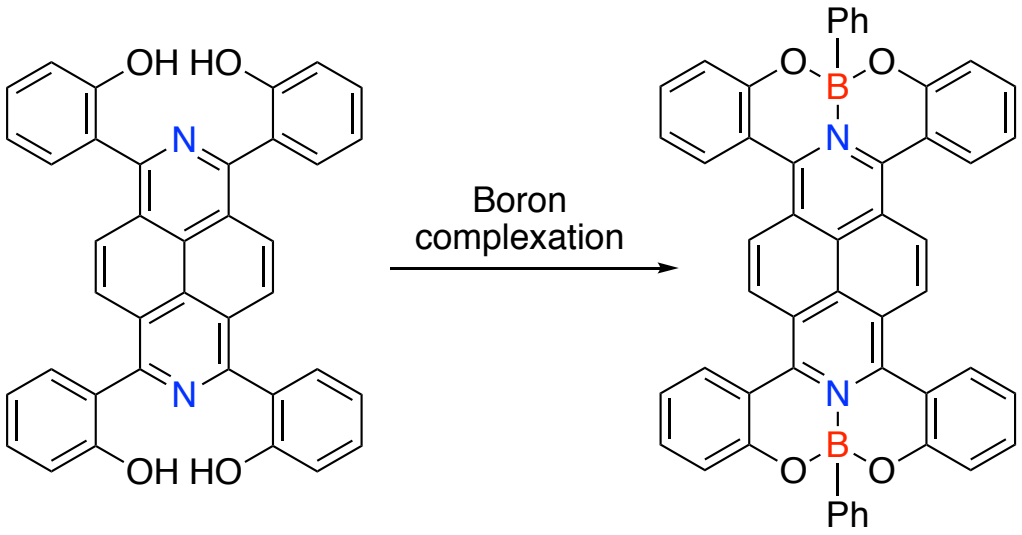

Contents

4-1. Introduction

As the author described in chapter 2, the protonation of tetrapentyldiazapyrene changes its UV-vis absorption and emission spectra, suggesting that modification of nitrogen atoms of 2,7-diazapyrenes is an effective method to modify their optical properties. Coordination of nitrogen atoms in 2,7-diazapyrene cores to boron center is a useful method to tune their electronic nature. Here, the author describes the synthesis of boron-diazapyrene complexes and the role of the peripheral aryl groups in the complexation. Optical and electrochemical properties as well as aggregation behaviors of boron-diazapyrene complexes are also investigated.

4-2. Synthesis of characterization of boron diazapyrene complex 4-1

First, diazapyrene-boron trifluoride complex (**4-1**) was synthesized as shown in Scheme 4-1. Treatment of **2-2b** with 6 equiv of boron trifluoride-ethyl ether complex (BF_3•Et_2O) afforded **4-1** in 57% yield. Figure 4-1 shows the electronic absorption and emission spectra of **2-2b** and **4-1** in THF and CH_2Cl_2 respectively. Absorption and fluorescence spectra of **4-1** in CH_2Cl_2 were bathochromically shifted compared to those of **2-2b**. On the other hand, optical spectra of **4-1** in THF exactly matched the absorption and fluorescence spectra of **2-2b**. These results suggest that B–N bonds in the boron complex **4-1** are dissociated in THF.

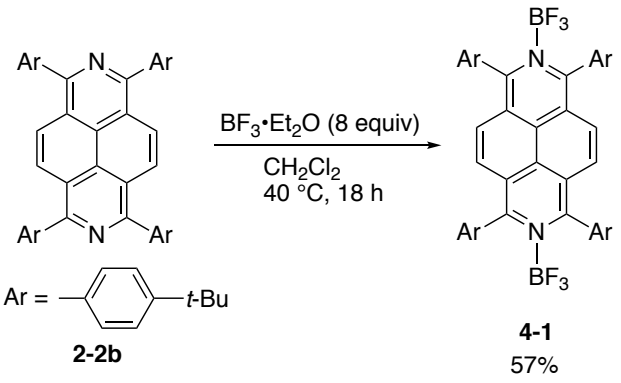

Scheme 4-1. Synthesis of boron-diazapyrene complex **4-1**.

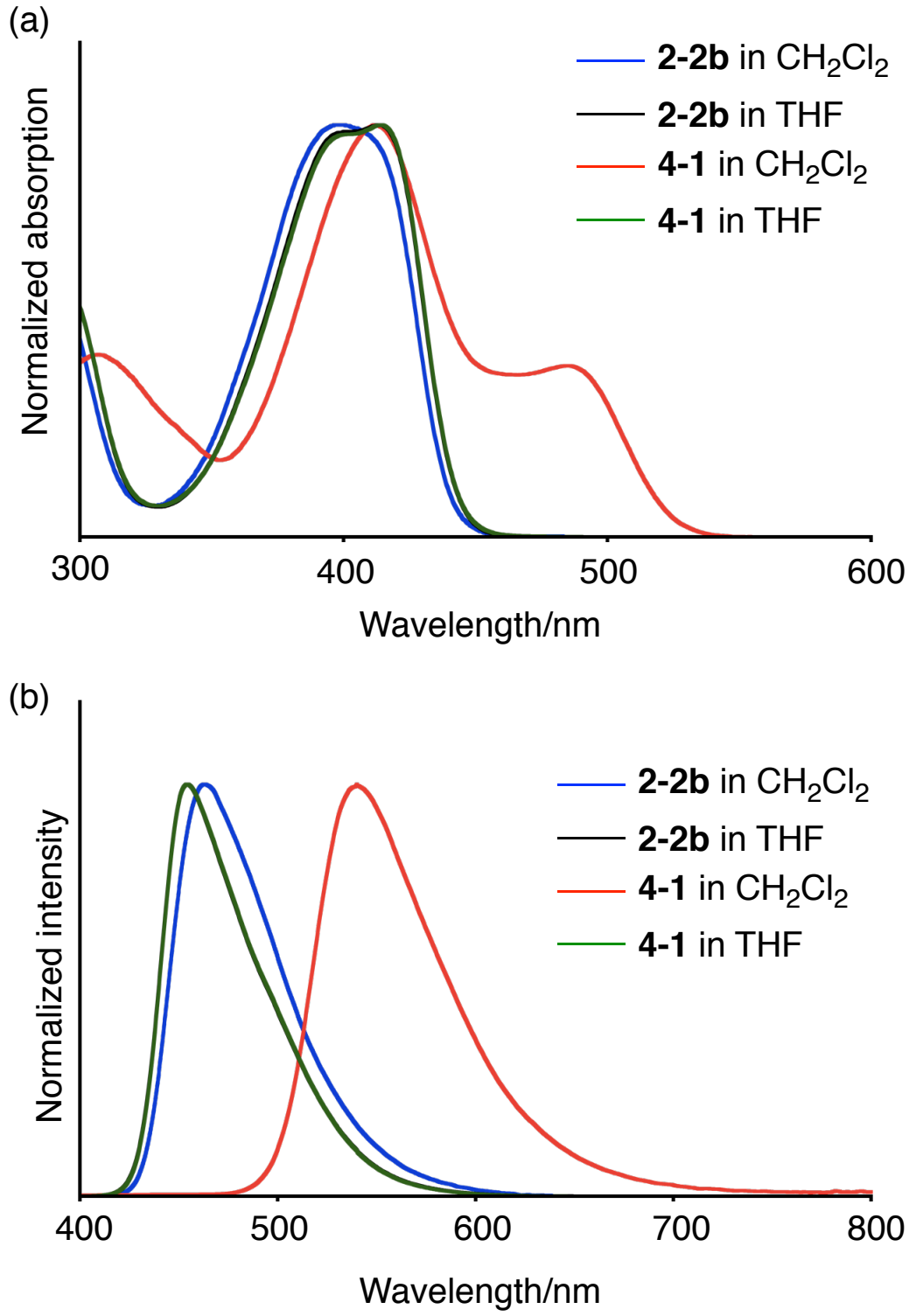

Figure 4-1. (a) UV-vis absorption and (b) emission spectra of **2-2b** and **4-1** in CH_2Cl_2 and THF.

Table 4-1. Summary of optical properties of **2-2b** and **4-1**.

Compound	solvent	λ_{ex} (nm)	Φ
2-2b	CH_2Cl_2	380	0.38
2-2b	THF	380	0.37
4-1	CH_2Cl_2	380	0.33
4-1	THF	380	0.36

4-3. Synthesis of boron-diazapyrene complexes 4-3

As described in the precious section, the dissociation of boron–nitrogen coordination bonds occurred easily in the presence of the coordinative solvents such as THF. The introduction of the additional coordination sites at the peripheral position of 2,7-diazapyrene ligands is a promising method for the stabilization of the boron complexes. Bidentate and tridentate ligands for organoboron compounds play an important role to establish their rigid structure to control the physical properties.[1-3] In particular, 2,2'-(pyridine-2,6-diyl)diphenolate (dppy) is a well-studied tridentate ligand to afford tetracoordinate boron complexes (Figure. 4-2a).[4-6] Consequently, the use of pyridine annulated π-conjugated molecules as ligands with boron is an attractive strategy for the tuning of their properties because the coordination of the nitrogen atom to a boron center results in the electronic perturbation to π-conjugated cores. Oda and Hatakeyama *et al*. have synthesized the pyrazine-based boron complexes to apply them to the cathode active materials for a lithium ion battery (Figure. 4-2b).[6] Based on this consideration, the author aimed to synthesize the boron-diazapyrene complex with dppy moiety to obtain the stable boron complex (Figure 4-2c).

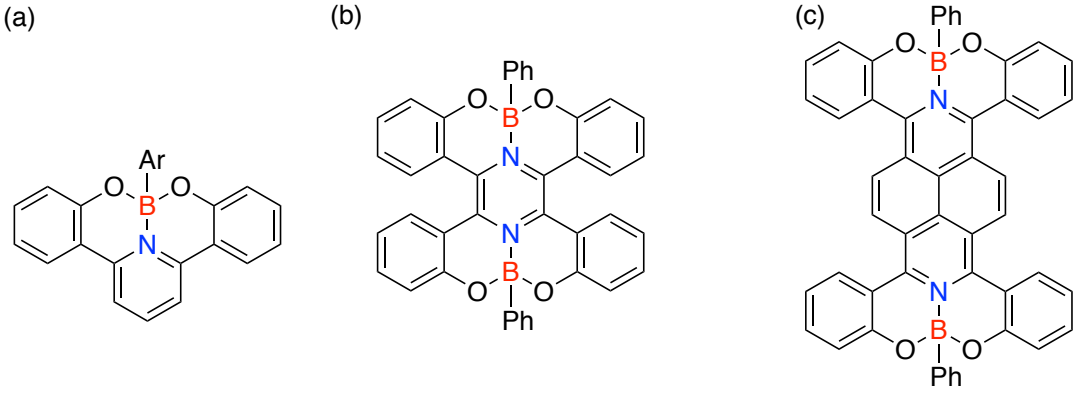

Figure 4-2. (a) Complexation of dppy with boron, (b) complexation of pyrazine with boron centers, and (c) complexation of 2,7-diazapyrene with boron centers.

The synthetic routes to boron-2,7-diazapyrene complexes **4-3** are shown in Scheme 4-2. Demethylation of **2-2d** with pyridine hydrochloride effectively provided 1,3,6,8-tetra(2-hydroxyphenyl)-2,7-diazapyrene (4) in 84% yield (Scheme 4-2a). The reaction of **4-2** with boron tribromide, and then the addition of PhMgBr afforded the target boron complex as a mixture of two stereoisomers. These isomers were separated by silica-gel column purification to furnish **anti-4-3** and **syn-4-3** as in 58% and 7% yields (Scheme 4-2b).[6] On the other hand, **syn-4-3** was obtained as a major product under different reaction conditions (Scheme 4-2c). The reaction of **4-2** with 8 equiv of phenyboronic acid in the presence of triethylamine provided **anti-4-3** and **syn-4-3** in 10% and 68% yield, respectively.[4b] Both boron-diazapyrene complexes **anti-4-3** and **syn-4-3** are stable under ambient conditions.

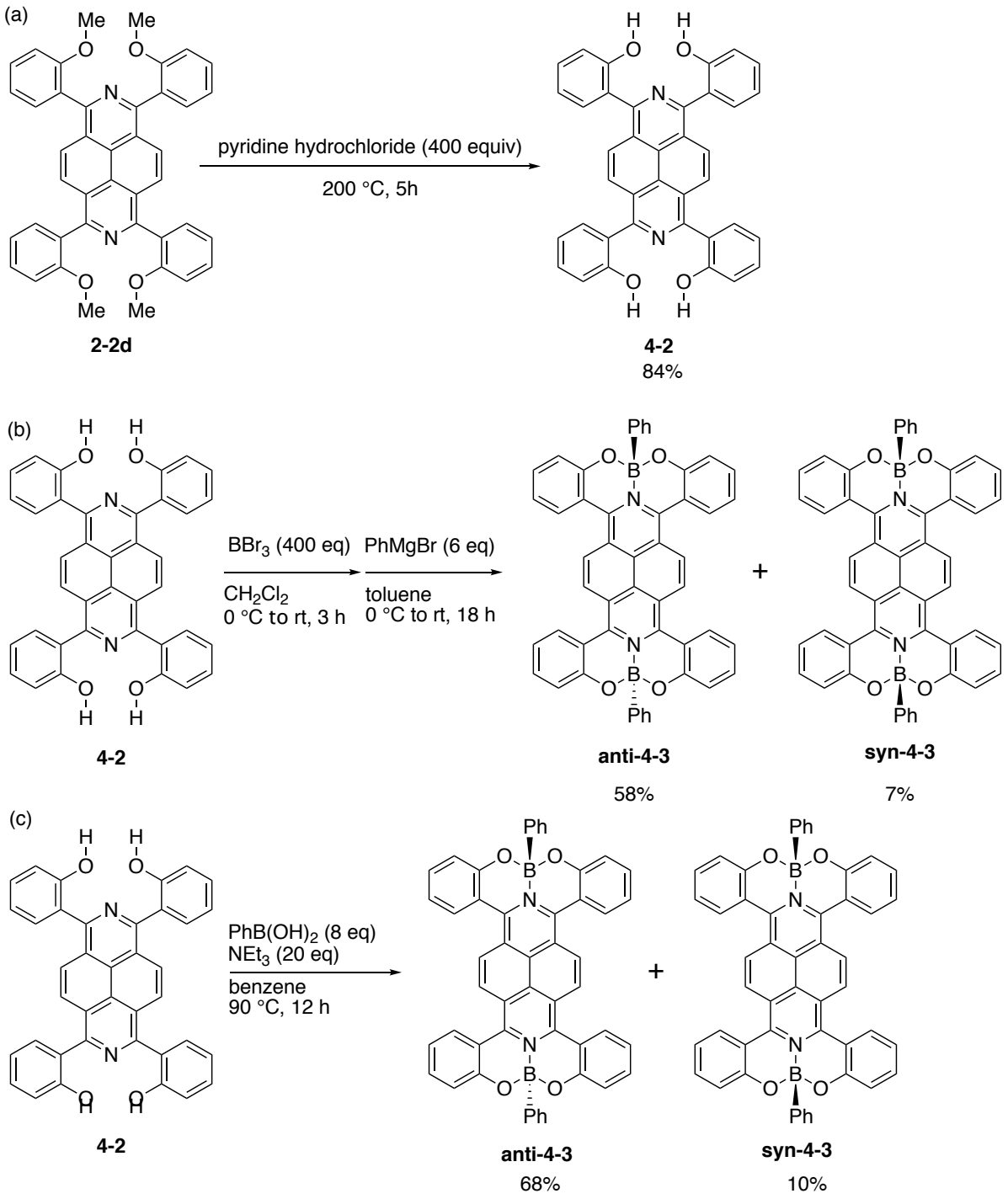

Scheme 4-2. Reduction reaction of *N,N'*-dimethyl-2,7-diazapyrenium dications.

4-4. Structural analyses

X-ray diffraction analysis unambiguously confirmed the molecular structures of **anti-4-3** and **syn-4-3** (Figure 4-3). Figure 4-3d shows one of the two independent molecules of **syn-4-3** in each unit cell. The configuration of the boron atom in both **anti-4-3** and **syn-4-3** adopts a distorted tetrahedral geometry. The B–O bond lengths (1.451(4)–1.458(5) Å), B–N bond lengths (1.619(5)-1.632(4) Å), and B–C bond lengths

(1.613(6)-1.614(4) Å) around boron atoms are comparable to those of the bis(2-hydroxyphenyl)pyridyl boron complexes and pyrazine boron complex (B–O: 1.442(3)–1.477(3) Å, B–N: 1.594(5)–1.613(3) Å, B–C: 1.614(5)–1.624(4) Å).[4b,6] Diazapyrene cores in **anti-4-3** and **syn-4-3** adopt the highly planar structures whose the mean plane deviations are 0.022 Å **(anti-4-3**) and 0.077 and 0.11 Å (**syn-4-3**). In the crystal packing, molecules of **anti-4-3** adopt a slipped-parallel one-dimensional alignment (Figure 4-3c). In contrast, **syn-4-3** forms a face-to-face stacked dimer, where one molecule is orthogonal to the other (Figure 4-3e, f). The distance between the diazapyrene cores in the dimer is 3.384 Å, which is shorter than sum of van der Waals radii of two carbon atoms. This value implies that attractive interaction exists between two molecules of **syn-4-3**.

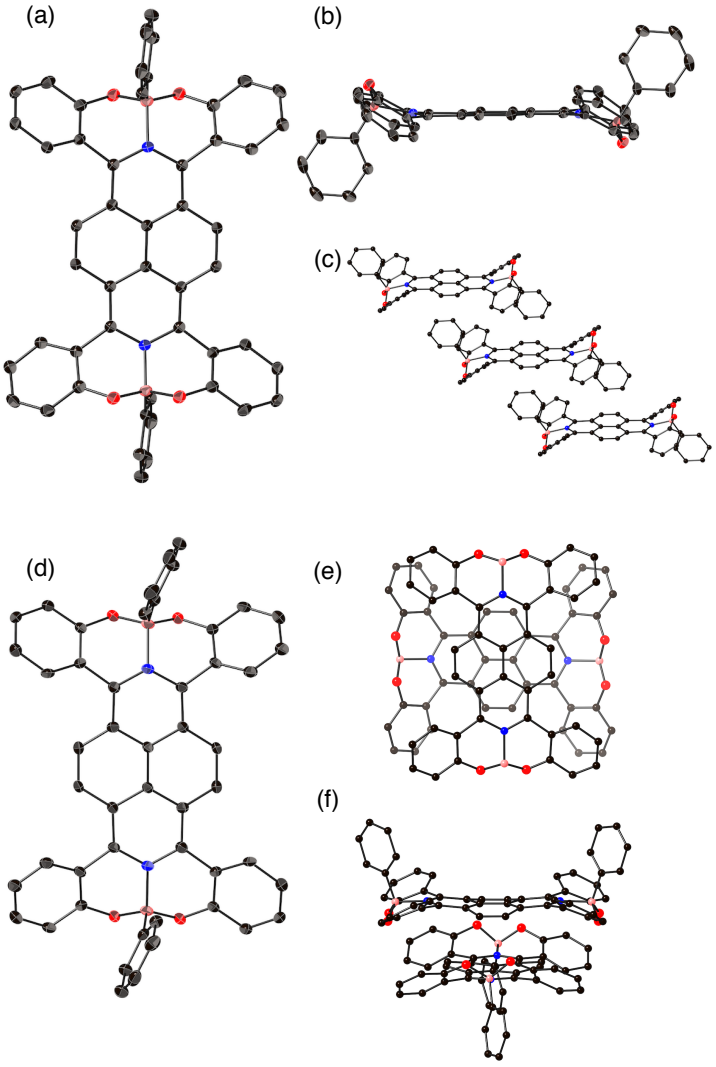

Figure 4-3. Molecular structures of **anti-4-3** and **syn-4-3**. (a) Top view, (b) side view, and (c) packing structure of **anti-4-3**. (d) Top view, (e) top and (f) side view of packing structures of **syn-4-3**.

To investigate the reasons for the dimer formation of **syn-4-3**, theoretical calculations were performed. The electrostatic potential map of **syn-4-3** dimer suggested the electron-deficiency of the diazapyrene core reduced electrostatic repulsion between two diazapyrene cores (Figure 4-4).

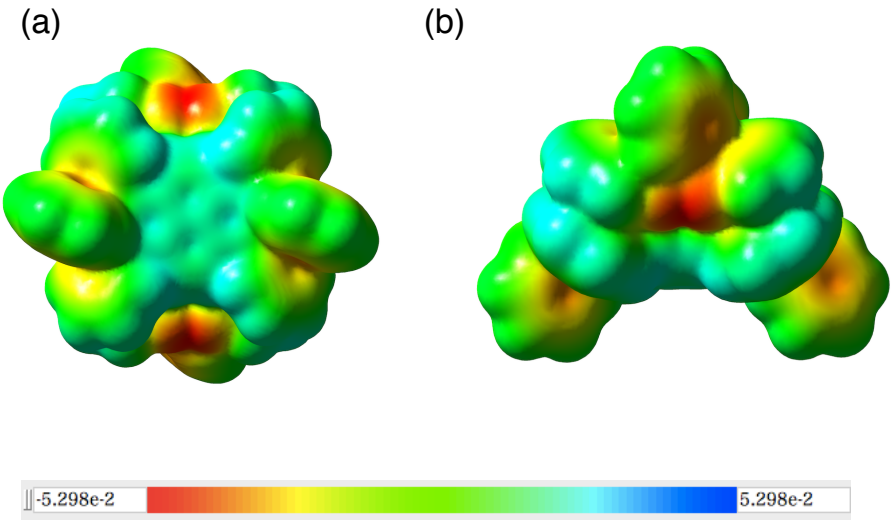

Figure 4-4. Electrostatic potential map of **syn-4-3** dimer. (a) top view and (b) side view of **syn-4-3** dimer calculated at B3LYP/6-31G(d) level of theory.

4-5. Association behavior

Interestingly, the chemical shift of the diazapyrene core of **syn-4-3** in $CDCl_3$ at 30 °C up-field shifted as concentration increased (Figure 4-5b). The chemical shift of the aromatic proton (H_a) in **syn-4-3** shifted from 8.58 to 8.29 ppm as the concentration increased from 0.63 mM to 12 mM. The upfield shift suggests the self-association of **syn-4-3** in $CDCl_3$. In sharp contrast, **anti-4-3** exhibited no change of its NMR spectra depending on concentrations (Figure 4-5a). The association constant of K_2 for **syn-4-3** was estimated using the dimer model under monomer−dimer equilibrium.[7,8] The curve fitting based on (eq 1) and (eq 2) was applied to estimate K_2; in these equations, the chemical shift of monomer **syn-4-3**, the chemical shift of dimer (**syn-4-3**)$_2$ and the total concentration of the substrate were represented by δ_m, δ_d, and C respectively. Figure 4-6 shows the dilution curve of **syn-4-3**. The K_2 value at 303 K was estimated to be 14497 ± 351 M^{-1}. The ^{1}H-NMR spectra of **syn-4-3** were also dependent on temperatures. The van't Hoff plot estimated thermodynamic parameters ΔG, ΔH, and ΔS at 303 K as –24.2 kJ mol^{-1}, –30.8 kJ mol^{-1}, and –21.9 J mol^{-1} K^{-1}, respectively (Figure 4-7). These values indicate that the dimer formation of **syn-4-3** was enthalpically driven owing to the low π-electron density induced by complexation of the diazapyrene core to the Lewis acidic boron center. The dimeric arrangement of **syn-4-3** in solution could be similar to that of the solid state structure of **syn-4-3** (Figure 4-3e, f)

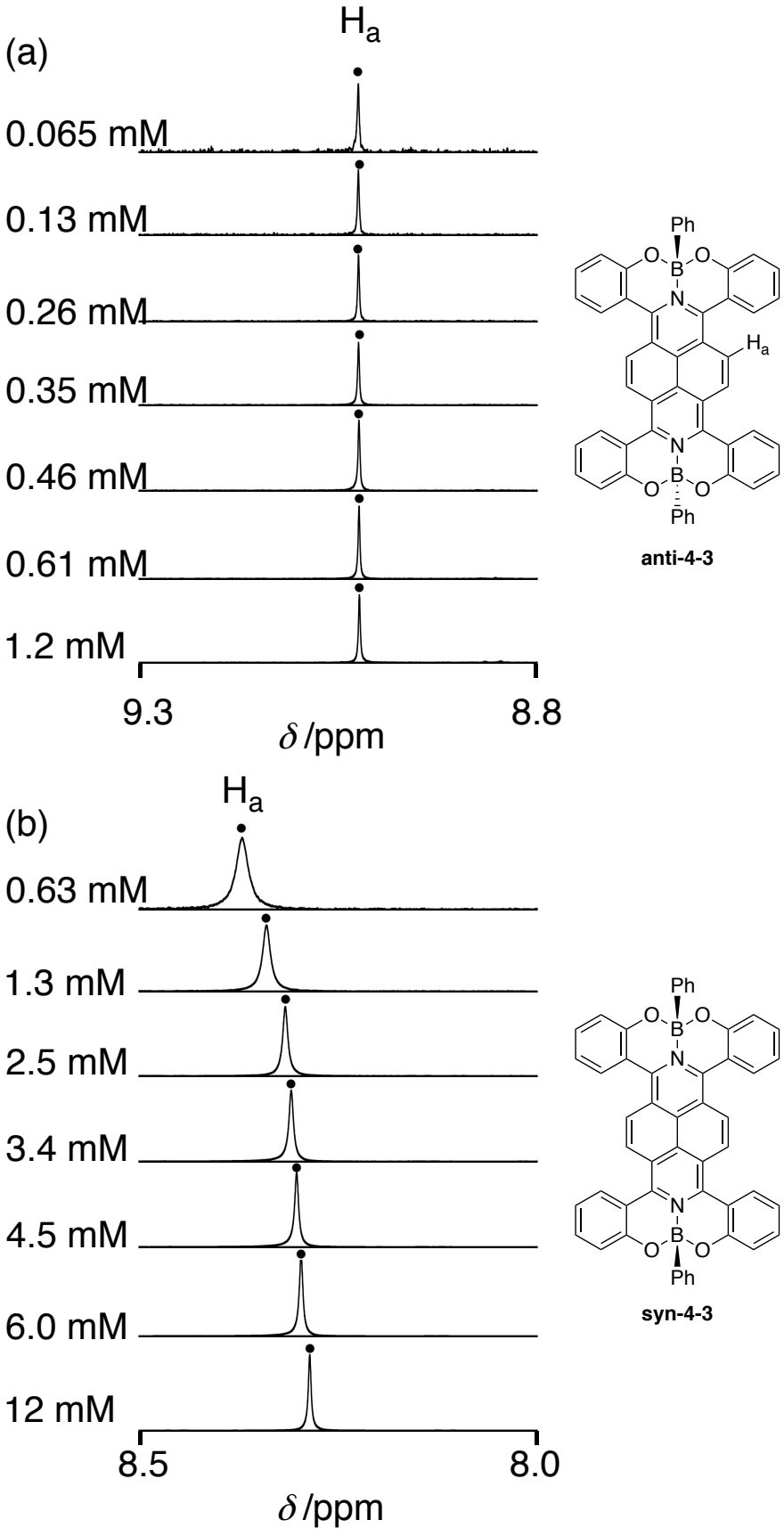

Figure 4-5. Concentration-dependent ^{1}H-NMR spectra of (a) **anti-4-3** and (b) **syn-4-3** in $CDCl_3$ at 30 °C.

$$K_2 = \frac{[(\mathbf{syn-1})_2]}{[\mathbf{syn-1}]^2} \quad \text{(eq 1)}$$

$$\delta = \delta_m + (\delta_d - \delta_m)\left[1 + \frac{1-\sqrt{8K_2C+1}}{4K_2C}\right] \quad \text{(eq 2)}$$

Table 4-2. Summary of chemical shifts of Ha of syn-4-2 in CDCl3, calculated association constants (K_2), and calculated chemical shifts of H_a proton for oligomer (δ_d) and monomer (δ_m).

Conc. (mM)	30 °C	35 °C	40 °C	45 °C	50 °C	55 °C
12	8.2857	8.2900	8.2944	8.2993	8.3042	8.3087
6.0	8.2965	8.3017	8.3073	8.3129	8.3185	8.3245
4.5	8.3022	8.3079	8.3135	8.3197	8.3262	8.3328
3.4	8.3090	8.3151	8.3218	8.3282	8.3353	8.3425
2.5	8.3165	8.3234	8.3304	8.3376	8.3454	8.3532
1.3	8.3400	8.3486	8.3573	8.3664	8.3759	8.3859
0.6	8.3706	8.3812	8.3920	8.4037	8.4154	8.4271
0.2	8.4583	8.4734	8.4892	8.5036	8.5187	8.5354
δ_d	8.2569 ± 0.0003	8.2590 ± 0.0004	8.2601 ± 0.0003	8.2613 ± 0.0006	8.2644 ± 0.0007	8.2655 ± 0.0004
δ_m	8.8022 ± 0.004	8.8121 ± 0.004	8.7926 ± 0.003	8.7705 ± 0.003	8.7949 ± 0.004	8.7945 ± 0.002
K_2	14497 ± 351	12750 ± 350	9700 ± 169	7311 ± 184	7080 ± 189	5912 ± 94

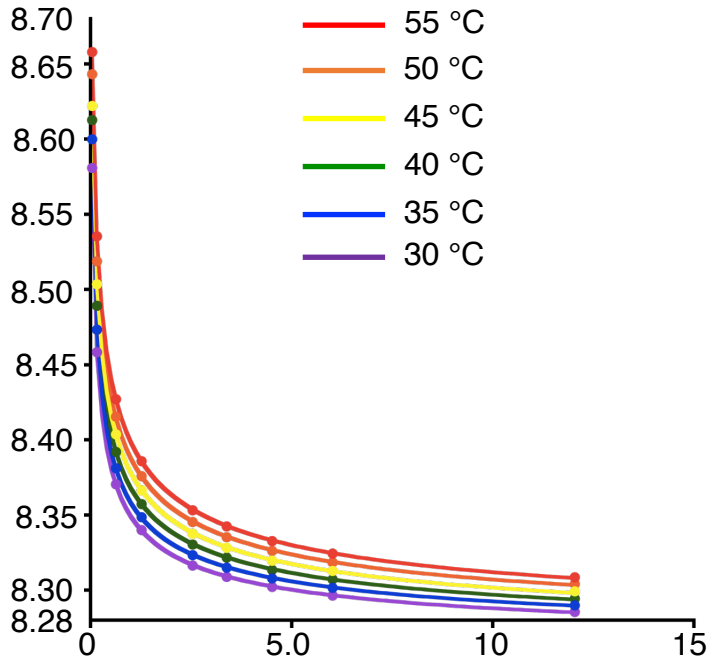

Figure 4-6. Curve fitting of **syn-4-3** in $CDCl_3$ at different temperatures.

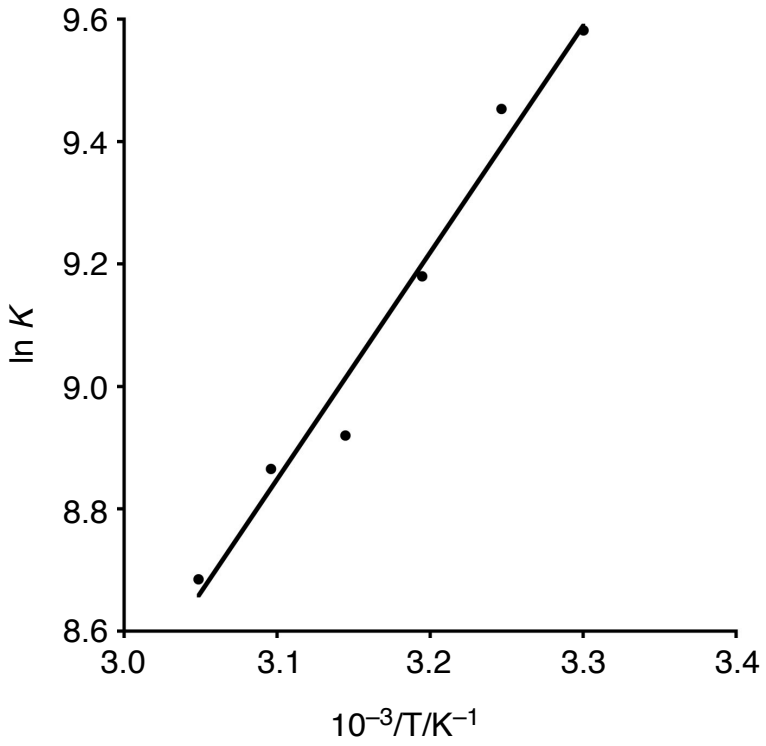

Figure 4-7. van't Hoff plots of **syn-4-3** in $CDCl_3$.

4-6. Optical properties

Figure 4-8 shows UV-vis absorption and emission spectra of **anti-4-3**, **syn-4-3**, and **2-2b** in CH_2Cl_2. The broad absorption bands of **anti-4-3** and **syn-4-3** from 400 to 600 nm are bathochromically shifted relative to

that of **2-2b** due to the boron complexation. Both diazapyrene boron complexes **anti-4-3** and **syn-4-3** were emissive, of which quantum yields were $\Phi = 0.25$ and 0.41, respectively. Bathochromic shift was also observed in emission spectra of **anti-4-3** and **syn-4-3** compared with **2-2b**.

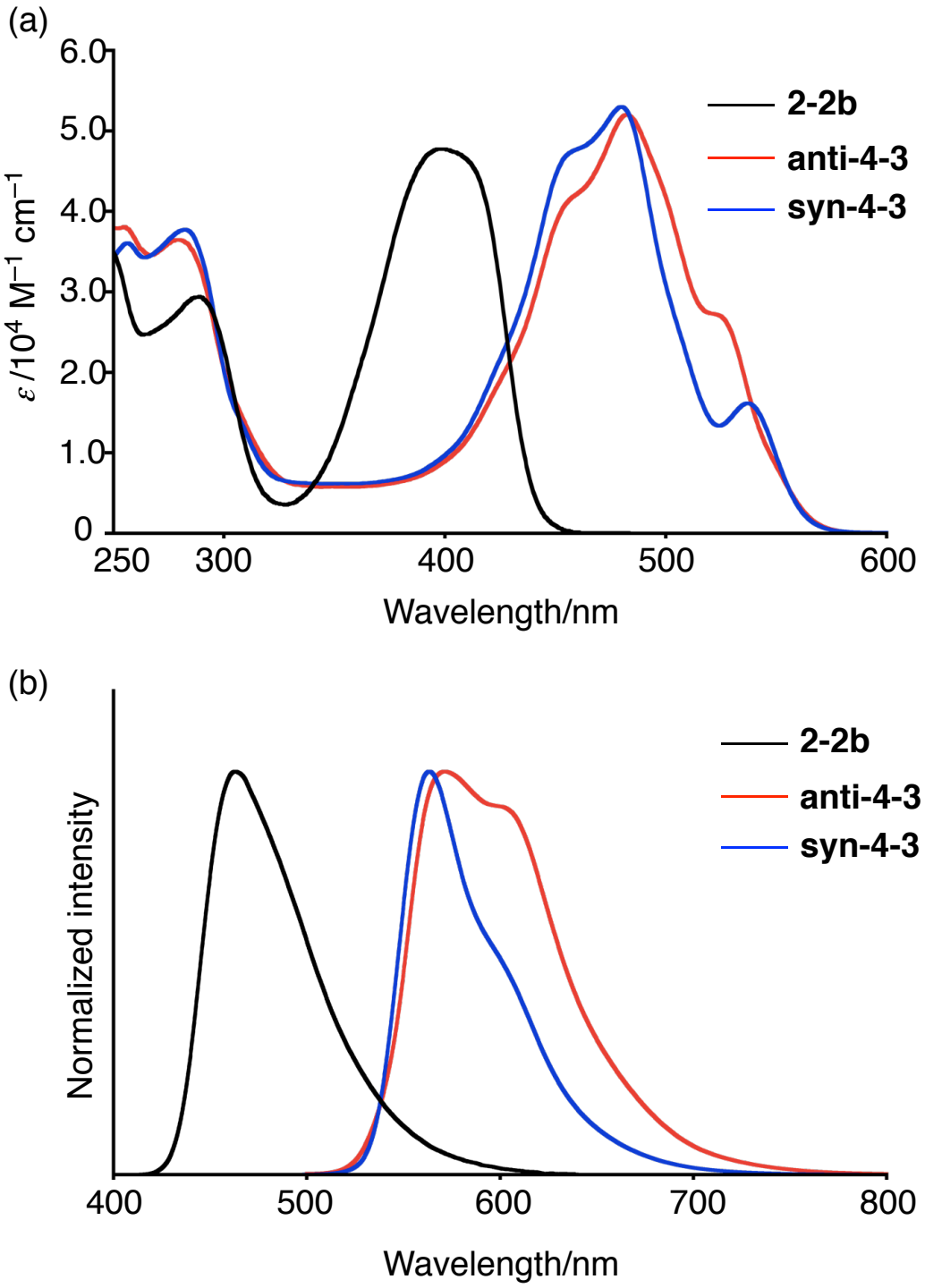

Figure 4-8. (a) Electronic absorption spectra of **anti-4-3**, **syn-4-3**, and **2-2b** in CH_2Cl_2. (b) Emission spectra of **anti-4-3**, **syn-4-3**, and **2-2b** in CH_2Cl_2.

Table 4-3. Summary of optical properties of **anti-4-3** and **syn-4-3**.

Compound	λ_{ex} (nm)	Φ (in CH_2Cl_2)
anti-4-3	450	0.25
syn-4-3	450	0.41

4-7. Electrochemical properties

Electrochemical properties of **anti-4-3**, **syn-4-3**, and **2-2b** were investigated by cyclic voltammetry (Figure 4-9). Two reversible reduction potentials were observed for **anti-4-3** (E_{red}^1 = –1.42 and E_{red}^2 = –1.88 V) and **syn-4-3** (E_{red}^1 = –1.44 and E_{red}^2 = –1.98 V) in THF. These values are shifted to higher potential field compared to diazapyrene **2-2b** (E_{red}^1 = –2.14 and E_{red}^2 = –2.53 V), indicating that the boron complexation enhances the electron deficient nature of the diazapyrene core.

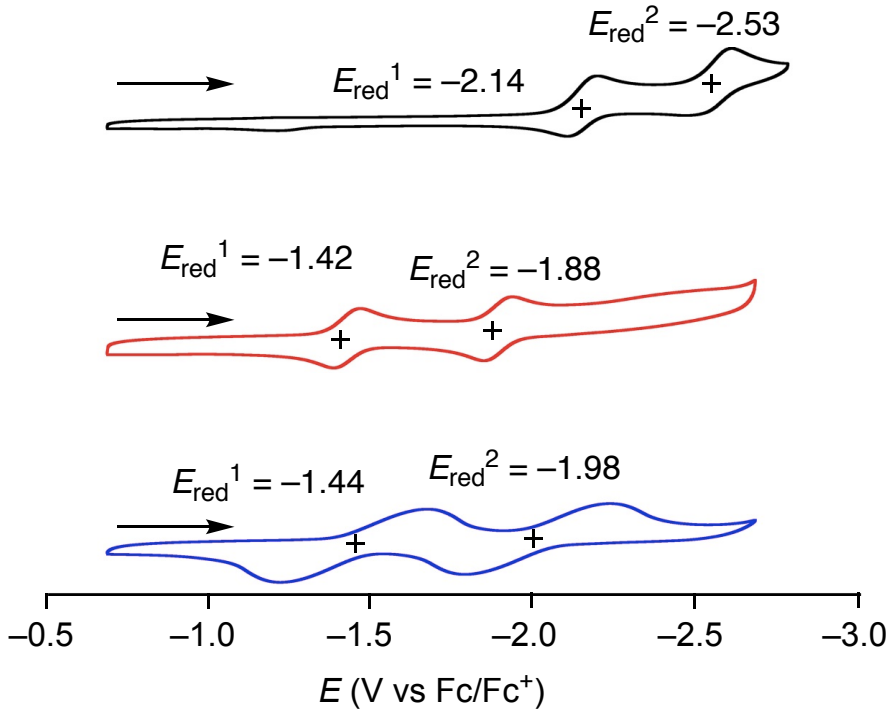

Figure 4-9. Cyclic voltammogram of **2-2b**, **anti-4-3**, and **syn-4-3** in THF.

4-8. Isomerization behavior

The author founds that boron complex **anti-4-3** underwent thermal isomerization into **syn-4-3** in both solution and solid state. The isomerization behavior of **anti-4-3** into **syn-4-3** in 1,2-dichlorobenzene-d_4 was monitored by ^{1}H-NMR measurement under heating conditions (at 130 °C). After 12 h, complete conversion of **anti-4-3** into **syn-4-3** was observed. Theoretical calculations revealed the multi-step isomerization pathway (Figure 4-10), indicates the rate-limiting step is the dissociation of the dative B–N bond to form a tri-

coordinate boron center in the transition state (TS3). The activation energy of 23.7 kcal mol^{-1} was calculated from **anti-4-3**. Interestingly, the isomerization of **anti-4-3** proceeded even in the solid state. Figure 4-11 shows the DSC measurement of **anti-4-3**. An exothermic peak was observed around 360.9 °C. ^{1}H-NMR measurement of the resulting sample revealed that **anti-4-3** was transformed to **syn-4-3** quantitatively.

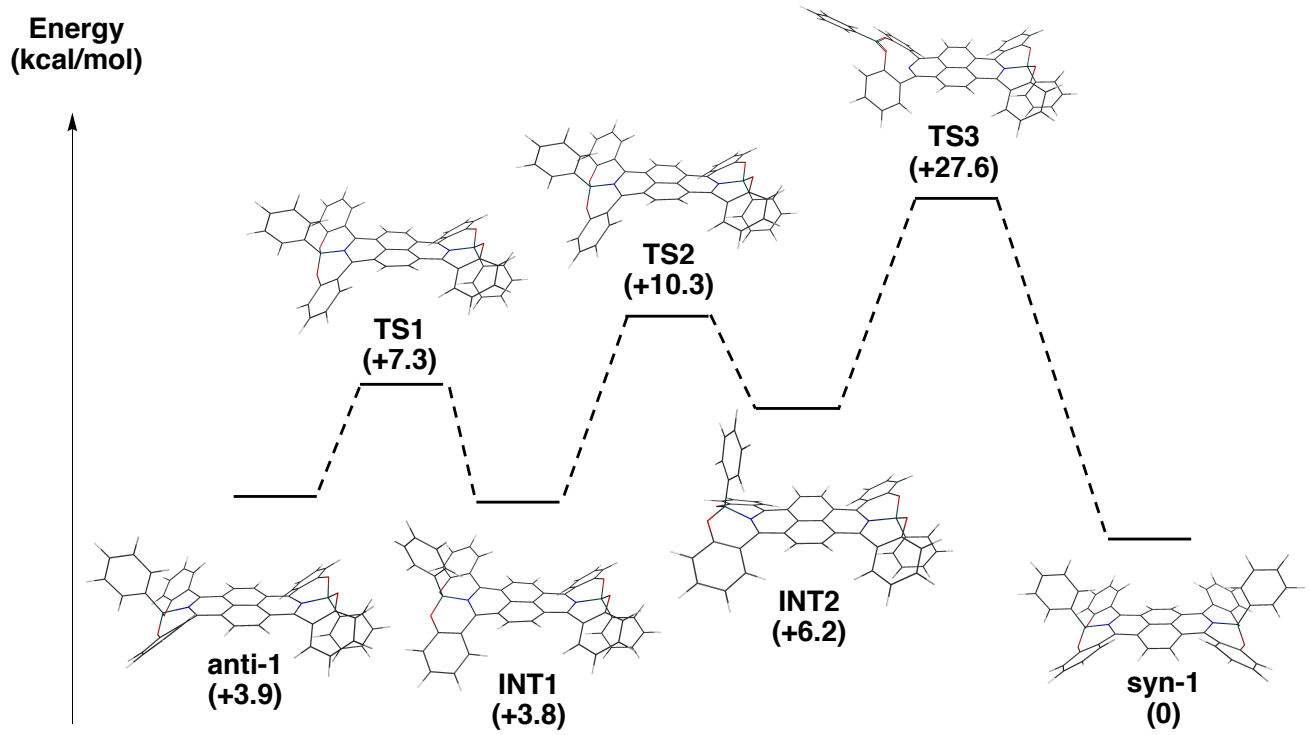

Figure 4-10. Energy diagram for the isomerization pathway of **anti-4-3** to **syn-4-3**. Free energies ΔG relative to **anti-4-3** are given in kcal mol^{-1} (B3LYP/6-31G(d)).

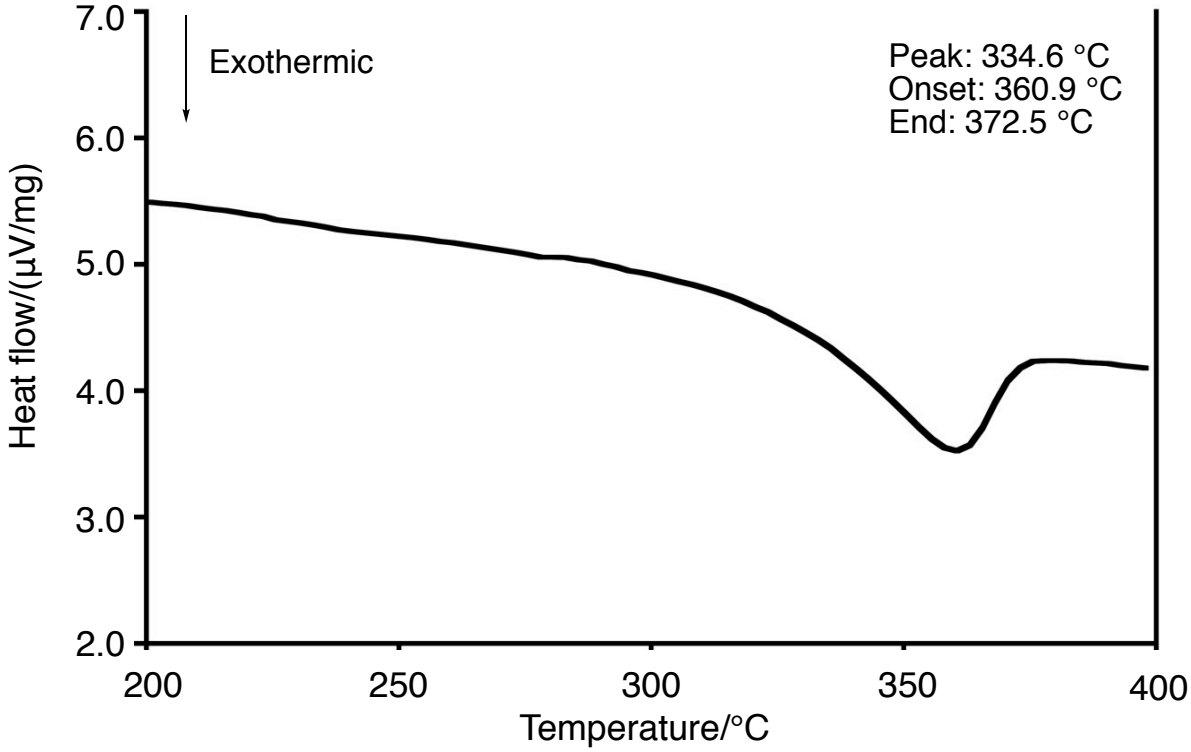

Figure 4-11. The DSC curve of **anti-4-3**.

4-9. Summary of Chapter 4

In summary, the author found the complexation of diazapyrene to boron centers provides the tetracoordinate boron complexes as separable stereoisomers **anti-4-3** and **syn-4-3**. Structural and electronical tune by the coordination is also found to perturbate the physical properties. In solution, **syn-4-3** exhibited the self-association behavior, while no association of **anti-4-3** was observed. Isomerization from **anti-4-3** to **syn-4-3** proceeded smoothly under heating conditions in the solution and solid states. Theoretical calculations revealed that the isomerization process occurred via a planar tricoordinate boron species in the transition state.

4-10. Refenences

1. 1 (a) Li, D.; Zhang, H.; Wang Y. *Chem. Soc. Rev.* **2013**, *42*, 8416-8433. (b) Shiu, Y.-J.; Cheng, Y.-C.; Tsai, W.-L.; Wu, C.-C.; Chao, C.-T.; Lu, C.-W.; Chi, Y.; Chen, Y.-T.; Liu; S.- H.; Chou, P.-T. *Angew. Chem., Int. Ed*. **2016**, *55*, 3017-3021. (c) Matsuo, K.; Yasuda, T.; *Chem. Commun*. **2017**, *53*, 8723-8726. (d) Mamada, M.; Tian, G. H.; Nakanotani, J.; Su, C.; Adachi, *Angew. Chem., Int. Ed*. **2018**, *57*, 12380-12384. (e) Fukagawa, H.; Sasaki, T.; Tsuzuki, T.; Nakajima, Y.; Takei, T.; Motomura, G.; Hasegawa, M.; Morii, K.; Shimizu, T. *Adv. Mater*. **2018**, *30*, 1706768.

2. (a) Sun, Y.; Rohde, D.; Liu, Y.; Wan, L.; Wang, Y.; Wu, W.; Di, C.; Yu, G.; Zhu, D. *J. Mater. Chem.* **2006**, *16*, 4499-4053. (b) Rao, Y.-L.; Wang, S. *Inorg. Chem.* **2011**, *50*, 12263-12274. (c) Hecht, R.; Kade, J.; Schmidt, D.; Nowak-Król, A. *Chem. Eur. J.* **2017**, *23*, 11620-11628. (d) Min, Y.; Dou, C.; Tian, H.; Geng, Y.; Liu, J.; Wang, L. *Angew. Chem. Int. Ed.* **2018**, *57*, 2000-2004. (e) Min, Y.; Dou, C.; Liu, D.; Dong, H.; Liu, J. *J. Am. Chem. Soc*. **2019**, *141*, 17015-17021.

3. Frath, D.; Massue, J.; Ulrich, G.; Ziessel, R. *Angew. Chem. Int. Ed*. **2014**, *53*, 2290-2310.

4. (a) Y.; Li, Y.; Liu, W.; Bu, J.; Guuo, Y.; Wang, *Chem. Commun.* **2000**, 1551. (b) H.; Zhang, C.; Huo, K.; Ye, P.; Zhang, W.; Tian, Y.; Wang, *Inorg. Chem.* **2006**, *45*, 2788-2794. (c) H.; Zhang, C.; Huo, J.; Zhang, P.; Zhang, W.; Tian, Y.; Wang, *Chem. Commun.* **2006**, 281. (d) H.; Zhang, Z.; Zhang, J.; Zhang, K.; Ye, H.; Gao, Y.; Wang, *CrystEngComm*. **2007**, *9*, 951-958. (e) Z.; Zhang, D.; Yao, S.; Zhao, H.; Gao, Y.; Fan, Z.; Su, H.; Zhang, Y.; Wang, *Dalton Trans.* **2010**, *39*, 5123-1529.

5. Li, P.; Chan, H.; Lai, Ng, S. -L.; M.; Chan, M. -Y.; Yam, V. W. -W. *Angew. Chem. Int. Ed*. **2019**, *58*, 9088-9094.

6. Oda, S.; Shimizu, T.; Katayama, T.; Yoshikawa, H.; Hatakeyama, T. *Org. Lett*. **2019**, *21*, 1770-1773.

7. Martin, R. B. *Chem. Rev*. **1996**, *96*, 3043-3064.

8. (a) Zhang, J.; Pesak, D. J.; Ludwick, J. L.; Moore, J. S. *J. Am. Chem. Soc*. **1994**, *116*, 4227-4239. (b) Tobe, Y.; Utsumi, N.; Kawabata, K.; Nagano, A.; Adachi, K.; Araki, S.; Sonoda, M.; Hirose, K.; Naemura, K. *J. Am. Chem. Soc*. **2002**, *124*, 5350-5364. (c) Kato, S.; Akahori, S.; Serizawa, Y.; Lin, X.; Yamauchi, M.; Yagai, S.; Sakurai, T.; Matsuda, W.; Seki, S.; Shinokubo, H.; Miyake, Y.; *J. Org. Chem*. **2020**, *85*, 62–69.

Chapter 5.

Synthesis and characterization of π-extended viologen

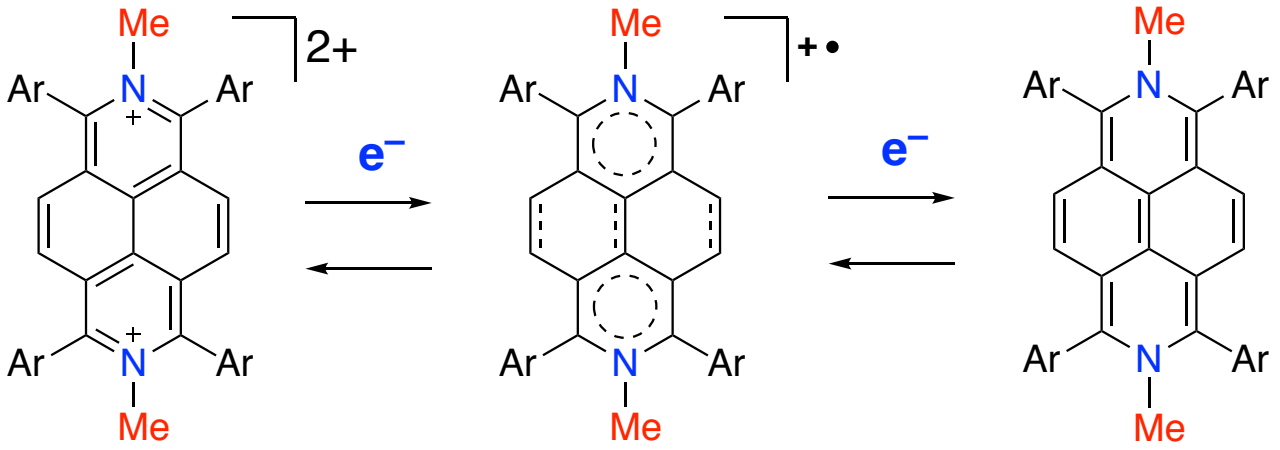

Contents

5-1. Introduction

Viologens, which are *N,N*′-disubstituted 4,4'-bipyridyls, have attracted significant attention as the promising candidates for organic materials such as electrochromic materials, redox flow batteries, and organic field effect transistors because of their highly electron-deficient nature.[1-4] Viologens also work as suitable acceptor units in donor/acceptor charge transfer complexes, which are often applied as the key component to construct the catenanes and the rotaxanes.[5] Two-step redox event of viologens provides three forms, the dication, the radical cation, and the neutral form.[6] Because methyl viologen (*N*,*N*'-dimethyl-4,4'-bipyridinium dication; abbreviated as MV^{2+}) is a representative viologen, the structures and optical properties of three forms of methyl viologen extensively studied until now. Kochi and co-workers reported that its two-electron reduced form (MV^0) has a dearomatized *para*-quinoid structure (Scheme 5-1a).[6b]

The connection between the two pyridine rings in the viologen core by the bridging units is a promising strategy for the tuning of their electronic nature. For example, the phosphorus-bridged viologen exhibits higher electron affinity than the parent viologen.[7] Oshita and co-workers have also reported that the silicon- and germanium-bridged viologens exhibited the enhanced phosphorescence in the solid state.[8]

N,N′-Dimethyl-2,7-diazapyrenes (**MDAP^{2+}**) can be regarded as π-extended **MV**$^{2+}$, where the two pyridine rings are bridged by two ethene units. Larger cross-section of **MDAP^{2+}** than **MV**$^{2+}$ should provide the stronger host-guest association with electron donors.[9] Furthermore, **MDAP^{2+}** can be used as fluorescent probe to detect organic molecules using donor-acceptor interaction because it exhibits strong emission due to the rigid π-conjugation system.[10] On the other hand, the two-electron reduced form (**MDAP^0**) is also an attractive target because **MDAP^0** would exhibit the antiaromatic character owing to the 16π electron conjugation via peripheral bridging units. In 1996, Wardör and Kaim reported the detection of **MDAP^0** through the two-electron reduction of **MDAP^{2+}** by its absorption spectrum. However, the isolation of **MDAP^0** has been unsuccessful and its structure and electrochemical properties have remained unexplored.[11] In this study, the author synthesized peripherally substituted **MDAP^{2+}** via *N*-methylation of tetraaryl-2,7-diazapyrenes to explore effects of the quaternization of nitrogen atoms. Furthermore, the two-electron reduced form **MDAP^0** was investigated.

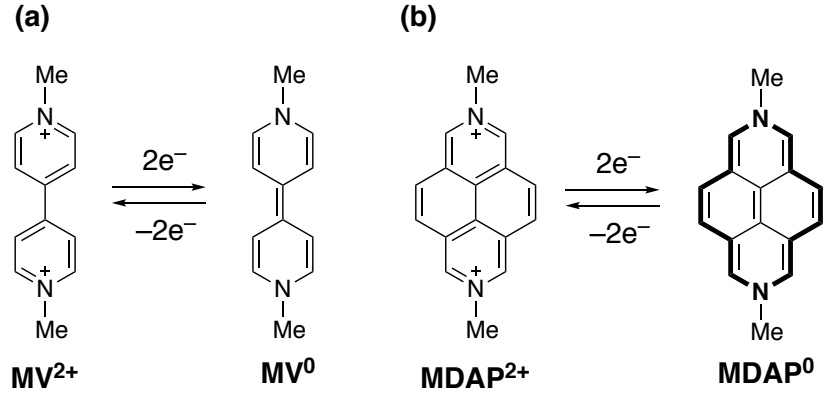

Scheme 5-1. (a) Dication and neutral forms of MV. (b) Dication and neutral forms of MDAP.

5-2. Synthesis and properties of *N*,*N*′-dimethyl-2,7-diazapyrenium dications

Scheme 5-2 shows the synthetic procedure of *N*,*N'*-dimethyl-2,7-diazapyrenium dications (**5-1**). Treatment of diazapyrenes **2-2a** and **2-2b** with 6 equiv of methyl triflate (MeOTf) in 1,2-dichloroethane at 80 °C for 6 h afforded **5-1a** and **5-1b** in 50% and 81% yield, respectively.

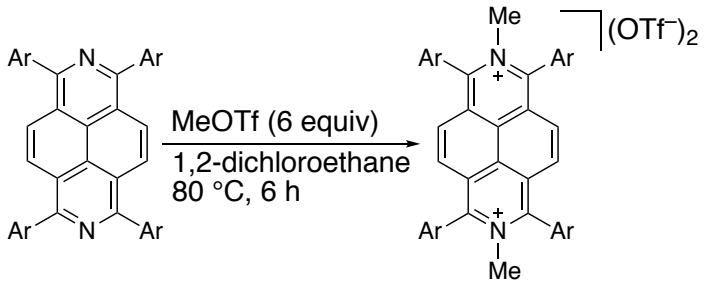

2-2a: Ar = C_6H_5
2-2b: Ar = 4-(*tert*-butyl)-C_6H_4
5-1a: Ar = C_6H_5 (50%)
5-1b: Ar = 4-(*tert*-butyl)-C_6H_4 (81%)

Scheme 5-2. Synthesis of *N*,*N'*-dimethyl-2,7-diazapyrenium dications.

The existence of two triflate anions as counter ions demonstrated the dicationic nature of **5-1a** (Figure 5-1). *N*,*N'*-Dimethyl-2,7-diazapyrenium dication **5-1a** has a highly planar structure. Dihedral angles between diazapyrene core and peripheral phenyl groups (65–67°) are larger than those of **2-2b** (33–34°) due to the steric repulsion between methyl groups on the nitrogen atoms and peripheral phenyl groups.

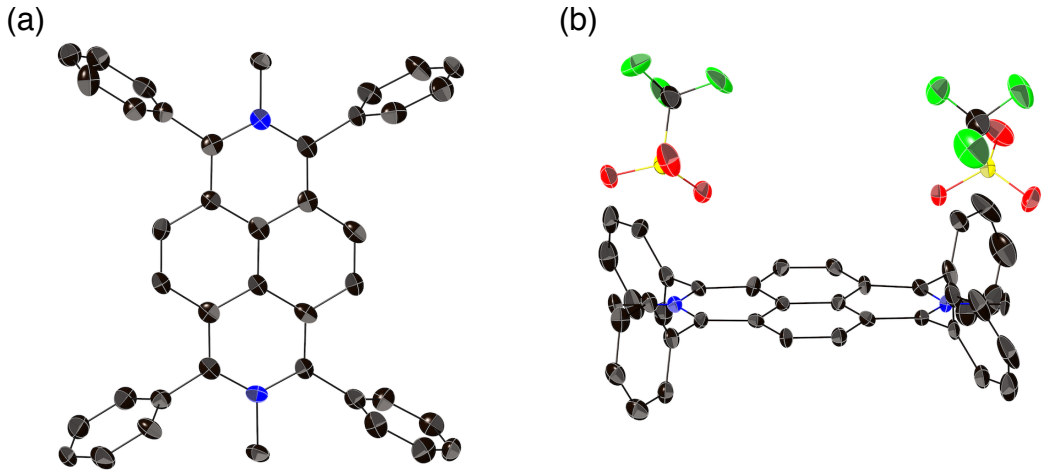

Figure 5-1. Molecular structures of **5-1a**. (a) Top view and (b) side view. Hydrogen atoms, solvent molecules, and counterions in (a) are omitted for clarity.

Figure 5-2 represents the UV-vis absorption and fluorescence spectra for **2-2b** and **5-1b** in CH_2Cl_2. In absorption spectrum of **5-1b**, bathochromic shift and the vibrational coarse structure were observed compared to **2-2b**. The emission quantum yield of **5-1b** (Φ = 0.78) was larger than **2-2b** (Φ = 0.38). These changes in optical properties result from not only the electric perturbation by the quaternization of nitrogen atoms but also the suppression of the rotation of the peripheral aryl groups due to the steric repulsion between methyl groups on the nitrogen atoms.

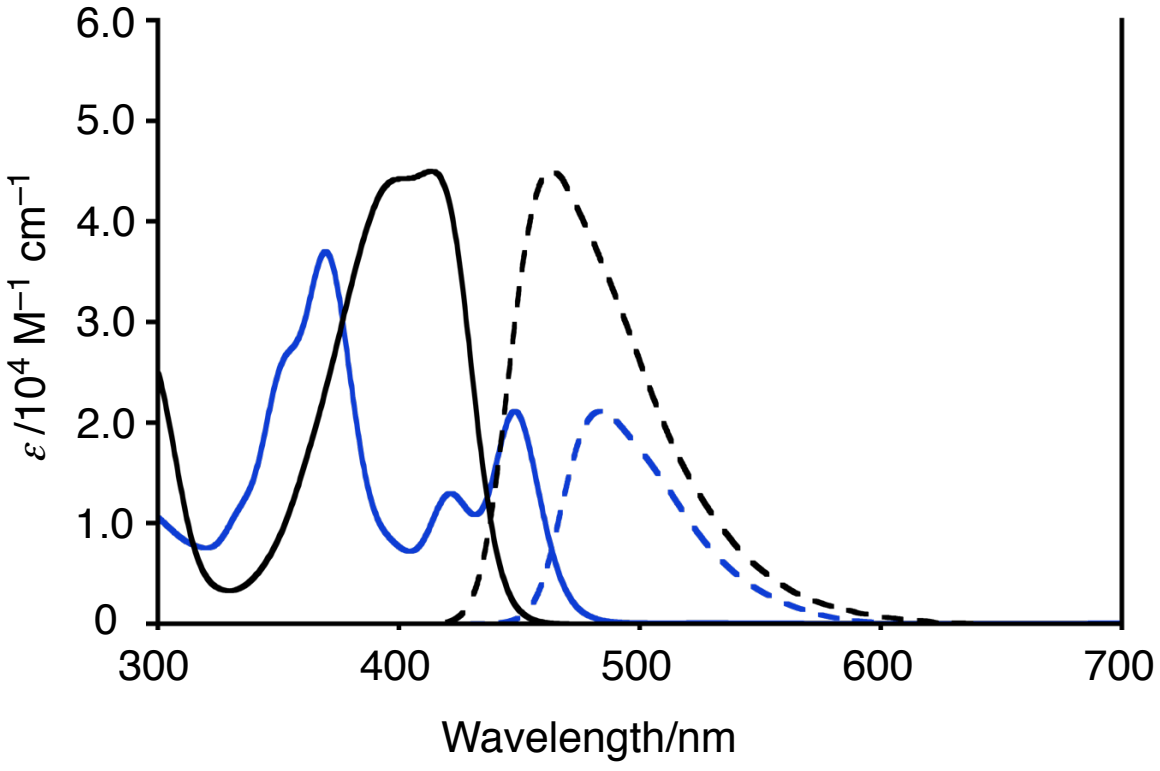

Figure 5-2. Electronic absorption (solid line) and fluorescence (dotted line) spectra of **1-2b** (black) and **5-1b** (blue) in CH_2Cl_2.

Table 5-1. Summary of optical properties of **1-2b** and **5-1b**.

Compound	λ_{ex} (nm)	Φ (in CH_2Cl_2)
2-2b	380	0.38
5-1b	370	0.78

Electrochemical properties of **2-2b, 5-1a** and **5-1b** were investigated with using cyclic voltammetry (Figure 5-4). Two reduction potentials were observed at $E_{red}^1 = -0.97$ V, $E_{red}^2 = -1.29$ V in **5-1a** and $E_{red}^1 = -1.01$ V, $E_{red}^2 = -1.34$ V in **5-2b**. These values are drastically shifted to the higher potential side than **2-2b** ($E_{red}^1 = -2.14$ V, $E_{red}^2 = -2.53$ V), indicating the highly electron accepting nature of **5-1**.

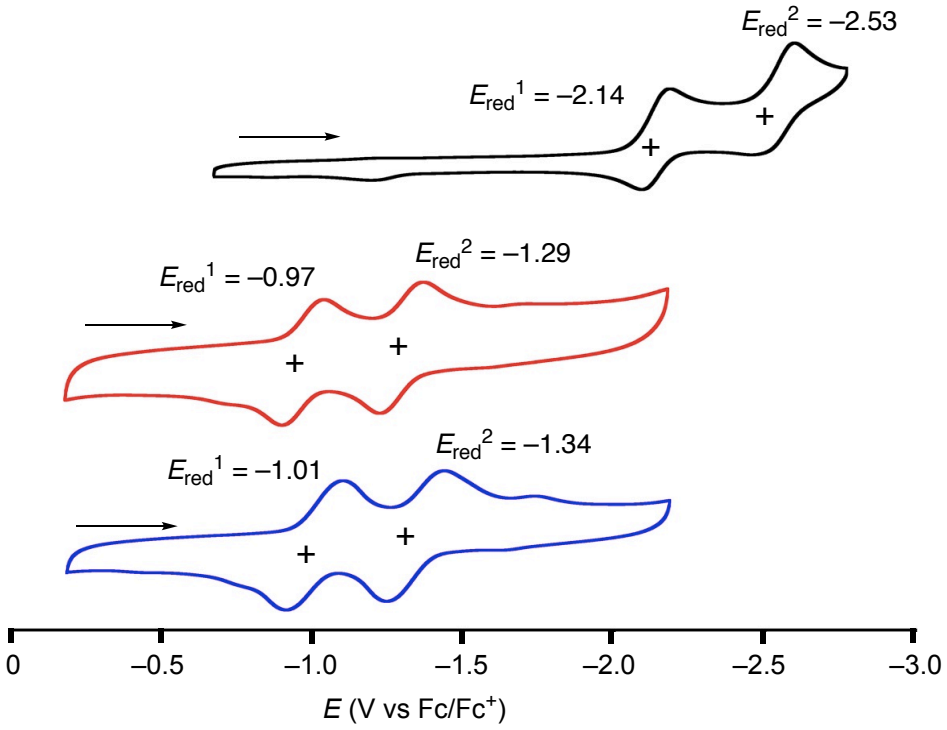

Figure 5-3. Cyclic voltammograms of **2-2b** (black line), **5-1a** (red line) and **5-1b** (blue line) in THF.

Table 5-2. Summary of reduction potentials of **2-2b**, **5-1a** and **5-1b** in THF.

Compound	E_{red}^1	E_{red}^2
2-2b	–2.14	–2.53
5-1a	–0.97	–1.29
5-1b	–1.01	–1.34

5-3. Reduction of *N,N'*-dimethyl-2,7-diazapyrenium dications and their properties

We conducted the two-electron reduction of **5-1** (Scheme 5-3). The reaction of **5-1a** and **5-1b** with 3 equiv of bis(pentamethylcyclopentadienyl)cobalt(II) ($CoCp^*_2$) in THF at room temperature for 3 h afforded the corresponding two-electron reduce forms **5-2a** and **5-2b** in 78 and 52% yields, respectively.

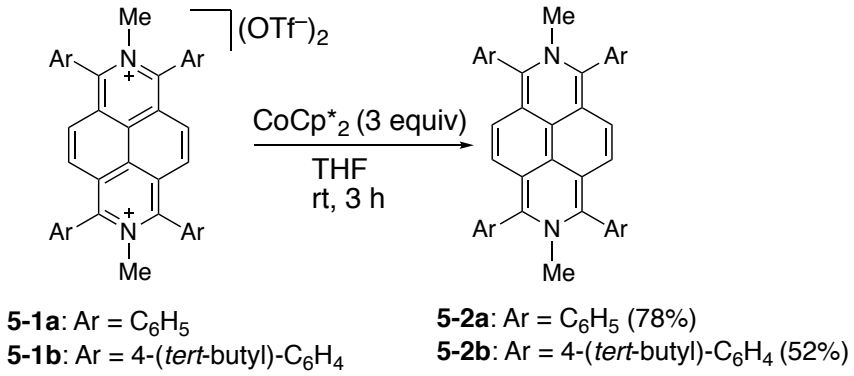

5-1a: Ar = C_6H_5
5-1b: Ar = 4-(*tert*-butyl)-C_6H_4

5-2a: Ar = C_6H_5 (78%)
5-2b: Ar = 4-(*tert*-butyl)-C_6H_4 (52%)

Scheme 5-3. Reduction reaction of *N,N'*-dimethyl-2,7-diazapyrenium dications.

The structure of **5-2a** was clearly determined X-ray analysis. Unlike the structure of **2-2b** and **5-1a**, **5-2a** adopts the slightly curved geometry with the mean plane deviation of 0.16 Å (Figure 5-4). Methyl groups on nitrogen atoms are displaced by 0.818 and 1.046 Å out of the nitrogen-based plane. This is in sharp contrast with MV^0, in which the methyl groups exist in the same plane of the six-membered rings including nitrogen atom.[6b] The structural distortion of **5-2a** would be caused by reducing 16π electron conjugation of the central core. In the packing structure, CH-π interaction between one methyl group and diazapyrene core of adjacent molecule was observed (Figure 5-4c).

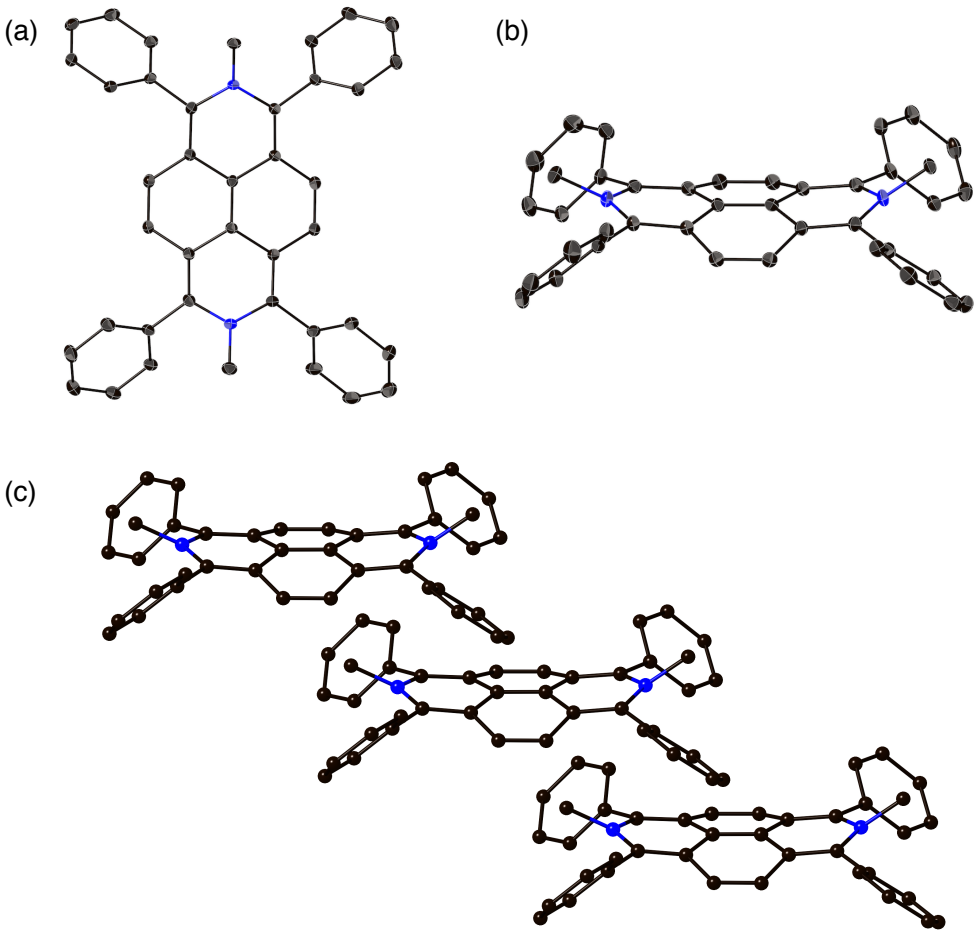

Figure 5-4. Molecular structures of **5-2a**. (a) Top view, (b) side view and (c) packing structure. Hydrogen atoms and solvent molecules are omitted for clarity.

Bond lengths of **5-2a** are summarized in Table 5-3. Compared to **2-2b**, the C13–C14 bond shortened (**5-2a**: 1.367(3) Å, **2-2b**: 1.436(2) Å), while the C–N bonds in the core became longer (**5-2a**: 1.404(3)–1.413(3) Å, **2-2b**: 1.341(2)–1.343(2) Å). In other bonds of **5-2b**, red bonds in Table 5-3 became shorter and black bonds became longer in comparison with those of **2-2b**. These values clearly indicate that **5-2a** adopts the quinoidal structure. The degree of bond length alternations in each ring was evaluated by harmonic oscillator model of aromaticity (HOMA) values (Figure 5-5).[12] In comparison with **2-2b**, the HOMA value of **5-2a** decreased in each ring, supporting the clear bond length alternations of **5-2a**.

Table 5-3. Summary of the selected bond length in the obtained from the crystal structure of **2-2b** and **5-2a**.

Selected bond	**2-2b (Å)**	**5-2a (Å)**
C13–C14	1.436(2)	1.367(3)
N1–C1	1.343(2)	1.413(3)
N1–C12	1.341(2)	1.410(3)
N2–C6	1.341(2)	1.403(3)
N2–C7	1.343(2)	1.404(3)
C2–C13	1.416(2)	1.456(3)
C11–C13	1.423(2)	1.460(3)
C5–C14	1.423(2)	1.457(3)
C8–C14	1.416(2)	1.456(3)
C1–C2	1.417(2)	1.413(3)
C11–C12	1.419(2)	1.364(3)
C3–C4	1.358(2)	1.344(3)
C9–C10	1.358(2)	1.346(3)
C5–C6	1.419(2)	1.367(3)
C7–C8	1.417(2)	1.363(3)

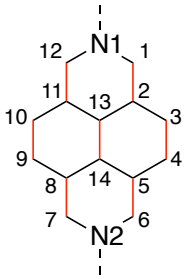

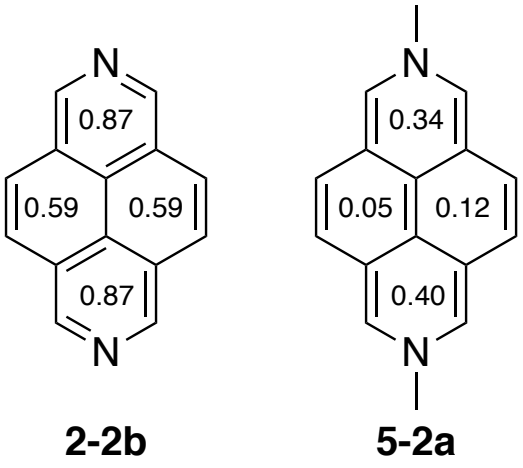

Figure 5-5. HOMA values for **2-2b** and **5-2a**.

5-4. Electrochemical properties

N,N'-Dimethyl-2,7-diazapyrenium dications **5-1** exhibits the high electron deficient nature derived from cationic imine-type nitrogen atoms. On the other hand, the two-electron reduced forms **5-2** should show electron-rich character. To evaluate the effects of converting cationic imine-type nitrogen to amine-type nitrogen, electrochemical properties of **5-2** were investigated with cyclic voltammetry. Both **5-2a** and **5-2b** shows two reversible oxidation waves in THF (Table 5-4). These values represent the high electron donating nature of **5-2**.

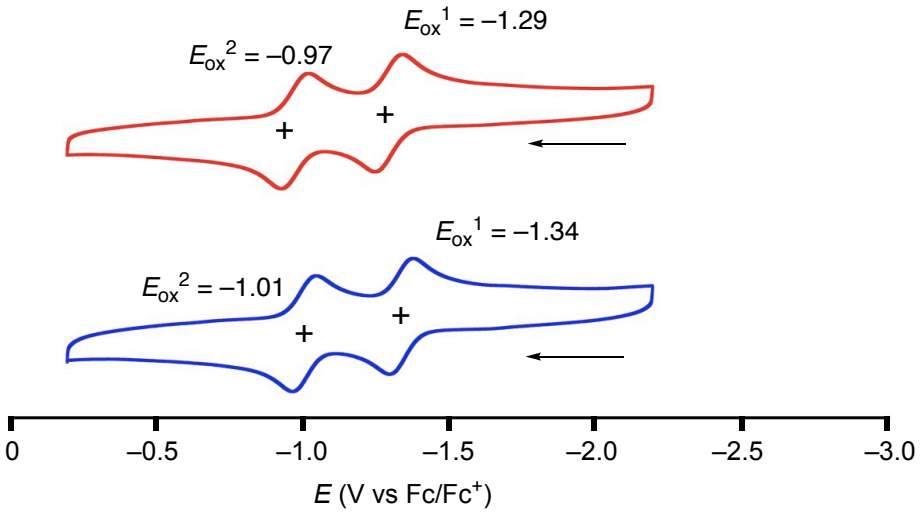

Figure 5-6. Cyclic voltammograms of **5-2a** (red line) and **5-2b** (blue line) in THF.

Table 5-4. Summary of oxidation potentials of **5-2a** and **5-2b** in THF.

Compound	E_{ox}^{1}	E_{ox}^{2}
5-2a	–1.29	–0.97
5-2b	–1.34	–1.01

5-5. Optical properties

Figure 5-7 shows UV-vis-NIR absorption spectra of **2-2b** and **5-2b** in THF. The absorption tail of **2-2b** was observed around 480 nm. In sharp contrast, **5-2b** exhibited the weak and broad absorption band reached to 1200 nm. According to the TD-DFT calculations (B3LYP/6-31G(d)), the lowest energy band of **5-2a** was assigned to the forbidden HOMO–LUMO transition. The HOMO–LUMO gap was estimated to be 1.87 eV, which is significantly smaller than that of aromatic 2,7-diazapyrene (3.08 eV). This result supports that **5-2a** have narrow HOMO–LUMO gap, which is the characteristic feature of antiaromatic compounds.

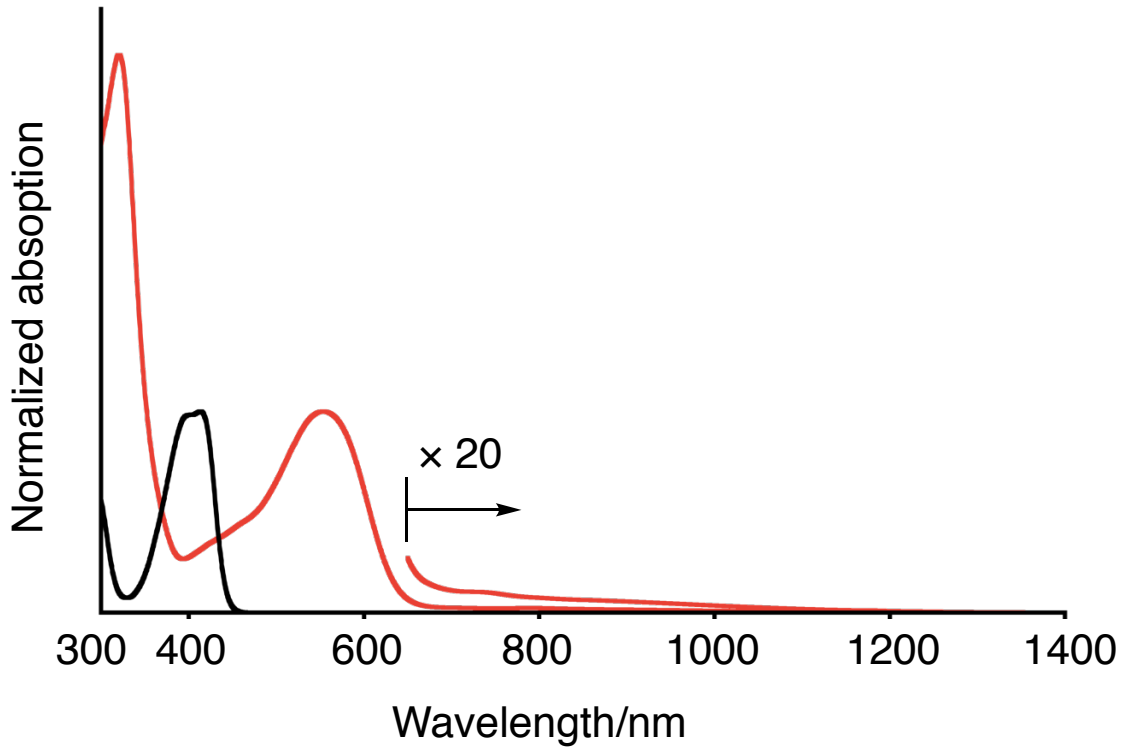

Figure 5-7. UV-vis-NIR absorption spectra of **1b** (black) and **3b** (red) in THF.

Table 5-5. Calculated excited wavelength (λ) and oscillator strength (f) of the lowest energy transitions of **2-2a** and **5-2a** calculated at the RB3LYP/6-31G(d) level of theory.

Compound	λ (nm)	f	Composition (%)
2-2a	443.47	1.0363	HOMO→LUMO (100%)
5-2a	1034.89	0.0000	HOMO→LUMO (100%)

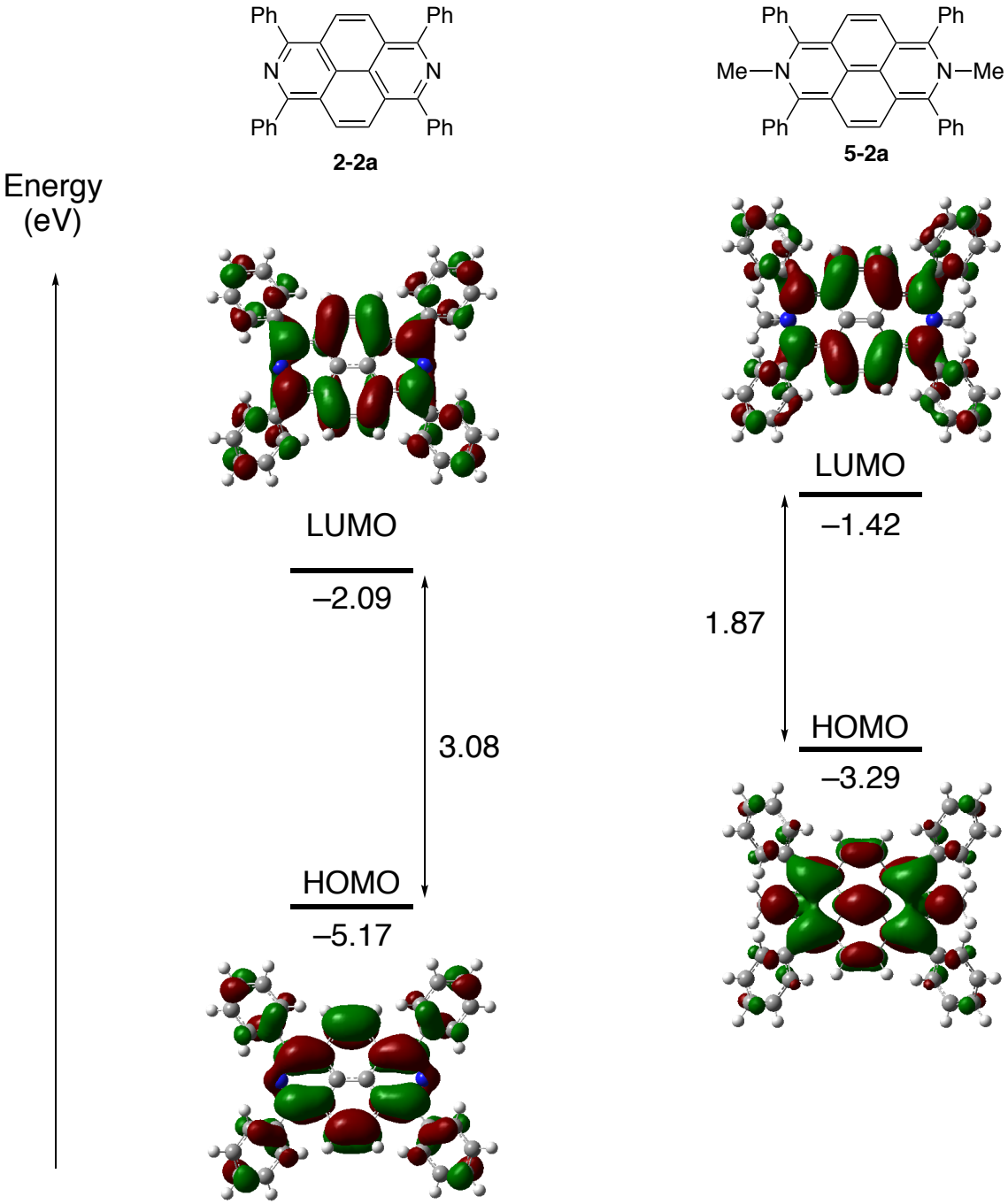

Figure 5-8. MO diagrams for **2-2a** and **5-2a** (RB3LYP/6-31G(d)) level of theory.

5-6. Evaluation of antiaromatic character

The magnitude of the magnetically induced ring current is one of the criteria to evaluate the antiaromatic character of cyclic π-conjugation systems. The proton on the diazapyrene core of **5-2b** in toluene-d_8 drastically high-field shifted to 4.5 ppm as compared to that of **2-2b** (Figure 5-9). This result suggests the presence of a paratropic ring current on **5-2b** derived from its antiaromatic character. To evaluate the paratropic ring current, NICS values were calculated using the optimized structure of **5-2a**.[13] As a result, **5-2a** exhibited positive values of the NICS(0) (8-19 ppm) at the center of the each ring (Figure 5-10a). ACID plot also supported the existence of paratropic ring current on **5-2a** (Figure 5-10b).[14] These experimental and theoretical results clearly revealed the antiaromatic character of **5-2**.

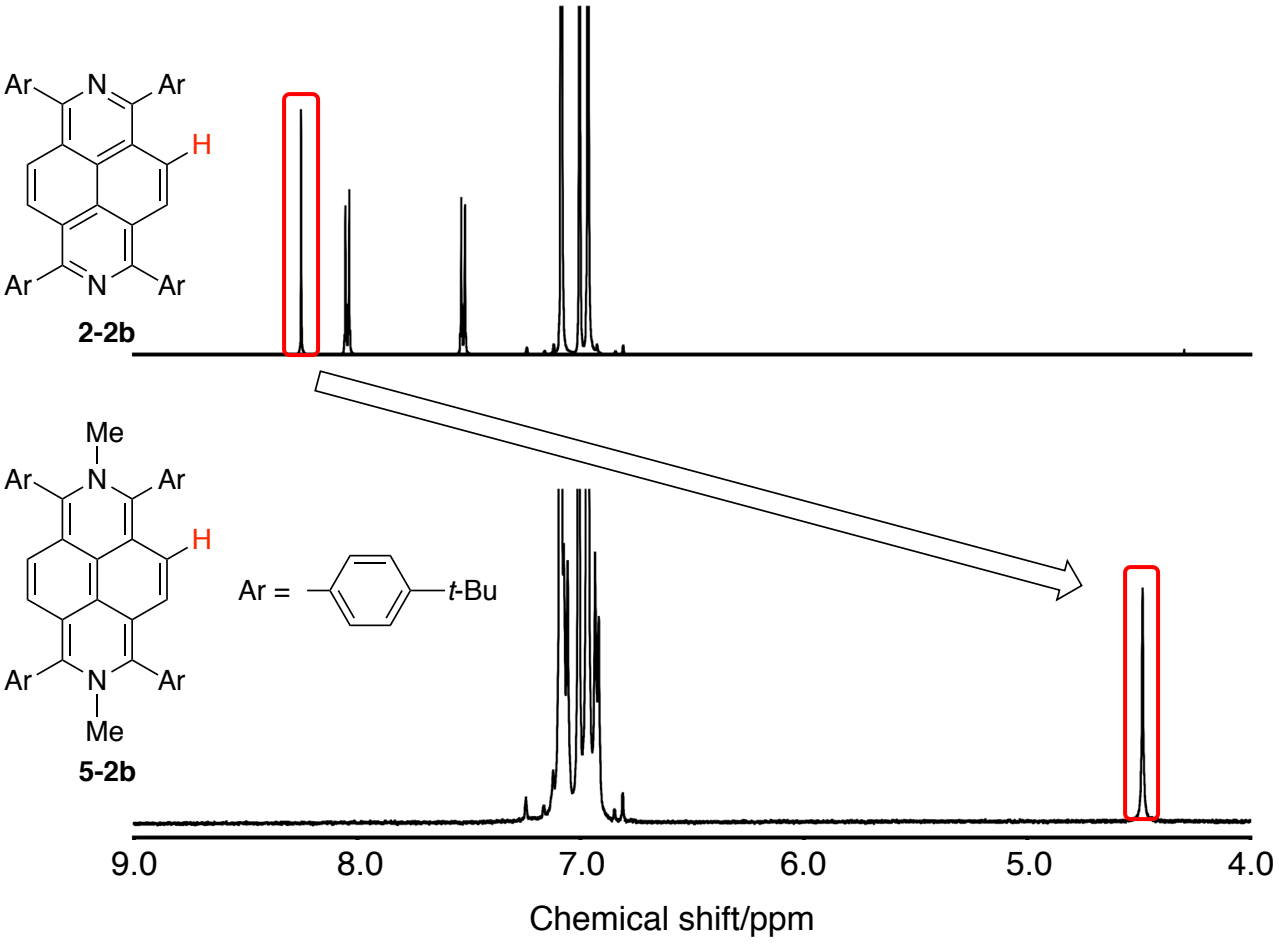

Figure 5-9. ^{1}H NMR spectra of **2-2b** (top) and **5-2b** (bottom) in toluene-d_6.

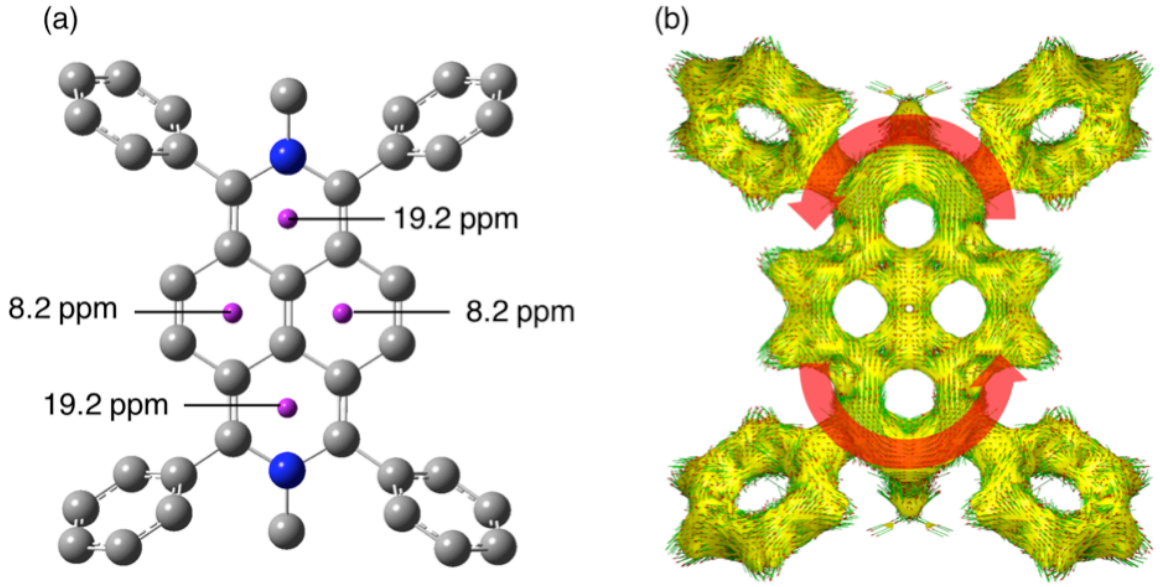

Figure 5-10. (a) NICS(0) values of **5-2a** calculated at the UB3LYP/6-31G(d) level of theory using X-ray crystal geometry. (b) The ACID-derived induced ring current map of **5-2a** calculated at the UB3LYP/6-31G(d) level of theory using X-ray crystal geometry.

5-7. Summary of Chapter 5

In summary, the author achieved the synthesis and characterization of *N,N'*-dimethyl-2,7-diazapyrenium dications **5-1** and the two-electron reduced forms **5-2** via methylation of tetraaryldiazapyrenes and two-electron reduction of **5-1**. Electrochemical analysis revealed highly electron-deficient nature of **5-1** reflecting dicationic character. X-ray analysis of **5-2a** elucidated its distorted geometry and quinoidal structure. The chemical shift of the proton on the diazapyrene core of **5-2b** in its ^{1}H NMR spectrum was high-field shifted compared with that of **2-2b**. Theoretical calculations supported the effect of the anticlockwise paratropic ring current. These results demonstrate that the two-electron reduced forms **5-2** exhibit the antiaromatic character owing to 16π electron conjugation.

5-8. References

1. (a) Monk, S. M. The Viologens: Physicochemical Properties, Synthesis and Applications of the Salts of 4,4'-Bipyridine, John Wiley& Sons, Chichester, 1998. (b) Bird, C. L.; Kuhn, A. T.; *Chem. Soc. Rev.* **1981**, *10*, 49-82. (c) Sliwa, W.; Bachowska, B.; Zelichowicz, N. *Heterocycles* **1991**, *32*, 2241-2273. (d) Ding, J.; Zheng, C.; Wang, L.; Lu, C.; Zhang, N.; Chen, Y.; Li, M.; Zhai, G.; Zhuang, X. *J. Mater. Chem. A* **2019**, *7*, 23337-23360.

2. (a) Hwang, E.; Seo, S.; Bak, S.; Lee, H.; Min, M.; Lee, H *Adv. Mater.* **2014**, *26*, 5129-5136. (b) Moon, H. C; Kim, C. -H.; Lodge, T. P.; Frisbie, C. D. *ACS Appl. Mater. Interfaces* **2016**, *8*, 6252-6260. (c) Madasamy, K.; Velayutham, D.; Suryanarayanan, V. M.; Kathiresan, K. -C. *J. Mater. Chem. C* **2019**, *7*, 4622-4637.

3. (a) Janoschka, T.; Martin, N.; Martin, U. Friebe, C.; Morgenstern, S.; Hiller, H. Hager, M. D. H.; Schubert U. S. *Nature* **2015**, *527*, 78-81. (b) Janoschka, T.; Martin, N.; Hager, M. D. Schubert, U. S. *Angew. Chem., Int. Ed.* **2016**, *55*, 14425-14428. (c) Hu, B.; DeBruler, C.; Rhodes, Z.; Liu, T. L. *J. Am. Chem. Soc.* **2017**, *139*, 1207-1214. (d) Wie, Z; Shin, W.; Jiang, H.; Wu, X.; Stickle, W. F.; Chen, G. Lu, J.; Greaney, P. A.; Du, F.; Ji, X. *Nat. Commun.* **2019**, ***10***, 3227.

4. (a) Sampath, A. C. S.; Late, D. J.; Barnes, J. C.; Kleinman, S. L.; Valley, N.; Hartlieb, K. J.; Liu, Z.; Dravid, V. P.; Schatz, G. C.; Van Duyne, R. P.; Stoddart, J. F. *ACS Nano* **2012**, *6*, 9964−9971. (b) A. Sagade, A.; Venkata, R. K.; George, S. J.; Dattac, A.; Kulkarni, U. G. A. *Chem. Commun.* **2013**, *49*, 5847-5849. (c) Osorio, H. M.; Catarelli, S.; Cea, P.; Gluyas, J. B.; Hartl, F.; Higgins, S. J.; Leary, E.; Low, P J.; Martin, S.; Nichols, R. J.; Tory, J.; Ulstrup, J.; Vezzoli, A.; Milan, D. C.; Zeng, Q. *J. Am. Chem. Soc.* **2015**, *137*, 14319-14328.

5. (a) Ashton, P. R.; Goodnow, T. T.; Kaifer, A. E.; Reddington, M. V.; Slawin, A. M. Z.; Spencer, N.; Stoddart, J. F.; Vicent, C.; Williams, D. J. A. *Angew. Chem., Int. Ed. Engl.* **1989**, *28*, 1396-1399. (b) Bissell, R. A.; Córdova, E.; Kaifer, A. E.; Stoddart, J. F.; *Nature* 1994, **369**, 133-137. (c) C. J. Bruns, D. Fujita, M. Hoshino, S. Sato, J. F. Stoddart, M. Fujita, *J. Am. Chem. Soc.* **2014**, *136*, 12027-12034. (d) Cantekin, S.; Markvoort, J. A.; Elemans, W. A. A. J.; Rowan, E. A.; Nolte, J. M. R.; Roeland, J. *J. Am. Chem. Soc.* **2015**, *137*, 3915-3923.

6. (a) Mohammad, M. *J. Org. Chem.* **1987**, *52*, 2779-2782. (b) Bockman, T. M.; Kochi, J. K. *J. Org. Chem.* **1990**, *55*, 4127-4135. (c) Porter, W. W.; Vaid, T. P.; *J. Org. Chem.* **2005**, *70*, 5028-5035.

7. (a) Durben, S.; Baumgartner, T.; *Angew. Chem. Int. Ed*. **2011**, *50*, 7948-7952. (b) Stolar, M.; Toonen, M.; Baumgartner, T. *J. Am. Chem. Soc*. **2015**, *137*, 3366-3371. (c) Bridges, C. R.; Borys, A. M.; Beland, V. A.; Gaffin, J. R.; Baumgartner, T. *Chem. Sci*. **2020**, *11*, 10483-10487.

8. (a) Oshita, J.; Murakami, K.; Tanaka, D.; Ooyama, Y.; Mizuno, T.; Kobayashi, N.; Higashimura, H.; Nakanishi, T.; Hasegawa, Y. *Organometallics* **2014**, *33*, 517-521. (b) Murakami, K.; Oshita, J.; Inagi, S.; Tomita, I. *Electrochemistry* **2015**, *83*, 605-608.

9. (a) Ashton, R. P.; Boyd, S. E.; Brindle, A.; Langford, S. J.; Menzer, S.; Perez-Garci, L.; Preece, J. A.; Raymo, F. M.; Spencer, N.; Stoddart, J. F.; Whiteb, A. J. P.; Williams, D. J. *New J. Chem.* **1999**, *23*, 587-602. (b) Zhang, Y. -M.; Wang, Z.; Chen, L.; Song, H.-B.; Liu, Y. *J. Phys. Chem. B* **2014**, *118*, 2433-2441. (c) Xing, H.; Wei, P.; Yan, X. *Org. Lett*. **2014**, *16*, 2850-2853

10. (a) Raymo, F. M.; Cejas, M. A. *Org. Lett.* **2002**, *4*, 3183-3185. (b) Cejas, M. A.; Raymo, F. M. *Langmuir* **2005**, *21*, 5795-5802.

11. Wardör, E. W.; Kaim, J. *Chem. Soc. Perkin Trans 2* **1996**, 1197-1204.

12. Krygowski, T. M.; Szatylowicz, H.; Stasyuk, O. A.; Dominikowska, J.; Palusiak, M, *Chem. Rev.* **2014**, *114*, 6383-6422.

13. Chen, Z.; Wannere, C. S.; Corminboeuf, C.; Puchta, R.; Schleyer, P. v. R. *Chem. Rev.* **2005**, *105*, 3842-3888.

14. Geuenich, D.; Hess, K.; Kohler, F.; Herges, R. *Chem. Rev.* **2005**, *105*, 3758-3772.

Chapter 6.

Summary of this thesis

In this thesis, the author described that the efficient synthetic methods for peripherally functionalized 2,7-diazapyrenes via reductive aromatization of naphthalene diimide as the key reaction and exploration of their properties and functions.

In Chapters 2 and 3, the author has developed efficient synthetic methods for aryl- and alkyl-introduced 2,7-diazapyrenes at the peripheral positions, respectively. In Chapter 2, the synthetic method for tetraaryl-2,7-diazapyrenes has been discussed. Reductive aromatization of naphthalene diimide with pivalic anhydride successfully provided 2,7-diazapyrene with pivaloxy groups as the useful synthetic intermediate. Introduced pivaloxy groups were converted to various aryl groups through Ni-catalyzed cross-coupling reactions. Tetrapentyl-2,7-diazapyrene was also synthesized by desulfurization of 2,7-diazapyrene with methylthienyl groups. Tetrapentyldiazapyrene showed spectral changes by protonation on nitrogen atoms. Moreover, FI-TRMC measurement revealed that diazapyrene with pentyl groups exhibited electron mobility. In Chapter 3, the synthetic method for tetraalkyl-2,7-diazapyrenes was described. Reductive aromatization of naphthalene diimide with methyl triflate afforded 2,7-diazapyrene with four methoxy groups. The cross-coupling reaction with alkyl Grignard reagents transformed methoxy groups into alkyl groups. X-ray analysis revealed that the length of peripheral alkyl groups dramatically affected their packing structure in the solid state. Furthermore, methyl and ethyl diazapyrene showed the electron mobility.

In Chapters 4 and 5, modification on nitrogen atoms of 2,7-diazapyrenes has been investigated. In Chapter 4, the author disclosed that the boron complexation of diazapyrene is an effective method to tune the structural and electronical properties of 2,7-diazapyrenes. The boron complexation of 2,7-diazapyrene with *o*-hydroxyphenyl groups afforded stable boron-diazapyrene complexes as stereoisomers of anti and syn form. Compared to the parent tetraaryl-2,7-diazapyrene, boron-diazapyrene complexes exhibited low-lying LUMO level and bathochromically shifted absorption and emission spectra. It was found that the syn-isomer forms the dimer in solution and solid state. The author also revealed that anti-form isomerizes to syn-form quantitatively under heating conditions. In Chapter 5, the author focused on the synthesis of *N*,*N*′-dimethyl-2,7-diazapyrenium dications with peripheral aryl groups and two-electron reduction of them. Quaternization of the two nitrogen atoms in diazapyrene was found to reduce the LUMO level in comparison with 2,7-diazapyrenes. Two-electron reduction of *N*,*N*′-dimethyl-2,7-diazapyrenium dications provided the corresponding reduced compounds. The X-ray analysis, ^{1}H NMR measurement, and theoretical calculations revealed that the two-electron reduced compounds exhibits antiaromatic character derived from the peripheral 16π electron conjugation including the lone pair electrons on nitrogen atoms.

Through this thesis, the author demonstrated the utility of the reductive aromatization of the naphthalene diimide for the construction of 2,7-diazapyrene skeleton and subsequent Ni-catalyzed cross-coupling reac-

tions for peripheral modifications. The reductive aromatization that is the key reaction in this thesis should be applicable to other aromatic diimide compounds. Consequently, the combination of reductive aromatization with the cross-coupling reaction provides peripherally functionalized aza-PAHs with various skeletons. Aza-PAHs have been widely studied because they are promising candidates for organic materials such as n-type semiconductor, stimuli-responsive materials, and components of supramolecular structures. The author hopes that the studies in this thesis accelerate the research on the synthesis and properties of aza-PAHs by offering the simple and efficient synthetic method.

In addition, the author disclosed that 2,7-diazapyrenes possess not only excellent optical properties derived from the pyrene skeleton, but also electron-deficient nature, Brønsted basicity, and Lewis basicity owing to the introduction of imine-type nitrogen atoms into the π-skeleton. The author expects that 2,7-diazapyrenes should be applied to photocatalysts or stimuli-responsive optical materials in the near future.

Experimental section

Contents

E-1. Instrumentation and materials

^{1}H NMR (500 MHz), ^{13}C NMR (126 MHz), ^{19}F NMR (470 MHz), and ^{11}B NMR (160 MHz) spectra were recorded on a Bruker AVANCE III HD spectrometer, and chemical shifts were reported as the delta scale in ppm relative to $CDCl_3$ (δ = 7.260 ppm), C_6D_6 (δ = 7.160 ppm), toluene-d_8 (δ = 2.080 ppm), CD_3CN (δ = 1.940 ppm), and DMSO-d_6 (δ = 2.500 ppm) for ^{1}H NMR, $CDCl_3$ (δ = 77.16 ppm), C_6D_6 (δ = 128.06 ppm), CD_3CN (δ = 118.26 ppm), and DMSO-d_6 (δ = 39.52 ppm) for ^{13}C NMR, hexafluorobenzene (δ = –164.90 ppm, as external standard) for ^{19}F NMR, and BF_3•OEt_2 (δ = 0.00 ppm, as external standard) for ^{11}B NMR respectively. UV/vis absorption spectra were recorded on a JASCO V670 spectrometer. Emission spectra were recorded using a JASCO FP-6500 spectrometer, and absolute fluorescence quantum yields were measured by the photon-counting method using an integration sphere. Fluorescence lifetimes were also measured on HAMAMATSU Photonics Quantaurus-Tau C11367-25. Mass spectra were recorded on a Bruker microTOF using positive mode for solid state with APCI-TOF methods and acetonitrile solutions with ESI-TOF method. X-ray data were taken on a Bruker D8 QUEST X-ray diffractometer equipped with PHOTON 100 CMOS active pixel sensor detector and IμS microfocus source using Mo-Kα radiation (λ = 0.71073 Å) or a Rigaku CCD diffractometer (Saturn 724 with MicroMax-007) with Varimax Mo optics using graphite monochromated Mo-Kα radiation (λ = 0.71075 Å). Melting points were measured by a SRS MPA100 OptiMelt Automated Melting Point System. Cyclic voltammograms were recorded on ALS electrochemical analyzer 612C. Measurements were performed in freshly distilled dichloromethane with 0.1 M tetrabutylammonium hexafluorophosphate as electrolyte. A three-electrode system was used and consisted of a grassy carbon as the working electrode, a platinum wire as the counter electrode, and an $Ag/AgClO_4$ as the reference electrode. All potentials are referenced to the potential of ferrocene/ferrocenium cation couple. The DSC measurement was recorded using NETZSCH DSC3500 Sirius at a heating rate of 10 K min^{-1}. Unless otherwise noted, materials obtained from commercial suppliers were used without further purification. All of reactions were conducted under argon atmosphere. Unless otherwise noted, materials obtained from commercial suppliers were used without further purification. Naphthalene diimide was prepared according to the literature.[1]

E-2. Theoretical calculations

All calculations were performed using the Gaussian 09 program.[2] Initial geometries were obtained from the X-ray structure. Full optimization was performed without any symmetric restriction with Becke's three-parameter hybrid exchange functional and the Lee-Yang-Parr correlation functional (B3LYP)[3] and the 6-31G(d) basis set for C, H, N, B and O atoms. In Chapter 4, the vibrational frequencies were calculated at the same level to check whether each optimized structure is an energy minimum (no imaginary frequency) or a transition state (one imaginary frequency) and to evaluate its zero-point vibrational energy (ZPVE) and thermal corrections at 298.15 K. The intrinsic reaction coordinates (IRC) were calculated using the global reaction route mapping (GRRM17) program[4] to track minimum energy paths from transition structures to the corresponding local minima.

E-3. Synthetic procedures and compound data

Chapter 2

Reductive aromatization of naphthalene diimide with pivalic anhydride (2-1)

In a 50 mL J-Young tube were placed naphthalene diimide (266 mg, 1.0 mmol), Zn (1.05 g, 16 mmol), pivalic anhydride (3.25 mL, 16 mmol), and 1,4-dioxane (10 mL) under Ar. The reaction mixture was stirred for 24 h at 120 °C. The suspension was filtrated through celite. The solution was concentrated in vacuo. Then, the remaining precipitate was washed with hexane. The residue was purified by column chromatography (SiO2) with CH2Cl2 as an eluent. After recrystallization from CH_2Cl_2/hexane, **2-1** (512 mg, 0.85 mmol, 85% yield) was obtained.

2-1: A white solid, m.p. 194.9 °C (decomp.). ^{1}H NMR ($CDCl_3$): δ 7.98 (s, 4H), 1.55 (s, 36H). 13C NMR (CDCl3): δ 176.6, 150.3, 132.1, 122.4, 117.9, 39.8, 27.4. HRMS(ESI) Calcd. For $C_{34}H_{41}N_2O_8$ [M+H]: 605.2857. Found: 605.2858.

1,3,6,8-tetra(4-*tert*-butylphenyl)-2,7-diazapyrene (2-2b)

Typical procedure for nickel-catalyzed cross-coupling reaction of **2-1** with a arylboronic acid is described below. In a 50 mL J-Young tube was placed K_3PO_4 (340 mg, 1.6 mmol) and was heated under the reduced pressure (120 °C, 1.0 Torr) for 1 h. After drying of K_3PO_4, **1b** (60.4 mg, 0.10 mmol) and 4-*tert*-butylphenylboronic acid (284.5 mg, 1.6 mmol) were added to the tube, and then $Ni(cod)_2$ (11.1 mg, 0.040 mmol), tricyclohexylphosphine (22.3 mg, 0.080 mmol), and toluene (3 mL) were taken in the reaction container in the globe box. The reaction mixture was stirred for 18 h at 60 °C. 10% Aqueous solution of ethylene diamine (3 mL) was added to the reaction mixture and the resulting solution was extracted with $CHCl_3$ (30 mL × 3). The combined organic layer was dried over Na_2SO_4 and concentrated in *vacuo*. The residue was purified by column chromatography (SiO_2) with $CHCl_3$/hexane (1/3) to give **2-2b** (43.3 mg, 0.059 mmol, 59% yield)

2-2b: A yellow solid, m.p. 209.9 °C (decomp.). ^{1}H NMR ($CDCl_3$): δ 8.36 (s, 4H), 7.89 (d, 8H, J = 8.5 Hz), 7.60 (d, 8H, J = 8.5 Hz), 1.42 (s, 36H). ^{13}C NMR ($CDCl_3$): δ 153.4, 151.7, 137.2, 130.7, 129.7, 126.2, 125.6, 122.6, 34.9, 31.5. HRMS(ESI) Calcd. For $C_{54}H_{57}N_2$ [M+H]: 733.4516. Found: 733.4512.

Isolated yields and spectroscopic data of other products are as follows:

1,3,6,8-Tetraphenyl-2,7-diazapyrene (2-2a)

2-2a: 26% yield (Purified by column chromatography (SiO_2) with CH_2Cl_2/hexane (1/20)). A pale yellow solid, m.p. 258.2 °C (decomp.). ^{1}H NMR ($CDCl_3$): δ 8.34 (s, 4H), 7.96-7.94 (m, 8H), 7.60 (t, 8H, J = 7.0 Hz), 7.54-7.51 (m, 4H). ^{13}C NMR could not be obtained due to the poor solubility. HRMS (APCI) Calcd. For $C_{38}H_{25}N_2$ [M+H]: 509.2018. Found: 509.2031.

1,3,6,8-Tetra(4-methoxyphenyl)-2,7-diazapyrene (2-2c)

2-2c: 50% yield (Purified by column chromatography (SiO_2) with $CHCl_3$ and recrystallization from $CHCl_3$/hexane). A yellow solid, m.p. 219.1 °C (decomp.). ^{1}H NMR ($CDCl_3$): δ 8.30 (s, 4H), 7.90 (d, 8H, *J* = 8.8 Hz), 7.12 (d, 8H, *J* = 8.8 Hz), 3.92 (s, 12H). ^{13}C NMR ($CDCl_3$): δ 160.2, 152.9, 132.6, 132.3, 129.9, 126.0, 122.3, 114.1, 55.6. HRMS(ESI) Calcd. For $C_{42}H_{33}N_2O_4$ [M+H]: 629.2435. Found: 629.2429.

1,3,6,8-Tetra(2-methoxyphenyl)-2,7-diazapyrene (2-2d)

2-2d: 30% (Purified by column chromatography (amino-SiO_2) with CH_2Cl_2/hexane (1/1)). A pale yellow solid, m.p. 225.8 °C (decomp.). ^{1}H NMR ($CDCl_3$ at 50 °C): δ 7.83 (s, 4H), 7.61 (br, 4H), 7.46 (dt, *J* = 1.8 and 8.0 Hz, 4H), 7.15 (t, *J* = 7.4 Hz, 4H), 7.08 (d, *J* = 8.1 Hz, 4H), 3.71 (s, 12H). ^{13}C NMR ($CDCl_3$): δ157.8, 151.7, 132.6, 130.0, 129.7, 127.9, 126.4, 124.3, 121.2, 111.7, 55.9. HRMS(APCI) Calcd. For $C_{42}H_{33}N_2O_4$ [M+H]: 629.2435. Found: 629.2439.

1,3,6,8-Tetra(4-trifluoromethylphenyl)-2,7-diazapyrene (2-2e)

2-2e: 18% yield (Purified by column chromatography (SiO_2) with $CHCl_3$ and recrystallization from $CHCl_3$/hexane). A yellow solid, m.p. 151.0 °C (decomp.). ^{1}H NMR ($CDCl_3$): δ 8.36 (s, 4H), 8.08 (d, 8H, *J* = 8.1 Hz), 7.88 (d, 8H, *J* = 8.1 Hz). ^{19}F NMR ($CDCl_3$): δ –65.76. HRMS(ESI) Calcd. For $C_{42}H_{21}F_{12}N_2$ [M+H]: 781.15131. Found: 781.15166.

1,3,6,8-Tetra(5-methylhienyl)-2,7-diazapyrene (2-2f)

2-2f: 30 % yield (at 70 °C) (Purified by column chromatography (SiO_2) with $CHCl_3$ and recrystallization from $CHCl_3$/hexane). A red solid, m.p. 110.1 °C (decomp.). ^{1}H NMR ($CDCl_3$): δ 8.63 (s, 4H), 7.62 (d, 4H, *J* = 3.6 Hz), 6.93 (dd, 4H, *J* = 3.6, 1.0 Hz), 3.92 (s, 12H). ^{13}C NMR ($CDCl_3$): δ 146.1, 143.9, 141.8, 130.4, 129.1, 126.6, 125.6, 120.9, 15.8. HRMS(ESI) Calcd. For $C_{34}H_{25}N_2S_4$ [M+H]: 589.0895. Found: 589.0880.

Chapter 3

Reductive aromatization of naphthalene diimide with pivalic anhydride (3-1)

In a 50 mL Schlenk was placed naphthalene diimide (266 mg, 1.0 mmol), Zn (1.05 g, 16 mmol), methyl triflate (0.66 mL, 6 mmol), and 1,4-dioxane (20 mL) under argon. The reaction mixture was stirred for 24 h at 60 °C. The suspension was filtrated through Celite. The filtrate was purified by alumina column chromatography with CH_2Cl_2 as eluent before concentration to give **3-1** (133 mg, 0.41 mmol, 41% yield).

3-1: A yellow solid, m.p. 199.2 °C (decomp.). ^{1}H NMR (C_6D_6): δ 8.10 (s, 4H), 3.89 (s, 12H). ^{13}C NMR (C_6D_6): δ 155.3, 133.89, 119.08, 109.74, 53.6. HRMS(APCI) Calcd. For $C_{18}H_{17}N_2O_4$ [M+H]: 325.1183. Found: 325.1190

1,3,6,8-Tetramethyl-2,7-diazapyrene (3-2a)

Typical procedure for nickel-catalyzed cross-coupling reaction of **3-1** with Grignard reagents is described below. In a flame-dried 50 mL J-Young tube was placed **3-1** and methylmagnesium iodide (0.77 mL, 0.6

mmol) and then $Ni(cod)_2$ (11.1 mg, 0.040 mmol), dicyclohexylphosphinoethane (17.1 mg, 0.040 mmol), and toluene (3 mL) were taken in the reaction container in the globe box. The reaction mixture was stirred for 24 h at 80 °C. 10% Aqueous solution of ethylene diamine (3 mL) was added to the reaction mixture and the resulting solution was extracted with $CHCl_3$ (30 mL × 3). The combined organic layer was dried over Na_2SO_4 and concentrated in *vacuo*. The residue was purified by column chromatography (SiO_2) with $CHCl_3$/ ethyl acetate (5/1) to afford **3-2a** (10.9 mg, 0.042 mmol, 42% yield).

3-2a: A pale yellow solid, m.p. 219.9 °C (decomp.). ^{1}H NMR ($CDCl_3$): δ 8.15 (s, 4H), 3.16 (s, 12H). ^{13}C NMR ($CDCl_3$): δ151.1, 127.8, 123.8, 122.8, 22.3. HRMS(APCI) Calcd. For $C_{18}H_{17}N_2$ [M+H]: 261.1386. Found: 261.1397.

Isolated yields and spectroscopic data of **3-2b** and **3-2c** are as follows:

1,3,6,8-Tetraethyl-2,7-diazapyrene (3-2b)

3-2b: 16% yield (Purified by column chromatography (SiO_2) with $CHCl_3$/ethyl acetate (10/1). A pale-yellow solid, m.p. 132.9 °C (decomp.). ^{1}H NMR (C_6D_6): δ 7.90 (s, 4H), 3.46 (q, 8H, J = 7.5 Hz), 1.58 (t, 12H, J = 7.5 Hz). ^{13}C NMR ($CDCl_3$): δ 156.0, 129.0, 123.36, 122.08, 28.7, 14.5. HRMS(APCI) Calcd. For $C_{22}H_{25}N_2$ [M+H]: 317.2012. Found: 317.2019.

1,3,6,8-Tetrapropyl-2,7-diazapyrene (3-2c)

3-2c: 12% yield (Purified by column chromatography (SiO_2)) with $CHCl_3$. A pale-yellow solid, m.p. 151.0 °C (decomp.). ^{1}H NMR ($CDCl_3$): δ 8.20 (s, 4H), 3.46 (t, 8H, J = 7.5 Hz), 1.96 (sextet, 8H, J = 7.5 Hz), 1.09 (t, 12 H, J = 7.5 Hz). ^{13}C NMR ($CDCl_3$): δ 155.2, 128.7, 123.6, 122.3, 37.6, 24.3, 14.4. HRMS(APCI) Calcd. For $C_{26}H_{33}N_2$ [M+H]: 373.2638. Found: 373.2655.

Chapter 4

Complexation of 2-2b with boron trifluoride

In a 20 mL Schlenk tube was placed compound **2-2b** (36.6 mg, 0.050 mmol). Then, dichloromethane (2 mL) and boron trifluoride-ethyl ether complex (50 μL, 0.20 mmol) were added under argon. After the reaction mixture was stirred for 1 h at 40 °C, the resultant mixture was added to toluene. The precipitates were filtered and washed with toluene to afford compound **4-1** (24.8 mg, 0.029 mmol, 57% yield).

4-1: A yellow solid, m.p. 151.0 °C (decomp.). ^{1}H NMR (CD_3CN): δ 8.57 (s, 4H), 7.90 (d, 8H, J = 8.6 Hz), 7.85 (d, 8H, J = 8.6 Hz), 1.46 (s, 36H). ^{13}C NMR (CD_3CN): δ 156.5, 151.2, 132.3, 130.9, 129.8, 128.6, 127.3, 127.1, 35.8, 31.3. ^{11}B NMR (CD_3CN): δ 1.48. ^{19}F NMR (CD_3CN) δ –152.3.

Demethylation of 2-2d

In a test tube were placed **2-2d** (62.9 mg, 0.10 mmol) and pyridine hydrochloride (1.85 g, 16 mmol). The mixture was stirred for 5 h at 200 °C. Aqueous solution of $NaHCO_3$ (50 mL) was added to the reaction

mixture, and the resulting solution was extracted with ethyl acetate (50 mL × 3). The combined organic layer was dried over Na_2SO_4 and concentrated in *vacuo*. The residue was purified by column chromatography (SiO_2) with CH_2Cl_2/ ethyl acetate (10/1) to give **4** (48.1 mg, 0.084 mmol, 84% yield)

4-2: A pale yellow solid, m.p. 250.8 °C (decomp.). ^{1}H NMR (DMSO-d_6 containing 0.05% of TMS): δ 9.99 (s, 4H), 8.04 (s, 4H), 7.56 (dd, J = 1.7 and 7.6 Hz, 4H), 7.40 (dt, J = 1.7 and 7.8 Hz, 4H), 7.09 (dd, J = 0.9 and 8.2 Hz, 4H), 7.05 (dt, J = 1.0 and 7.5 Hz, 4H). ^{13}C NMR (DMSO-d_6 containing 0.05% of TMS): δ 155.3, 151.0, 132.0, 130.1, 127.5, 126.2, 125.7, 122.8, 119.2, 116.2. HRMS(APCI) Calcd. For $C_{38}H_{24}N_2O_4$ [M]: 572.1731. Found: 572.1737.

Complexation of 4-2 with BBr_3 and sequential reaction with Grignard reagent

A 20 mL Schlenk tube containing **4-2** (28.6 mg, 0.050 mmol) was evacuated and then refilled with N_2. A solution of BBr_3 (10.8 mmol, 12 mL, 17% CH_2Cl_2 solution) was added to the tube at 0 °C. The mixture was stirred at r.t. for 5 h. The volatiles were removed in *vacuo* and the tube was refilled with N_2. Dry and degassed toluene (2 mL) was added. To the solution was added phenylmagnesium bromide (0.30 mmol, 0.33 mL, 0.89 M THF solution) at 0 °C. After stirring at room temperature for 18 h, 20 mL of 1 M aq. HCl was added to the solution. The aqueous layer was separated and extracted with dichloromethane (20 mL × 3). The combined organic layer was concentrated in *vacuo*. The residue was purified by column chromatography (SiO_2) with CH_2Cl_2 to give **anti-4-3** (21.6 mg, 0.029 mmol, 58% yield) and **syn-4-3** (2.60 mg, 0.0035 mmol, 7% yield)

anti-4-3: A pale yellow solid. ^{1}H NMR ($CDCl_3$): δ 9.03 (s, 4H), 7.99 (dd, J = 1.4 and 7.9 Hz, 4H), 7.44 (td, J = 1.5 and 7.8 Hz, 4H), 7.23 (dd, J = 1.1 and 8.2 Hz, 4H), 7.15 (dd, J = 1.6 and 7.5 Hz, 4H), 7.05 (td, J = 1.1 and 8.1 Hz, 4H), 6.97-6.93 (m, 6H). ^{11}B NMR ($CDCl_3$): δ 6.65. HRMS(ESI) Calcd. For $C_{50}H_{31}N_2O_4B_2$ [M+H]: 745.2480. Found: 745.2479.

syn-4-3: A pale yellow solid. ^{1}H NMR ($CDCl_3$): δ 8.30 (s, 4H), 7.60 (d, J = 7.3 Hz, 4H), 7.24 (td, J = 1.4 Hz, 7.8 Hz, 4H), 7.00 (td, J = 1.1 Hz, 7.6 Hz, 4H), 6.88-6.80 (m, 14H). ^{11}B NMR ($CDCl_3$): δ 6.07. HRMS(ESI) Calcd. For $C_{50}H_{31}N_2O_4B_2$ [M+H]: 745.2480. Found: 745.2466.

Complexation of 4-2 with phenylboronic acid

In a 20 mL Schlenk tube, **4-2** (28.2 mg, 0.050 mmol) and phenylboronic acid (48.7 mg, 0.40 mmol) were dissolved in benzene (2 mL). Triethylamine (0.18 mL, 2.0 mmol) was added and the reaction mixture was stirred at 90 °C for 12 h. The resulting solution was evaporated to remove solvents. The residue was purified by column chromatography (SiO_2) with CH_2Cl_2 to give **anti-4-3** (3.75 mg, 0.0050 mmol, 10% yield) and **syn-4-3** (23.1 mg, 0.031 mmol, 68% yield).

Chapter 5

Methylation of 1,3,6,8-tetraphenyl-2,7-diazapyrene (5-1a)

Typical procedure for the reaction of **2-2a** with methyl triflate is described below. In a 20 mL Schlenk tube was placed compound **2-2a** (25.4 mg, 0.050 mmol). Then, 1,2-dichloroethane (6 mL) and methyl triflate (33 μL, 0.30 mmol) were added under argon. After the reaction mixture was stirred for 6 h at 80 °C, the resultant mixture was cooled to room temperature. Volatiles were evaporated in *vacuo*. The precipitates were filtered and washed with $CHCl_3$ to afford compound **5-1a** (20.9 mg, 0.025 mmol, 50% yield).

5-1a: A yellow solid, m.p. 228 °C (decomp.). ^{1}H NMR (CD_3CN): δ 7.98 (s, 4H), 7.86-7.80 (m, 12H), 7.60 (t, 8H, J = 7.0 Hz), 7.75-7.73 (m, 8H), 7.08 (s, 4H). ^{19}F NMR δ –79.3. HRMS (APCI) Calcd. For $C_{40}H_{30}N_2$ [M]: 538.2409. Found: 538.2427.

Isolated yields and spectroscopic data of other products are as follows:

5-1b: 81% yield (Purified by column chromatography (SiO_2)) with CH_2Cl_2/ethyl acetate (1/1). A yellow solid, m.p. 239 °C (decomp.). ^{1}H NMR (CD_3CN): δ 7.97 (s, 4H), 7.85 (d, 8H, J = 8.5 Hz), 7.64 (d, 8H, J = 8.5 Hz), 4.09 (s, 6H), 1.44 (s, 36H). ^{13}C NMR (CD_3CN): δ 156.4, 154.1, 130.8, 130.5, 129.8, 128.3, 128.2, 48.8, 35.9, 31,4. ^{19}F NMR: δ –79.3. HRMS (APCI) Calcd. For $C_{56}H_{62}N_2$ [M]: 762.4908. Found: 742.4929.

Two-electron reduction of *N,N′*-dimethyl-2,7-diazapyrenium dications (5-2a)

Typical procedure for the two-electron reduction of **2-2a** is described below. A flask containing compound **5-1a** (42.0 mg, 0.050 mmol) was placed in the argon-filled glove box. Then, THF (10 mL) and bis(pentamethylcyclopentadienyl)cobalt(II) (65.6 mg) were added to the flask. The mixture was stirred at room temperature for 3 h. The reaction mixture was filtrated through celite and wash with toluene. The filtrate was evaporated to remove the solvent and the obtained residue was recrystallized from toluene/hexane in the glove box to afford **5-2a** as a purple solid (14.0 mg, 0.026 mmol, 52% yield).

5-2a: A purple solid. ^{1}H NMR (C_6D_6): δ 6.93-6.84 (m, 20H), 4.50 (s, 4H), 1.65 (s, 6H). ^{13}C NMR: δ 140.4, 136.4, 129.0, 128.7, 128.6, 127.5, 127.2, 124.1, 41.3.

The isolated yield and spectroscopic data of **5-2b** are as follows:

5-2b: 78% yield. A purple solid. ^{1}H NMR (C_6D_6): δ 7.08 (d, 8H, J = 8.0), 6.96 (d, 8H, J = 8.5), 4.56 (s, 4H), 1.79 (s, 6H), 1.11 (s, 36H). ^{13}C NMR: δ 150.7, 140.4, 133.6, 128.5, 127.7, 127.3, 125.9, 124.2, 41.4, 34.5, 31.3.

E-4. Crystallographic data

compound	**2-2b**	**2-2f**
Formula	$C_{54}H_{56}N_2$	$C_{34}H_{24}N_2S_4$
Formula weight	733.01	588.79
Crystal system	triclinic	monoclinic
Space group	*P*-1 (No. 2)	*P*2/c (No. 14)
Crystal color	yellow	orange
Crystal description	prism	block
a [Å]	7.2959(4)	15.9885(7)
b [Å]	10.3488(6)	6.2625(3)
c [Å]	14.0322(7)	14.7453(6)
α [°]	96.970(2)	90
β [°]	98.0126(4)	111.597(5)
γ [°]	100.566(4)	90
V [Å^3]	1019.50(10)	1372.77(12)
Z	1	2
d_{calcd} [g cm^{-3}]	1.194	1.424
R_1 ($I > 2\sigma(I)$)	0.0444	0.0461
wR_2 (all data)	0.1235	0.1250
Goodness-of-fit	1.042	1.098
Temperature [K]	101(2)	93(2)
Solvent	toluene/acetonitrile	chlorobenzene/acetonitrile

compound	**2-3**	**3-1**
Formula	$C_{34}H_{48}N_2$	$C_{18}H_{16}N_2O_4$
Formula weight	484.74	324.34
Crystal system	orthorhombic	triclinic
Space group	$Pna2_1$ (No. 33)	$P\bar{1}$ (No. 2)
Crystal color	colorless	yellow
Crystal description	needle	prism
a [Å]	21.6241(8)	6.5353(2)
b [Å]	4.7229(3)	7.3858(3)
c [Å]	27.9845(9)	8.2199(3)
α [°]	90	102.097(3)
β [°]	90	99.004(3)
γ [°]	90	105.886(3)
V [Å^3]	2858(2)	363.36(2)
Z	4	1
d_{calcd} [g cm^{-3}]	1.127	1.482
R_1 ($I > 2\sigma(I)$)	0.0675	0.0399
wR_2 (all data)	0.1878	0.1181
Goodness-of-fit	1.053	1.089
Temperature [K]	93(2)	93(2)
Solvent	acetonitrile	dichloroethane/hexane

compound	**3-2a**	**3-2b**
Formula	$C_{18}H_{16}N_2$	$C_{22}H_{24}N_2$
Formula weight	260.33	316.43
Crystal system	orthorhombic	triclinic
Space group	*Pbam* (No. 55)	*P*-1 (No. 2)
Crystal color	pale-yellow	pale-yellow
Crystal description	block	prism
a [Å]	17.5029(4)	4.4909(3)
b [Å]	11.0272(3)	8.3869(4)
c [Å]	6.7696(2)	11.3304(7)
α [°]	90	79.258(5)
β [°]	90	89.682(5)
γ [°]	90	86.088(4)
V [Å^3]	1306.59(12)	418.29(4)
Z	4	1
d_{calcd} [g cm^{-3}]	1.323	1.256
R_1 ($I > 2\sigma(I)$)	0.0943	0.0603
wR_2 (all data)	0.3216	0.1802
Goodness-of-fit	1.088	1.067
Temperature [K]	93(2)	93(2)
Solvent	$CHCl_3$/hexane	$CHCl_3$/acetonitrile

compound	**anti-4-3**	**syn-4-3**
Formula	$C_{50}H_{30}B_2N_2O_4$	$C_{50}H_{30}B_2N_2O_4$
Formula weight	744.42	744.42
Crystal system	triclinic	orthorhombic
Space group	*P*-1 (No. 2)	*P21212* (No. 18)
Crystal color	orange	pale yellow
Crystal description	block	block
a [Å]	9.5439(2)	17.5029(4)
b [Å]	10.6657(2)	11.0272(3)
c [Å]	14.8023(3)	6.7696(2)
α [°]	86.851(2)	90
β [°]	73.687(2)	90
γ [°]	74.975(2)	90
V [Å^3]	1396.40(5)	1306.59(12)
Z	2	4
d_{calcd} [g cm^{-3}]	1.595	1.323
R_1 ($I > 2\sigma(I)$)	0.0634	0.0943
wR_2 (all data)	0.1579	0.3216
Goodness-of-fit	1.097	1.088
Temperature [K]	93(2)	93(2)
Solvent	$CHCl_3$	toluene/octane

compound	**5-1a**	**5-2a**
Formula	$C_{50}H_{30}B_2N_2O_4$	$C_{50}H_{30}B_2N_2O_4$
Formula weight	836.82	538.24
Crystal system	monoclinic	triclinic
Space group	$P2_1$ (No. 4)	$P\bar{1}$ (No. 2)
Crystal color	yellow	brown
Crystal description	block	plate
a [Å]	13.5923(4)	7.4295(2)
b [Å]	23.4067(6)	10.3077(2)
c [Å]	14.4963(4)	11.5948(3)
α [°]	90	101.5399(17)
β [°]	108.166(3)	107.796(2)
γ [°]	90	92.2346(16)
V [Å^3]	4282.1(2)	823.58(4)
Z	2	1
d_{calcd} [g cm^{-3}]	1.523	1.272
R_1 ($I > 2\sigma(I)$)	0.0871	0.0426
wR_2 (all data)	0.2303	0.1209
Goodness-of-fit	1.030	1.024
Temperature [K]	93(2)	93(2)
Solvent	tetrachloroethane/hexane	toluene/acetonitrile

E-5. References

1. Sotiriou-Leventis, C.; Mao, Z. *J. Heterocyclic Chem.* **2000**, *37*, 1665-1667.

2. Frisch, M. J.; Trucks, G. W.; Schlegel, H. B.; Scuseria, G. E.; Robb, M. A.; Cheeseman, J. R.; Montgomery, Jr., J. A.; Vreven, T.; Kudin, K. N.; Burant, J. C.; Millam, J. M.; Iyengar, S. S.; Tomasi, J.; Barone, V.; Mennucci, B.; Cossi, M.; Scalmani, G.; Rega, N.; Petersson, G. A.; Nakatsuji, H.; Hada, M.; Ehara, M.; Toyota, K.; Fukuda, R.; Hasegawa, J.; Ishida, M.; Nakajima, T.; Honda, Y.; Kitao, O.; Nakai, H.; Klene, M.; Li, X.; Knox, J. E.; Hratchian, H. P.; Cross, J. B.; Bakken, V.; Adamo, C.; Jaramillo, J.; Gomperts, R.; Stratmann, R. E.; Yazyev, O.; Austin, A. J.; Cammi, R.; Pomelli, C.; Ochterski, J. W.; Ayala, P. Y.; Morokuma, K.; Voth, G. A.; Salvador, P.; Dannenberg, J. J.; Zakrzewski, V. G.; Dapprich, S.; Daniels, A. D.; Strain, M. C.; Farkas, O.; Malick, D. K.; Rabuck, A. D.; Raghavachari, K.; Foresman, J. B.; Ortiz, J. V.; Cui, Q.; Baboul, A. G.; Clifford, S.; Cioslowski, J.; Stefanov, B. B.; Liu, G.; Liashenko, A.; Piskorz, P.; Komaromi, I.; Martin, R. L.; Fox, D. J.; Keith, T.; Al-Laham, M. A.; Peng, C. Y.; Nanayakkara, A.; Challacombe, M.; Gill, P. M. W.; Johnson, B.; Chen, W.; Wong, M. W.; Gonzalez, C.; Pople, J. A. Gaussian, Inc., Wallingford CT, Pittsburgh, PA, **2009**.

3. (a) Becke, A. D. *Phys. Rev. A* **1988**, *38*, 3098-3100. (b) Lee, C.; Yang, W.; Parr, R. G. *Phys. Rev. B* **1988**, *37*, 785-789.

4. Maeda, S.; Harabuchi, Y.; Takagi, M.; Saita, K.; Suzuki, K.; Ichino, T.; Sumiya, Y.; Sugiyama, K.; Ono, Y. *J. Comput. Chem.* **2018**, *39*, 233-251.

List of Publications

1. Nakazato, T.; Kamatsuka, T.; Inoue, J.; Sakurai, T.; Seki, S.; Shinokubo, H.; Miyake, Y. *Chem. Commun*. **2018**, *54*, 5177-5180.
2. Nakazato, T.; Matsuda, W.; Sakurai, T.; Seki, S.; Shinokubo, H.; Miyake, Y. *Chem. Lett*. **2020**, *49*, 465-468.
3. Nakazato, T.; Shinokubo, H.; Miyake, Y. *Chem. Commun.* **2021**, *57*, 327-330.

The following papers are not included in this doctoral thesis.

4. Nakamura, Y.; Nakazato, T.; Kamatsuka, T.; Shinokubo, H.; Miyake, Y. *Chem. Eur. J.* **2019**, *25*, 10571-10574.

5. Acknowledgements

The study described here has been carried out under the super vision of Prof. Dr. Hiroshi Shinokubo at Graduate School of Engineering, Nagoya University during the period from 2016 to 2021. The author would like to express his deepest gratitude for Prof. Dr. Hiroshi Shinokubo for his precious guidance and encouragement throughout this thesis. The author would like to express the deepest appreciation to Assoc. Prof. Dr. Yoshihiro Miyake whose comments and suggestions were innumerably valuable throughout the course of the study of this thesis. The author is deeply grateful to Assoc. Prof. Dr. Satoru Hitroto, Assist. Prof. Dr. Norihito Fukui, and Prof. Dr. Ji-Yong Shin for their kind and helpful discussions and suggestions of this study.

The author wishes to express deep appreciation to Prof. Dr. Shigehiro Yamaguchi at Graduate School of Science, Nagoya University and Prof. Dr. Makoto Yamashita at Graduate School of Engineering, Nagoya University, for their helpful suggestions and discussion on his dissertation committee.

The author gratefully acknowledges to Prof. Dr. Shu Seki, members of the Seki Group at Graduate School of Engineering, Kyoto University, and Senior Junior Assoc. Prof. Dr. Tsuneaki Sakurai at Kyoto Institute of Technology for the evaluation of carrier conductivity using TRMC technics.

The author also gratefully acknowledges to Prof. Dr. Wu Jishan and Assoc. Prof. Chi Chunyan at Department of Chemistry, National University of Singapore, Singapore, for their invaluable guidance and financial support during the stay in NUS as a visiting student. The author extends grateful thanks to members of the Wu and Chi Groups for their heartfut friendship and enormous help. The three months spent at NUS have been an irreplaceable experience for the author.

The author gratefully acknowledges to Prof. Dr. Shigeo Komoto, Prof. Dr. Keiki Kishikawa, and, Dr. Masahiro Takahashi at Department of Applied Chemistry and Biotechnology, Chiba University, for their precious guidance, advices, and encouragement through the author's previous study at Faculty of Engineering, Chiba University from 2015 to 2016. The author also would like to show appreciation to former members of the Komoto Group for discussions and encouragement.

The author would like to acknowledge to following members of the Shinokubo Group for their friendly competition and consideration.

Dr. Satoru Ito
Mr. Yuya Hiraoka
Dr. Takuya Yoshida
Mr. Yuki Ando
Mr. Hideo Tsuboi
Mr. Tsubasa Yonezawa
Mr. Tatsuya Ochiai
Mr. Tsubasa Nishimura
Mr. Yasutaka Nakamura
Mr. Syuto Yokoyama
Ms. Asahi Takiguchi
Mr. Yuki Tanaka
Mr. Tomoya Yokota
Mr. Hiroyuki Kawashima
Mr. Kazuya Miyagawa
Mr. Atsumi Yagi
Mr. Masaki Kato
Ms. Mao Komura
Mr. Yuki Tanaka
Ms. Ayako Kimata
Dr. Kazuma Oda
Mr. Hiroki Yokoi
Dr. Hiroto Omori
Ms. Ayako Ushiyama
Ms. Juri Nagasaki
Mr. Shuhei Akahori
Mr. Motoki Takeda
Mr. Kazuhiro Kubokoya
Ms. Sakiho Hayakawa
Mr. Syuto Yokoyama
Ms. Siham Asyiqin Shafie
Ms. Wen Xi Chia
Ms. Siyu Liu
Mr. Takahiro Sakurai
Ms. Shiho Mori
Ms. Mai Odajima
Mr. Ryohei Noge
Mr. Shota Kino
Mr. Shigetatsu Tsugimoto
Dr. Ayaka Yamaji
Mr. Naruhiko Wachi
Dr. Ryo Nozawa
Mr. Hiroyuki Kawashima
Mr. Yuya Nagata
Ms. Shiori Itabuchi
Mr. Tomohiro Nagai
Mr. Yuma Shiratani
Mr. Daisuke Yamashita
Mr. Nathan Hikaru Faialaga
Ms. Haruka Takekoshi
Mr. Hiroyasu Murase
Dr. Jean-François Longevial
Mr. Keita Tajima
Mr. Shusaku Ukai
Mr. Masahiro Odawara
Mr. Kensuke Hanida
Mr. Yoshihiro Takeo
Mr. Takumi Hayashi

The author expresses sincere thanks to his all friend inside and outside the world of academia for their friendship and warm encouragement.

Last but not least, I desire to express my deepest gratitude beyond description to my parents, Mr. Hitoshi Nakazato, Ms. Izuru Nakazato, my young brother Mr. Masaki Nakazato, my young sister Ms. Shiori Nakazato, my grandparents Mr. Reizo Nakazato, Ms. Mieko Nakazato, Mr. Shosei Yamazato, Ms. Chiyoko Yamazato, my uncle Mr. Katsuya Nakazato, my aunt Ms. Yaeko Nakazato, and Ms. Rei Yamazato.

Takumi NAKAZATO
仲里　巧
January 2021